Order Number 9130376

Diamond chemical vapor deposition: Thermodynamic analysis and growth studies

Sommer, Marianne, Ph.D.

City University of New York, 1991

DIAMOND CHEMICAL VAPOR DEPOSITION: THERMODYNAMIC ANALYSIS AND GROWTH STUDIES

by

Marianne Sommer

A dissertation submitted to the Graduate Faculty in Physics in partial fulfillment of the requirements for the degree of Doctor of Philosophy, The City University of New York.

1991

This manuscript has been read and accepted for the Graduate Faculty in Physics in satisfaction of the dissertation requirements for the degree of Doctor of Philosophy.

April 18, 1991
Date

Frederick W. Smith
Chair of Examining Committee

May 7, 1991
Date

Executive Officer

Supervisory Committee

The City University of New York

Abstract

DIAMOND CHEMICAL VAPOR DEPOSITION: THERMODYNAMIC ANALYSIS AND GROWTH STUDIES

by

Marianne Sommer

Adviser: Professor Frederick W. Smith

The chemical vapor deposition of carbon films is analyzed using the thermodynamic quasiequilibrium (QE) model and a phase diagram for the carbon-hydrogen system is obtained. When the enhanced etching of graphite by hydrogen is included in the model, a region appears in the phase diagram where diamond is predicted to be the only stable phase of carbon, in agreement with the experimental results of Matsumoto *et al.* [*J. Mater. Sci.* **17**, 3106 (1982)]. The QE model can also explain the experimentally observed effects on the CVD of diamond resulting from variations in the available growth parameters (substrate temperature, reactant ratio, etc.). When the QE thermodynamic model is extended to reactions between carbon, hydrogen, and oxygen the stability region of solid carbon in the C-H-O phase diagram is predicted to shrink considerably due to the formation of CO. In particular, it is predicted that no carbon can be deposited from gas mixtures whose C/O ratio equals unity.

In a series of experiments the interactions of tungsten and rhenium filaments with gas mixtures typical of the diamond growth environment have been analyzed. It has been demonstrated that the filaments themselves can act as high temperature substrates

for the deposition of graphitic carbon and that the filaments then lose their ability to dissociate the reactant gases. The filament resistance, spectral emissivity, power consumption, and partial pressures of stable gases in the reaction chamber have been found to depend critically both on the filament temperature and on the reactant ratio. Specifically, both W and Re filaments show sharp jumps in power consumption at essentially the same temperature, signaling strong increases in filament activity and, hence, production of atomic hydrogen. This behavior can be related to the removal of nonreactive carbon from the filament surface via etching by atomic hydrogen. Upon the addition of small amounts of oxygen to C-H mixtures these transitions from deposition to etching of graphitic carbon from the filament surface are shifted to lower temperatures. The results of these experimental studies are consistent with the predictions of the QE thermodynamic model for both the C-H and C-H-O systems and the implications of these observations for filament-assisted diamond CVD are discussed.

Samples deposited from various gas mixtures under different growth conditions have been found to be in good agreement with the predictions of the QE model.

Acknowledgements

There are many people who have helped me, in one way or another, and to whom thanks are due. I am grateful to all of them, Joe Altmann and "his crew" from the Machine Shop with their special skills, Jack Downey who taught me how to use the Scanning Electron Microscope, fellow students, and the members of my doctoral committee who contributed through spirited discussions. Financial support was provided by the US Department of Energy under contract DE-FG02-87ER45317.

I am especially grateful to Professor Fred W. Smith for his vital support, encouragement, and guidance during the course of this research. His advice, not only as supervisor, but also as friend are greatly appreciated.

My colleagues, Zhiping Yin, Antony Galea, and Ruobao Wang, deserve special mention for making this place so supportive, inspiring and fun.

Special thanks go to my friends Martin Muschol and Wolfgang Polifke, who accompanied me on my journey to New York and through Graduate School. They offered support when it was needed, and put up with me when I was most unbearable. Their friendship remains invaluable. Last but not least, I thank my family for their love, support, and understanding.

Contents

Tables

Figures

"I love diamonds, and I like them to be taken seriously."

– Harry Winston (1965)

Chapter 1

Introduction

The unsurpassed beauty of diamonds, their very high brilliance and "fire", has made them supreme gem stones from time immemorial. Other minerals such as zircon or topaz also show high brilliance, but they are scratched easily and deteriorate in time. Only "a diamond is forever". Diamond is one of the few minerals that has served mankind in two very different ways: as a gem stone and in industrial applications. Due to its unique properties (section 1.4) it stands out in both fields.

In the period between the world wars diamond as a tool was appreciated mainly for its hardness. It was found to be a most efficient tool for grinding and shaping hard and abrasive materials. From the mid-thirties on the demand for industrial diamonds has risen steadily. Although in one respect diamonds are said to last forever, in industrial processes they are used up so rapidly that it was necessary to look for substitutes or to intensify efforts to make diamonds synthetically. In the following section we shall give a brief summary of the history of diamond growth under metastable conditions.

1.1 Historical Perspective of CVD Diamond Growth

In 1955 General Electric announced that diamonds had been made by dissolving carbon in molten nickel and then applying high pressures and temperatures to induce crystallization (Bundy *et al.* 1955). This success was based on the knowledge that

diamond is the thermodynamically favored form of carbon under high pressure, high temperature (HPHT) conditions (Berman & Simon 1955), as is illustrated in the diamond-graphite phase diagram in Fig. 1.1. Shown is the thermodynamic equilibrium line between diamond and graphite under certain temperature-pressure conditions. However, this figure does not show that diamond can exist indefinitely as a metastable phase on the earth's surface, i.e. in the graphite stability region.

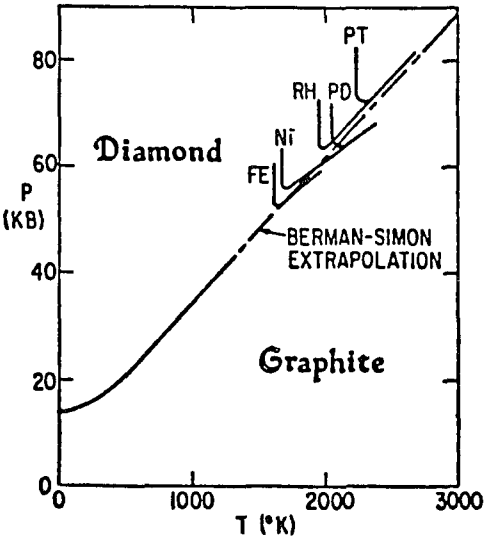

Figure 1.1 Thermodynamic stability regions of diamond and graphite, based on the calculations of Berman and Simon (1955) and the experimental work of Bundy *et al.* (1955).

A few tons of synthetic diamonds are made by metal-solvent methods each year in various countries around the world. Since many applications of diamond, however, require thin films or coatings which cannot be produced from either natural or HPHT synthetic diamonds, a considerable amount of work was invested into growing diamond from low-pressure gases. Since in this work we are concerned with chemical vapor deposition we will limit ourselves to processes that are based on that principle. For a more detailed discussion of the synthesis of diamond under metastable conditions we

suggest the excellent review paper by DeVries (1987) with over 200 citations or a review paper written by Angus and Hayman (1988).

The first person who claimed to have achieved diamond growth from low-pressure gases was von Bolton in 1911. He used acetylene in the presence of mercury vapor to deposit diamond on diamond seed crystals. Very little attention was given to his claim and nobody seemed interested in reproducing his result. Many other attempts to synthesize diamond failed but resulted in the discovery of a new dense form of carbon in 1921 (Tammann).

It was not until the early 1950s that systematic studies of diamond vapor deposition processes began. Successful reports came almost simultaneously from parallel research projects in the Soviet Union and the United States. In 1956 Spitsyn received a USSR Author's Certificate on a method to grow diamond (Spitsyn & Deryagin). The patent was not issued until 1980. Starting with CBr_4 and CCl_4 at temperatures of 800-1000°C and pressures of about 3×10^{-6} torr he had synthesized diamond on pre-existing diamond seeds. Eversole at the Union Carbide Company reported growth of diamond on diamond from decomposition of carbon-containing gases at 600-1600°C and pressures of 0.1-1.0 torr. Patents were filed in 1958/59 and issued in 1961/62 (Eversole 1962).

It is interesting to note that the accomplishments of Spitsyn and Eversole almost coincide with General Electric's discovery of the HTHP method (Bundy *et al.* 1955). But, in contrast to the latter, the low-pressure technique relies on the presence of diamond seeds. Unfortunately these early processes were plagued by low deposition rates (Å/hr) and codeposition of graphite which made it necessary to alternate diamond growth with graphite removal cycles. During the succeeding years, until approximately 1975, much time was invested into reproducing and possibly improving the early experiments. Angus and colleagues (1968) used hydrogen-diluted gases (still no activation) and also produced boron-doped material (Poferl *et al.* 1973). The application of a metal catalyst

increased growth rates dramatically (Angus & Gardner 1969). The Soviet group around Deryagin developed a theoretical description of the relative nucleation rates of diamond and graphite (Deryagin & Fedoseev 1977).

Experimental data by Lander and Morrison (1966) provided evidence that hydrogen was essential for diamond epitaxy. Low energy electron diffraction (LEED) studies revealed that a (111) diamond surface did not reconstruct when it was saturated with hydrogen. Chauhan *et al.* (1976) and Fedoseev *et al.* (1977) demonstrated that addition of hydrogen to the hydrocarbon feed gas suppresses the growth of graphite more than it suppresses the growth of diamond.

In 1971 Angus *et al.* came very close to a major breakthrough. They used a hot filament to activate the hydrogen, unfortunately only during the graphite etch cycle. Finally in 1976 Deryagin recognized that growth and etch cycles could be combined into one process if atomic hydrogen was present *during* the growth period. Unfortunately the method of growth was not described aside from the mentioning of "an electric discharge" (Deryagin *et al.* 1976). Only later did Varnin *et al.* (1984) report more details of the experimental setup.

It was Deryagin's ingenious recognition which really marked the beginning of a new era. Atomic hydrogen not only improves the diamond growth rates and eliminates codeposition of graphite, it also permits nucleation of diamond crystals on *nondiamond* substrates. The many roles of atomic hydrogen in the diamond deposition process will be discussed in chapter 2. Due to the most unfortunate circumstances (Deryagin's involvement in the polywater affair) these results received little attention or were treated with much skepticism outside the Soviet Union and Eastern Europe.

Japan's involvement in metastable diamond growth started in the mid 1970s. A group of researchers at the National Institute for Research in Inorganic Materials (NIRIM) was particularly successful. Among the key figures were Kamo, Sato, Matsumoto, and Setaka. They were the first ones to develop a variety of gas activation

techniques which allowed rapid growth of diamond. It is fair to say that the current world-wide interest in the new diamond technology can be traced back to the accomplishments of the NIRIM group. Examples of their discoveries are given below.

In 1982 it was reported that diamond had been synthesized using a hot filament to activate CH_4/H_2 gas mixtures (Matsumoto *et al.* 1982). Shortly thereafter diamond growth was achieved in a microwave-plasma reactor (Kamo *et al.* 1983) which was later extended to a magneto-microwave system (Kawarada *et al.* 1987). In 1985 a radio-frequency (rf) glow discharge apparatus was utilized for large area diamond deposition (Matsumoto 1985). Sawabe and Inuzuka (1985) tried a variation on the hot-filament method by applying a DC voltage between the filament and the substrate. They named this electron-assisted chemical vapor deposition (EACVD) since it resulted in electron bombardment of the growing film. In 1988 Hirose and Kondo introduced a novel technique which made it possible to deposit diamond in the ambient atmosphere: the oxyacetylene welding torch. In the next stage thermal plasma CVD was added to the already long list of diamond growth techniques. Kurihara *et al.* (1988) presented the DC plasma jet reactor which yields, due to the high degree of gas dissociation, extremely high growth rates. The latest breakthrough in metastable diamond synthesis came in 1990 from an American group. Patterson *et al.* (1990) achieved growth of crystalline diamond in a simple flow tube reactor from carbon-hydrogen-halogen gas mixtures with *hardly any* activation of the feed gas molecules.

In the next chapter we shall describe in more detail some of the techniques that have been mentioned above. Table 1.1 contains in chronological order the key experimental events in the development of metastable diamond growth by chemical vapor deposition.

Table 1.1 Chronology of the Development of Metastable Diamond Growth by Chemical Vapor Deposition.

Date	Author[a]	Description
1911	von Bolton	Claimed growth of diamond from C_2H_2 (on diamond)
1956	Spitsyn	Author's certificate on diamond growth from CBr_4 and CCl_4
1958-59	Eversole	Patents on low pressure diamond growth filed (issued in 1961/62)
1966	Lander	LEED study of diamond surface demonstrates importance of hydrogen for diamond epitaxy
1971	Angus	Thermal activation of hydrogen in graphite etch cycle
1976	Deryaguin	Growth of faceted crystals on nondiamond substrates in presence of atomic hydrogen
1981-85	Kamo, Setaka, Matsumoto, Sato	Growth of diamond on nondiamond substrates from hot-filament, microwave- and rf-plasma techniques
1988	Hirose	Diamond from oxyacetylene torch
1988	Kurihara	Diamond from DC plasma jet
1990	Patterson	Diamond from carbon-hydrogen-halogen gas mixtures with hardly any gas activation

a) Principal Author only

1.2 Chemical Vapor Deposition Processes

According to K. Spear (1982) chemical vapor deposition (CVD) is defined as a process 'in which a gaseous phase chemically reacts to produce one or more condensed phases (deposit) plus gaseous product species.' The application of chemical vapor deposition has become a cornerstone in today's modern technology. Its primary use is centered around the production of thin films for solid state electronic and optical devices, erosion and corrosion resistant coatings for tools or exposed surfaces etc. One of the advantages of CVD is its versatility. A large number of elements and compounds can be deposited under different process conditions with a wide range of parameters. The accurate stoichiometric composition of the deposited materials is relatively easy to control and there is no other technique which is as suited for the growth of layer structures.

Important materials being prepared by CVD include Si, Ge, Si_3N_4, SiO_2, GaAs, a-C (for electronic and optical devices) and titanium carbide, titanium nitride, chromium carbide, aluminum oxide (as protective coatings) and of course diamond whose potential applications will be discussed in section 1.4.

A typical setup for chemical vapor deposition comprises a dynamic flow system in which the following events will take place. After forcing the gaseous reactants into the system they have to reach the heated substrate surface which will most likely involve diffusion through a boundary layer adjacent to the substrate. The interaction with the surface consists of a number of individual steps such as adsorption, surface diffusion, chemical reaction, and desorption. After the product gases are formed they have to diffuse back through the boundary layer before they can exit the system together with the bulk unreacted gas.

It is apparent from the foregoing discussion that CVD processes are not simple processes. In order to gain insight into the various mechanisms involved one has to be

knowledgeable in many classical fields. Fluid dynamics, transport phenomena, reaction chemistry, and film growth aspects such as nucleation need to be considered. Furthermore the effects of process variables such as temperature, pressure, and input concentration must be understood. Many theoretical models have been developed to help with the understanding of CVD processes.

Thermodynamics has proven to be a helpful tool in relation to CVD since it can provide quantitative information about the feasibility of the process under consideration (Sommer *et al.* 1989, 1990a). In particular it can predict certain trends associated with a variation of the process parameters. In chapter 3 we will demonstrate how quasi-equilibrium thermodynamics can be applied to diamond CVD to predict evaporation rates and obtain a C-H phase diagram. A chemical reaction which is thermodynamically feasible might involve some intermediary steps that proceed at such a slow rate that the overall reaction becomes essentially unimportant. Thus, when deviations from equilibrium are observed kinetic descriptions have to be put forward. It should be noted that to a certain degree kinetic factors can even be incorporated into a thermodynamic model (as has been done in this work).

In situ analysis of chemical vapor deposition processes such as flow visualization, mass spectroscopy, absorption spectroscopy, and gas chromotography can help clarify the complex mechanisms involved.

1.3 Phases and Crystal Structures of Carbon

A carbon atom can in principle take on three different bonding configurations, sp^3, sp^2, and sp (Fig. 1.2). At a carbon sp^3 site each of the four valence electrons is assigned to a tetrahedrally directed sp^3 hybridized orbital which then forms a strong σ bond with a neighboring atom. An sp^2 bonded carbon contributes three of its four valence electrons to trigonally directed sp^2 hybridized orbitals which form σ bonds; the fourth

electron is found in a p_z ($p\pi$) orbital lying normal to the σ bonding plane. The $p\pi$ orbital forms weaker π bonds with adjacent $p\pi$ orbitals. In the sp configuration only two of the electrons are assigned to σ bonds while the other two are left in orthogonal p_y and p_z orbitals to form π bonds. A σ bond between two sites is called a single bond, and is represented by a single line (C-C) whereas a σ-π bond pair is called a double bond and is represented by two lines (C=C).

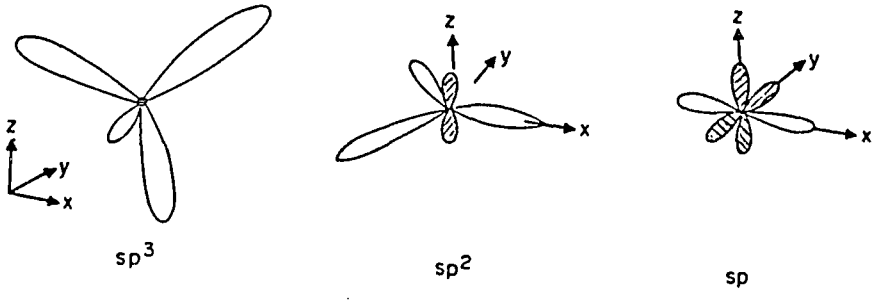

Figure 1.2 Schematic presentation of sp^3, sp^2, and sp^1 hybridized atoms.

Depending on the various proportions of sp^3, sp^2, and sp orbitals and their local arrangement we obtain different forms of carbon with remarkably different properties. Diamond and the less common lonsdaleite (also called hexagonal diamond) consist entirely of sp^3 bonded carbons. Graphite is formed completely from sp^2 sites while the disordered forms of carbon consist of mixtures of sp^3, sp^2, and sp bonds. The area of disordered carbon covers a wide range of materials, such as glassy carbon, amorphous carbon (a-C) and hydrogenated amorphous carbon (a-C:H) which, due to its high hydrogen content, is not a pure form of carbon. Aisenberg and Chabot (1971) first reported on deposited material that had properties very similar to those of diamond and they referred to it as "diamondlike" carbon (DLC). For example, their films were electrically insulating, harder than glass, radiation resistant and had an index of refraction > 2.0.

Many publications on disordered carbon are available. For a detailed review of the atomic and electronic structures of the various types of amorphous and hydrogenated

amorphous carbons we suggest a paper by Robertson (1986). The article by Angus *et al.* (1986) or Koidl's overview of deposition, properties and applications of dense amorphous carbon films was also found to be very useful (Koidl *et al.* 1989).

From now on our main emphasis will lie on the more common, naturally occurring forms of carbon, namely diamond, lonsdaleite and graphite. The space lattice of diamond is face-centered cubic (fcc) with a primitive basis of two identical atoms at relative positions (000) and $(\frac{1}{4}\frac{1}{4}\frac{1}{4})$ associated with each lattice point. An equivalent way of describing the structure uses two interpenetrating fcc lattices displaced from each other by one-quarter of a cube diagonal. Diamond consists entirely of sp^3 sites so that each atom has 4 nearest neighbors and there are 8 atoms in a unit cell. Lonsdaleite has 4 atoms in the unit cell and exhibits hexagonal symmetry. Schematic drawings of the unit cells of diamond and lonsdaleite are presented in Fig. 1.3(a,b). Since lonsdaleite has only tetrahedrally bonded carbon atoms it has the same nearest-neighbor coordination as diamond. Upon comparison of these two structures one wonders how such different looking objects can be so closely related to each other?

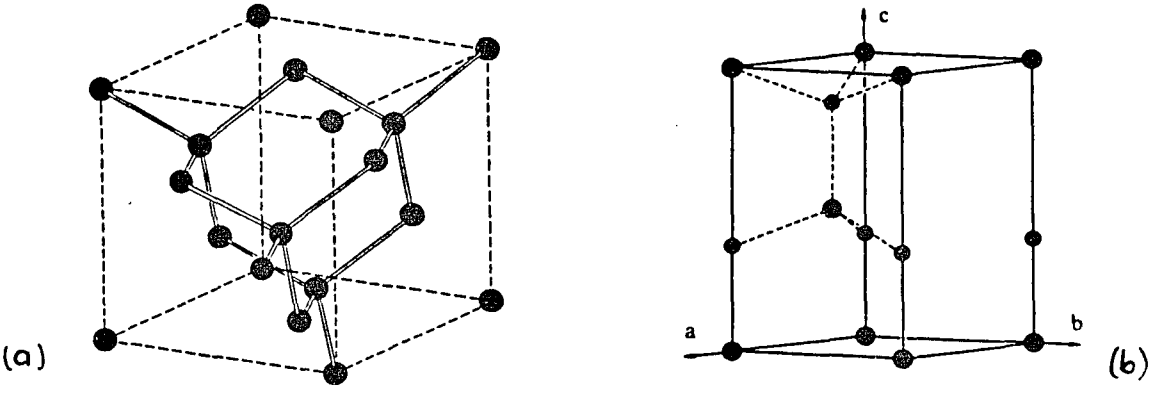

Figure 1.3 Schematic diagrams of the unit cells of (a) diamond and (b) londsdaleite.

To understand the similarities between the two let us take a look at the atomic arrangements in graphite, diamond and lonsdaleite which are presented schematically in

Fig. 1.4[(a)-(c)]. It is seen that graphite consists of a succession of layers with each layer containing hexagonally linked carbon atoms. The carbon atoms in one sheet are trigonally bonded (see above) and therefore the binding is strong. The binding between two adjacent sheets is of the Van der Waals type and hence weak. If the layers are stacked in a sequence ABAB, as depicted in Fig. 1.4(a) one gets a crystal with hexagonal symmetry. However, there are some graphites which display the rhombohedral stacking sequence ABCABC as a result of deformation by either glide or twinning. It is apparent that certain properties of graphite, such as thermal or electrical resistivity and strength can be expected to differ greatly along the basal plane and along the c axis (perpendicular to basal planes).

We note that the (111) planes of diamond are identical to the (001) planes in lonsdaleite. Each plane is composed of puckered six-membered rings of carbon atoms, a configuration which is usually referred to as the "chair". The difference between the cubic and hexagonal form of diamond lies in the second-nearest-neighbor coordination i.e. the stacking of the planes. While in diamond these planes are joined by other six-membered rings in chair form, in lonsdaleite the six-membered rings joining the planes look like "boats". The stacking sequence in diamond is ABCABC, in lonsdaleite it is ABAB. Another way of illustrating this difference in second-nearest-neighbor coordination is by looking down a C-C bond in the stacking direction. In diamond, the three carbon atoms at each end of the bond are staggered with respect to one another. In lonsdaleite, these same carbons eclipse each other. Since the eclipsed bonds lead to a slightly higher repulsive interaction between next-nearest neighbors this structure is less stable and therefore less common in nature.

We would also like to comment on the similarity between the basal planes in graphite and the (111) planes in diamond (or (001) in lonsdaleite), as depicted in Fig. 1.4. It is easy to imagine how the puckered rings of a cleaved (111) surface of diamond, for instance, can collapse into a planar structure similar to graphite. In chapter 2 we

will show that atomic hydrogen will saturate dangling bonds and thereby prevent the reconstruction of the growing diamond surface.

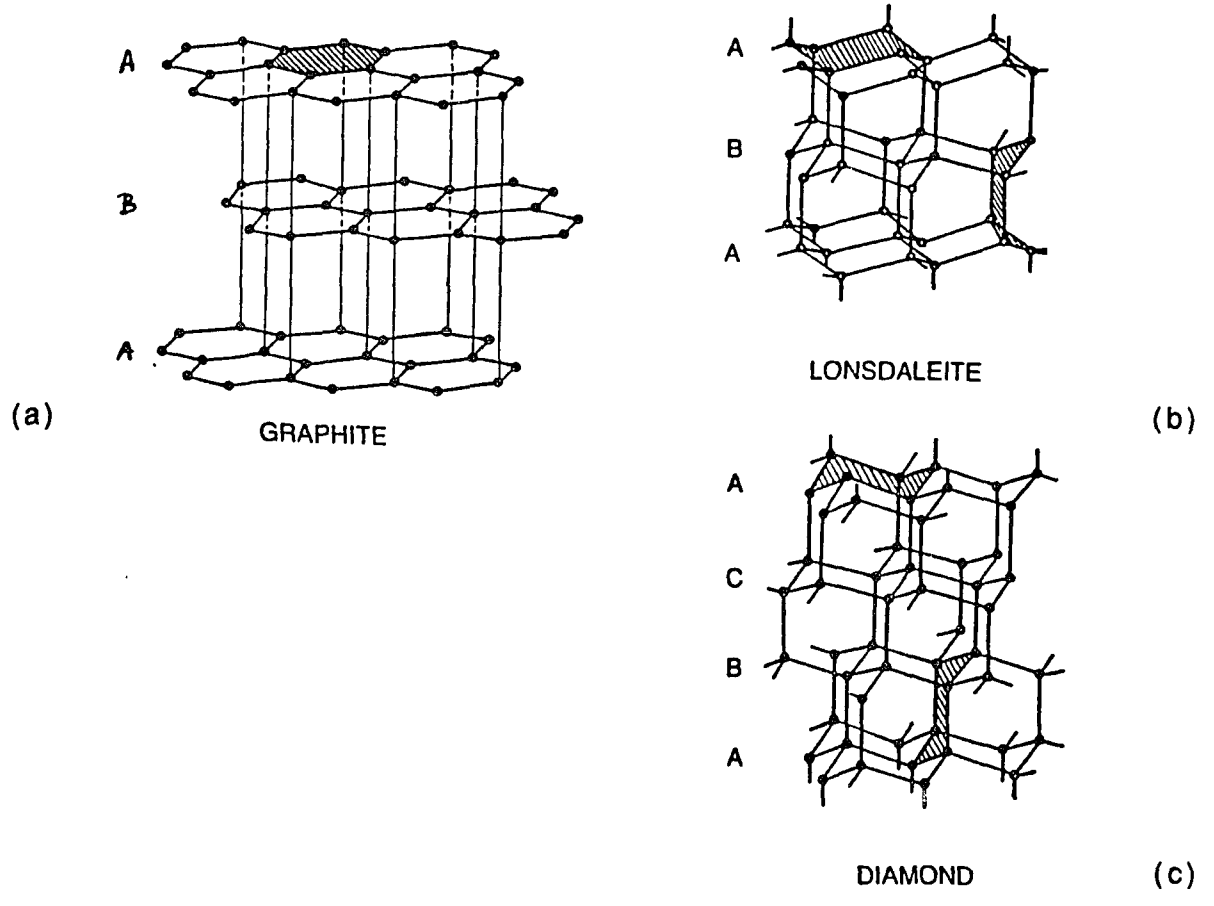

Figure 1.4 Schematic drawings of the atomic arrangements in (a) hexagonal graphite, (b) hexagonal londsdaleite, and (c) cubic diamond. Note the shaded hexagonal rings of carbons in these three structures: planar (a), boat-form (b), and chair-form (c).

Natural diamonds have been classified as type I and type II in relation to their different absorption spectra in the infrared, visible, and ultraviolet regions and their different x-ray diffraction patterns (Evans 1976). It has been found that type I diamonds are less perfect crystals than type II due to their relatively high concentration of defects or impurities (mainly nitrogen). Type I diamonds are further divided depending on whether they are paramagnetic (Ib) or not (Ia). Most diamonds are extremely good

insulators, but a small number of type II diamonds are semiconductors. The *non*-conducting type II diamonds are referred to as type IIa and the *semi*-conducting diamonds as type IIb. 98% of all natural diamonds are type Ia, while almost all synthetic diamonds belong to type Ib (Badzian *et al.* 1986). It should be noted that some properties of diamond (e.g. thermal conductivity) are sensitive to the amount of impurities in the specimen (see below).

In the next section we shall look at the properties of diamond and outline how they can lead to advanced applications in the tooling industry or in solid state electronics.

1.4 Properties and Applications of Diamond

The increase in diamond activity over the last decade reflects the strong commercial interest in this material. Due to its unique mechanical, thermal, chemical, electronic, and optical properties (see Table 1.2) diamond is a candidate for many industrial applications. It will be shown below that actually it is the *combination* of various properties which makes diamond so unique. Once again we refer to the review paper by Spear (1989) as a source for additional information on this topic. The book by Berman (1965) on the 'Physical Properties of Diamond' was also very useful.

One of the factors that makes diamond stand out, both as a gem and as a tool, is its extreme hardness which is derived from its strong, uniform atomic structure. Since the day that diamond first appeared on the industrial scene it has been used with cutting tools, such as in turning or milling, in drill crowns, as abrasive grit in lapping and polishing, etc. Compared to other hard materials diamond has the highest thermal conductivity at room temperature, a small coefficient of friction and a low thermal expansion, and these play important roles in the industrial use of the stone. When a tool works a material moving at high speed it is essential that heat be removed from the cutting edge in order to reduce problems of burning or thermal fracture. This

demonstrates that it is the combination of extreme hardness and high thermal conductivity which makes diamond so valuable a tool.

A key characteristic of diamond is its high electrical resistivity. This feature combined with the high thermal conductivity makes diamond an appealing material for electronic applications. No other substance is simultaneously as good a heat conductor and electrical insulator, especially at elevated temperatures. The use of diamond films as heat sinks for integrated circuits would allow higher packing densities and higher operating speeds. Ravi and Landstrass (1989) point out the benefits of CVD diamond films beneath thin Si films in Silicon on Insulator (SOI) structures. Since nobody has succeeded in growing single crystal diamond heteroepitaxially they discuss a new approach that is capable of incorporating polycrystalline films.

Table 1.2 Some Properties of Natural Type IIa Diamond

Mass density	3.51 g/cm^3
Hardness	Vickers: 7000-10,000 kg/mm^2; Mohs: 10
Thermal conductivity	20 W/cm K (at 20 °C)
Thermal expansion coefficient	1.34×10^{-6} (20-100 °C)
Coefficient of friction	0.05-0.15
Refractive index	2.42 (at 589 nm)
Optical bandgap	5.5 eV
Electrical resistivity	$> 10^{16}$ (Ω cm)
Dielectric constant	5.7 (at 20 °C)
Saturated electron velocity	2.7×10^7 cm/s

Data taken from DeVries (1987) and Schnetzer (1990).

Diamond is chemically inert to all acids, even at high temperatures. It can only be attacked by alkalis and strong oxidants. In addition it has a high radiation tolerance (due to its large band gap of 5.5eV). These properties suggest that electronic devices made from diamond material could be employed in severe environments, such as automobile engines or telecommunication systems in space.

Schnetzer (1990) discusses the use of diamond films in a high energy particle calorimeter for the Superconducting Supercollider (SSC). In the calorimeter layers of 6mm of uranium or tungsten (active medium) would alternate with layers of 200μm of diamond (dense medium). As a high energy particle crossed a diamond layer, it would produce ionization charges which would then be accelerated across the layer by a high voltage and collected in the active medium. The collected charge would be proportional to the ionizing energy, which, in turn would be proportional to the energy of the incident particle. This application would take advantage of the following properties of diamond: the high breakdown field , the high radiation resistance, and the high saturated electron velocity (i.e. the velocity at which electrons move through the semiconductor at very high fields). The latter would guarantee a high detection rate of one event every 10 nanoseconds since the ionization charge produced in the 200μm diamond layer could be collected in approximately 10^{-9} s.

Another important application of diamond is related to its optical properties. Due to its large bandgap diamond does not respond to electromagnetic radiation in the visible and infrared (IR) regions and is therefore a perfect substance for ultraviolet (UV) detectors. The combination of mechanical, chemical, and thermal properties and its transparency make diamond also ideal as window or lens material operating in the visible and IR regions. Spear (1989) reports that transmission losses in the IR spectrum can be up to four orders of magnitude lower in diamond than in competing materials.

It must be realized, however, that many of the properties listed above depend greatly on the concentration of impurities in the specimen. For example, natural type IIa diamond which contains very little nitrogen conducts heat five times better than copper at room temperature. On the other hand type Ia diamond can contain up to 0.2% nitrogen (Evans 1976) and its thermal conductivity is about one third of that of type IIa. General Electric has succeeded in synthesizing isotopically enriched carbon-12 diamonds with a room temperature thermal conductivity that is 50% higher than that of natural diamond (Anthony *et al.* 1990a). The amount of metal inclusions (from the solvent) has a pronounced influence on the properties of HPHT diamonds. The properties of CVD diamond films and hence their ability to perform as electronic devices largely depends on the presence of sp^2-bonded carbon in the films. In the next chapter we will show how the various process parameters (substrate temperature, carbon concentration, etc.) determine the quality of the synthesized films. Since an increase in the carbon concentration in the feed gas typically leads to higher sp^2/sp^3 ratios (see next chapter) we expect the thermal conductivity to drop with higher carbon content in the feed.

Although there have been major achievements in terms of utilizing the unique properties of diamond for technological applications in the form of polycrystalline films, many problems remain unsolved. For example, lowering the substrate temperature and controlling film adhesion to a variety of substrate materials is an important issue, since that would make it possible to furnish plastics with a scratch-proof surface. Other necessary improvements include the control of nucleation rates and defect densities, the production of n-type diamond, and most important of all, the growth of single crystal films on *nondiamond* substrates which is essential for many electronic devices. At this point diamond films used on tools as protection against wear and chemical attack seem by far the most widespread application.

Chapter 2

Summary of Experimental Observations

Ever since the discovery that crystalline diamond could be grown at low pressures where it is the metastable form of carbon, diamond synthesis has held a special attraction. Strong commercial interests in new materials and products together with reports of breakthroughs in the 1970s (e.g. deposition of diamond on *nondiamond* substrates, increased growth rates and less codeposition of graphite) has spurred an enormous activity around the world. The diversity of techniques to deposit diamonds from the vapor phase is truly astonishing and the imagination of researchers seems inexhaustible. Although the designs for the various techniques differ quite significantly from each other they do have one feature in common. They supply energy to a carbon-containing gas mixture (e.g. CH_4 in H_2) to decompose the source gas molecules. However, recently the growth of diamond films has been achieved from a carbon-hydrogen-halogen gas mixture with *hardly any* activation of the reactants (Patterson *et al.* 1990). In the first section of this chapter we shall discuss some of the techniques that have been successfully employed for diamond synthesis.

2.1 Methods of Gas Activation

The earliest and probably simplest method uses a hot filament for gas activation (Matsumoto *et al.* 1982). The reactant gas molecules flow past the hot filament

($T_f \sim 2200^oC$) where they will be thermally excited or dissociated (hardly any ionization occurs) and then impinge on a heated substrate ($T_s \sim 800^oC$). Extensive studies of the thermal dissociation process of hydrogen have already been carried out at the beginning of this century by Langmuir and Mackay (1914). One advantage of the thermal technique, in addition to its simplicity, is the relative ease with which it can be scaled up for large area deposition. It is always possible to add more filaments and extend the existing structure to any desired shape. One has to realize however that the filament itself can act as a high temperature substrate for the deposition of graphitic carbon and then loose its ability to dissociate the reactant gases. We have shown (Sommer & Smith 1990b, c) that this limitation can be easily overcome if the filament is operated at a high enough temperature so that its surface is free of carbon. The common materials from which filaments are formed all have high melting points. They include tungsten (W), rhenium (Re), and tantalum (Ta) whose melting points are 3410, 3180, and 3000 ^oC, respectively. Diamond growth rates are typically of the order of 1-2 microns/hour and depend on the filament to substrate distance as well as the filament temperature.

Since in this work we use a hot-filament reactor for the CVD of diamond we will present more quantitative results of our filament studies later. In chapter 4 the experimental setup will be described in detail and chapters 5 and 6 include an investigation of the filament activity in the growth environment.

Another method commonly employed is microwave-assisted deposition. Microwave power generated by a magnetron is transmitted to the vacuum chamber and applied to the gas mixture to induce a ball-shaped glow discharge. Growth rates depend greatly on the power input into the plasma and are generally much higher than for the hot-filament method. However the ball-like geometry of the plasma does not allow deposition of uniform diamond films over large areas. Since the substrate, which could be a silicon wafer with electronic devices, is immersed in the plasma it is likely to be damaged by

energetic particles or radiation from the plasma. One advantage of this method is that the discharge occurs without electrodes, and hence the synthesized diamond is not contaminated by electrode materials, unlike in DC plasma CVD (see below).

Due to its simplicity the oxyacetylene welding torch has become a very attractive technique for the deposition of diamond. Since growth occurs in the ambient atmosphere the process does not require any vacuum equipment and so diamonds can be grown quite cost-effectively.

The oxygen-acetylene flame can be divided into three regions: The inner core consisting of unburned gas, the mantle or feather region containing the burned gas, and the outer core where the burning continues due to diffusion of oxygen from the surrounding atmosphere. The hottest and most luminous part of the flame is the feather. When used for diamond CVD, growth occurs only in the feather region and the material deposited on the substrate is symmetrically distributed about the central axis of the flame. High quality diamonds are typically observed in the central part while the quality deteriorates as one moves radially outwards (Hanssen *et al.* 1988). The length of the feather depends not only on the O_2/C_2H_2 flow ratio but also on the geometry of the nozzle, e.g. its orifice diameter. High quality diamond is deposited when the flow ratio is near unity, although various workers have obtained somewhat different results with regard to the O_2/C_2H_2 flow ratio. Diamond growth rates can average 100 microns per hour. The synthesis of diamond from an oxygen-ethylene flame, although with lower growth rates, has been achieved (Carrington *et al.* 1989). In chapter 3 we will present some theoretical predictions for the rates of evaporation and deposition of carbon based on the QE thermodynamic model and also some experimental results obtained from careful studies of the oxyacetylene torch.

The highest diamond growth rates reported so far have been achieved in a DC plasma jet reactor. A thermal plasma containing many activated radicals is generated via a DC arc discharge and then sprayed (in the form of a plasma jet) onto a water-cooled

substrate. The source gases are almost entirely decomposed into hydrogen and carbon atoms at the arc leading to growth rates of hundreds of microns per hour (Kurihara *et al.* 1988). However, one disadvantage of this method is the high level of impurity inclusions, which suggests possible limitations on the diamond it produces. Electrode materials that can withstand the high temperatures (~4000 K) and the attack by atomic hydrogen are not readily available.

Other methods that will only be mentioned here include UV-, laser-, and electron beam-assisted gas activation, as well as radio-frequency plasma methods (both inductively and capacitively coupled).

For the first time in the history of low-pressure diamond synthesis diamond films have been grown with very limited gas activation. Recently Patterson *et al.* (1990) reported growth of diamond particles from carbon-hydrogen-halogen mixtures at atmospheric pressure. In their setup the reactant gases flow along a resistively heated monel tube into which a heated substrate (700-900°C) has been placed. Wall temperatures are between 750 and 950°C with temperature gradients along the axis of the tube. These temperature gradients appear to be important for chemical reactions and we speculate that the monel tube might have some catalytic effect on the growth process. The source gases consist of fluorine/hydrocarbon or hydrogen/halocarbon mixtures and the carbon-containing gas is typically held to less than 5% of the overall gas composition. Since the diatomic binding energy of fluorine (44 kcal/mole) is less than that of hydyrogen (104 kcal/mole) less energy is necessary to dissociate fluorine molecules. In other words, the hot walls might be sufficient to generate an appreciable amount of atomic fluorine. This could explain why diamond growth is possible even without additional gas activation. Although growth rates at this stage of development are still low, the halogen-based system offers many advantages over other currently employed diamond growing techniques, one being its simplicity.

After having introduced some of the most common or unusual techniques for CVD diamond synthesis let us now turn to other experimental observations reported in the literature concerning CVD diamonds. In the next section we shall discuss the effects of source gases on the diamond deposition process.

2.2 The Starting Materials and Growth Mechanisms

In all the processes described above the common denominator is the deposition of diamond from a carbon-containing gas. Here are some of the compositions that have been successfully used for diamond synthesis: Hydrogen mixed with CH_4 (Matsumoto *et al.* 1982, ...), C_2H_2, C_2H_4 (Mitomo *et al.* 1990), CO (Ito *et al.* 1988, ...), CH_3OH, C_2H_5OH, $(CH_3)_2CHOH$, CH_3COCH_3, $[(CH_3)_2CH]_2O$, $C_2H_5OC_2H_5$, CH_3COOCH_3, CH_3CHO, and $(CH_3)_3N$ (Hirose & Terasawa 1986), CH_3F, CH_2F_2, CHF_3, CF_4, $CHClF_2$, CCl_2F_2, CCl_4, $F_2C{=}CH_2$, $ClFC{=}CF_2$, $CHBr_3$, and CH_3I (Patterson *et al.* 1990), CH_4/H_2 mixtures with additions of O_2 (Kawato & Kondo 1987, ...), CO_2 (Meyer *et al.* 1989), H_2O (Saito *et al.* 1988), or mixtures such as C_2H_2/O_2 (Hirose & Kondo 1988, Hanssen *et al.* 1988, ...), F_2/CH_4 and F_2/C_2H_4 (Patterson *et al.* 1990). The source gases are typically very rich in hydrogen (or other solvent for carbon), e.g. a common composition is 1% CH_4 in H_2. Growth takes place from an environment containing molecules, molecular fragments and radicals. Although this has initiated a large number of scientists to propose different models for growth mechanisms, to this day very little is known about the nucleation and growth processes involved in the chemical vapor deposition of diamond.

Tsuda *et al.* (1987) applied quantum chemical calculations to find the lowest energy path of diamond growth on (111) diamond surfaces from a CH_4/H_2 plasma. Their proposed mechanism for epitaxial growth relies on a positively charged surface due to methyl ions and a supply of methyl radicals. Chu *et al.* (1990) also identified methyl

radicals and/or methane molecules as the dominant carbon source for diamond growth based on their experimental results from carbon-13 studies.

Frenklach and Spear (1988) suggest an alternative mechanism in which the main monomer growth species is acetylene. It basically consists of two alternating steps. First, the creation of an active site by removal of a surface-bonded hydrogen atom and second, the subsequent addition of a carbon-containing specie to this surface-activated carbon radical. Quantum mechanical computations performed by the same group (Huang *et al.* 1988) indicate that the acetylene addition mechanism of diamond growth is energetically more favorable than the mechanism proposed by Tsuda *et al.* (1987). In addition, in situ measurements of the activated gas mixture show that under harsh environments such as those found in plasmas, combustion, etc. most hydrocarbon species chemically transform to the most stable product (i.e. C_2H_2) under those conditions. When a tungsten filament is heated to above ~2000°C it can be shown that CH_4/H_2 or C_2H_2/H_2 mixtures with equal initial carbon fractions yield identical gas compositions (Wu *et al.* 1990, Sommer & Smith 1990b,c).

Harris (1990) injected either methane or acetylene into a flow of partially dissociated hydrogen gas at 800°C and found that diamond could be grown from both methyl radicals (or CH_4) and from acetylene, although more and higher quality diamond was formed when methane was added.

The fact that neither the method of activation nor the nature of the input hydrocarbon species influences the general structure of the deposited crystallites leads to the conclusion that either the same general growth species are produced by all activation methods or that there exist different channels for CVD diamond growth. We feel that the latter description is more likely, namely that there is no unique diamond precursor and that different mechanisms may prevail on the different surfaces. For example, insertion of CH_3 may be more probable on (100) surfaces while acetylenic species may be favored for addition on (111) surfaces.

Moreover, none of the mechanisms proposed so far includes third elements such as oxygen or fluorine whose influence on process chemistry has been widely demonstrated.

2.3 The Growth Parameters

There is a flood of scientific papers that are concerned with the growth parameters of low-pressure synthesis of crystalline diamond. The typical "recipe" to synthesize diamond calls for small concentrations of carbon-containing gases in hydrogen, such as 1% CH_4 in H_2, substrate temperatures in the range of 800 to 1000°C, pressures below 1 atm, and, as has been pointed out above, some means to decompose or activate the source gas molecules. Many papers have been published that claim successful diamond growth for different ranges of parameters, for example, deposition at lower temperatures, higher carbon atom fractions, lower/higher pressures. What are the optimum conditions to achieve diamond growth in its metastable region? In chapter 3 we will illustrate that there is not a unique answer to this question. It will be shown that there exists an interdependence between the various growth parameters. For instance, both the substrate temperature and the carbon atom fraction suited for diamond deposition depend on the total pressure, the substrate temperature in turn depends on the carbon fraction etc. Depending on the CVD process used there might also be other important factors, such as filament temperature or microwave power input into the system. In this section we shall describe some of the tendencies that have been observed when growth conditions deviate from the above prescribed values.

How do we know whether the synthesized diamond is of "good" or "bad" quality? According to Messier *et al.* (1987) crystalline diamond material should have the following properties: (i) a crystalline morphology visually discernible by microscopic methods, (ii) a single-phase crystalline structure identifiable by x-ray and/or

electron diffraction, and (iii) a Raman spectrum characteristic for crystalline diamond. Of all these charaterization techniques, Raman spectroscopy is the most sensitive tool for identifying the various forms of carbon. A peak at 1332±1 wavenumber (cm^{-1}) is characteristic of diamond (Solin & Ramdas 1970) while broad peaks in the 1500 to 1600 wavenumber range indicate disordered sp^2-type carbon in the deposit (Wagner *et al.* 1989). Since sp^2-bonded graphite has a Raman efficiency 50 times greater than that for sp^3-bonded diamond, small amounts of sp^2-bonded carbon incorporated in the diamond deposits can be easily detected.

Matsumoto *et al.* (1982) used a hot filament reactor to deposit diamond films on various substrates from CH_4/H_2 mixtures at a pressure of about 36 torr. Interesting variations in the quality of the deposited material were observed when the substrate temperature was raised form 600 to 1000°C at a given CH_4/H_2 ratio of 1%. The particles changed from very small (~0.5-1 μm dia) and poorly defined at 610°C to well-defined diamond crystals (1-2 μm dia) between 700 and 880°C and then to spherically-shaped, cauliflower-type particles (> 2 μm dia) at 970°C. Another series of measurements consisted of varying the concentration of CH_4 in H_2 at a fixed substrate temperature of 800°C. This time transitions from poorly defined (0.5% CH_4/H_2) to well-crystallized (0.67-1%), to cauliflower-type particles (2%) were observed with increasing CH_4 concentration. These results have been confirmed in many other experiments (Kobashi *et al.* 1988, Setaka 1989, ...). It is common knowledge by now that an increase in the carbon concentration leads to a higher nucleation density (see section 2.5) and the formation of polycrystalline films unless the substrate temperature is lowered. Polycrystalline films, however, tend to have Raman spectra with a broadened "diamond line" and a high level background due to sp^2 bonded carbon.

Hsu *et al.* (1989) announced the achievement of diamond film deposition on silicon at temperatures lower than typically used. They reported growth down to ~500°C with 2% CH_4 in H_2 at 40 torr (5.3 kPa). They further argued that by maintaining the

substrate at lower temperatures they were able to operate with higher CH_4/H_2 ratios and still obtain good quality diamond. On the other hand, films deposited at 1000°C and higher CH_4/H_2 ratios had cauliflower-type appearance and their Raman peak at 1332 cm^{-1} had almost vanished.

Buckley *et al.* (1989) used Raman spectroscopy to examine diamond films prepared by filament-assisted CVD from a CH_4/H_2 gas mixture. Their study entailed varying the total pressure from 5 to 100 torr but holding all other deposition parameters constant (2% CH_4/H_2 and $T_{substrate}$=950°C). The Raman spectra of films grown at less than 30 torr displayed a broad feature near 1550 cm^{-1}, in addition to the diamond line at 1332 cm^{-1}, indicating the presence of disordered graphite in the film. In particular, the film prepared at 5 torr exhibited a ball-like morphology and a Raman spectrum typical of amorphous carbon. For higher pressures (60 and 100 torr) the diamond line was well-developed but the peak at 1580 cm^{-1} was still present suggesting that even at this high a pressure a graphitic component was still included in the film.

Matsumoto *et al.* (1987) investigated the growth of diamond films at atmospheric pressure using rf induction heating to generate a thermal plasma. They were able to demonstrate that growth at this pressure required up to 10% CH_4 in H_2.

To conclude this section let us now summarize the observed tendencies associated with a variation of the growth parameters. We have learned 1) that an increase in the carbon concentration at constant temperature and pressure leads to inclusions of graphitic carbon in the deposit, 2) that raising the substrate temperature too much while keeping the carbon fraction the same results in a deterioration of the synthesized diamond, 3) that lowering the substrate temperature requires an increase in the carbon fraction, and 4) that the relative contribution of sp^2 bonded types of carbon increases with decreasing pressure for constant temperature and CH_4/H_2 ratio .

A final remark concerning points 2) and 3) above is appropriate. Clearly, there will exist both an upper and a lower temperature limit for the vapor growth of diamond.

At low temperatures kinetic barriers might limit the growth of diamond, for example due to slow reaction rates. On the other hand, it has been observed that diamond cannot be synthesized for substrate temperatures higher than 1200°C (Matsumoto 1985). This may be due to the spontaneous graphitization of diamond at high temperatures or the desorption of hydrogen from the growing diamond surface. It will be shown in section 2.6 that one of the many roles of atomic hydrogen is to maintain the bonding of the surface carbon atoms in the sp^3 state. Electron-stimulated desorption studies have demonstrated that almost all the hydrogen desorbs from the (111) diamond surface upon heating to ~1275 K (Kubiak *et al.* 1990).

2.4 Substrates for Deposition and Their Surface Treatment

The first successes in the synthesis of diamond from the gas phase required the presence of diamond seed crystals. Since then low pressure diamond has been grown on a variety of substrate materials including Si, SiO_2, β-SiC, α-SiC, Si_3N_4, Al_2O_3, Cu, Au, W, WC, Mo, Mo_2C, BN, and Ni. Essentially any material that can withstand the high substrate temperatures needed for deposition may qualify. (Diamond cannot be used on ferrous metals due to the solution of iron in diamond). By far the most common substrates are single crystal silicon wafers. While diamond particles nucleate almost immediately on a diamond substrate they do not readily nucleate on commercially available mirror-polished silicon. In fact, induction periods of up to several hours have been observed for hot filament- and microwave-assisted deposition processes. However large diamond particle populations are typical in areas of crystal defects such as cracks or microscratches.

Kobashi *et al.* (1988) reported that the diamond nucleation density on carbide-forming substrates, such as Si, W, and Mo was 1-2 orders of magnitude higher than on

non-carbide-forming substrates. Belton *et al.* (1989) utilized x-ray photoelectron spectroscopy (XPS) to show that prior to growth their silicon substrate was covered by an oxide layer which was removed after a short period and replaced by a layer of SiC whose thickness increased with time. Finally, diamonds were seen to nucleate and grow on the SiC layer. A layer of β-SiC was also found by Williams and Glass (1989). Similar results were obtained for molybdenum substrates where a layer of Mo_2C formed between the substrate and the diamond film (Meilunas *et al.* 1989). These observations seem to imply that diamond nucleation on the surface competes with the removal of carbon from the surface by diffusion into the substrate. Only when the surface layer is saturated with carbon (or a layer of some low carbon diffusion coefficient material is formed, e.g. carbide) will diamond begin to grow.

When it was realized that the diamond induction period could be shortened considerably if active sites for nucleation were provided, scratching the substrate with diamond powder and/or coating it with some form of carbon prior to deposition became the rule. The exact mechanism of enhancement is not well understood. One possibility is that small diamond crystals that remain on the substrate surface after scratching serve as seeds for diamond growth. Another possibility is the saturation of the substrate surface with carbon.

The degree of perfection of the substrate surface is expected to influence the occurrence of defects, i.e. when the surface is mechanically scratched stacking faults are most likely to originate at the interface. Therefore, a compromise between the high nucleation rate and the structural perfection of diamond films is necessary. Many experiments have been conducted to investigate how various substrate treatments can influence the diamond nucleation density and crystallinity of the resulting film.

Meyer *et al.* (1988) used rf-plasma assisted CVD to attempt diamond growth on glass, quartz, Si, Ni, and h-BN. Silicon surfaces were either polished or roughened by sandpaper, sandblasting, or "Si-Si abrasion". No surface modification was undertaken

for any of the other materials. Very thin films of diamond-like amorphous carbon were observed on glass and quartz, and spherically-shaped particles were sparsely distributed on BN, Ni and sandblasted Si. While sandpaper produced the largest particle population density, "Si-Si abrasion" gave the best results in terms of quality. Polished Si showed deposits only on surface defects, a result which is common knowledge by now.

Pehrsson and Morrish (1990) studied the effects of hydrocarbon oil on diamond nucleation on both carbide- (Si, Mo) and non-carbide-forming (Ag, Cu) substrates in a hot filament reactor. All of the substrates that were oil-treated *plus* diamond scratched demonstrated enhanced nucleation densities over the substrates that were *only* diamond scratched, at least during the initial stages of growth. No improvement in nucleation density for oil-treated *un*scratched substrates indicates that oil does not contribute nucleation sites.

Without a doubt, the above mentioned experiments have shed some light on the diamond nucleation process. We have learned that carbon saturation of the substrate surface is necessary to enhance the concentration of surface carbon and thereby increase the carbon flux to the growing crystals. But the mystery of how these growing crystals ended up on the substrate in the first place remains unsolved.

2.5 Deposit Morphologies

The structure and properties of diamond grown by activated CVD vary greatly depending on the growth parameters. If conditions deviate from the optimum, structural defects involving sp^2 carbon become more prominent. Gas composition and substrate temperature seem to be the most critical parameters in determining whether the synthesized diamond will consist of individual crystals or polycrystalline films. Faceted crystallites are dominated by (111) or (100) surfaces; (110) faces are rare. Secondary nucleation is typical on (111) faces while for (100)-dominated films secondary

nucleation occurs primarily between the grains. Micrographs of vapor-grown diamond often reveal a large number of defects such as stacking faults and twins. Decahedral crystals containing a fivefold twin or even icosahedrons with 20 twin planes are not unusual. Examples of these defective crystals will be shown in chapter 7. Since these crystals have x-ray diffraction patterns that are distinctly different from that of diamond, it is proposed that they be considered a new form of carbon. Recently, Spear (1990) has described a series of diamond polytype structures in terms of a new stacking notation.

Kobashi *et al.* (1988) reported interesting changes in deposit morphology with varying CH_4/H_2 concentration. For less than 0.4% CH_4 in H_2 the deposit consisted mainly of (111) faces, between 0.4 and 1.2% (100) faces were dominant, and for CH_4/H_2 greater than 1.5% a microcrystalline texture was observed. Their diamonds were synthesized in a microwave reactor at a total pressure of 30 torr (≈4000 Pa) and a substrate temperature of 800°C. This implies that for lower CH_4 concentrations the (100) planes are the faster growing planes, while for higher concentrations the (111) planes grow fastest. Polycrystalline films result from a high nucleation rate and small crystal sizes at very high carbon concentrations. The same dependence of morphology on CH_4 concentration has been confirmed by Williams and Glass (1989) and by Badzian *et al.* (1988) who additionally noted a dependence on temperature. Below 900°C, mainly (100) faces were observed while for temperatures above 1000°C, (111) faces were predominant.

Based on Raman spectra and cathodoluminescence studies Sato (1990) illustrated that single crystal diamond prepared at lower methane concentrations was of high crystal quality. The spectra for polycrystalline films showed appreciable amounts of non-diamond structures and the diamond line at 1332 cm^{-1} was broadened considerably. Polycrystalline films were subject to higher defect density and strain when compared with single crystals.

As has been pointed out above, the synthesized diamond crystals contain (111) faces that are highly defective and/or (100) faces that are not very susceptible to "parasitic" nucleation. Badzian *et al.* (1990) succeeded in growing a single crystal film 160 μm thick by continuing homoepitaxial growth on the (100) face for six days. Is there a simple explanation for these observations? Spear (1989) provides the following arguments concerning diamond growth at the gas-solid interface. When a (111) plane is completed, continuation of growth on that surface *requires* nucleation of a new (111) plane. Stacking faults and twin planes can therefore be easily introduced during nucleation of the new (111) plane. On the other hand nucleation of new planes is *not required* for (100) surfaces since addition of carbon species to these planes results in new active growth sites. Defects *cannot* be easily introduced during growth.

Using these arguments one can interpret most of the experimental results reported in the literature.

2.6 The Role of Atomic Hydrogen

The first section of this chapter contains an introduction to the large number of methods that have been used to generate atomic hydrogen. Let us now examine the many roles that atomic hydrogen serves in the chemical vapor deposition of diamond at low pressures. For a nice overview of the various functions of atomic hydrogen and potential substitutes we recommend a paper by R. Anthony (1990b).

All bonds in diamond are sp^3 hybridized orbitals while graphite consists of a mixture of hybrid sp^2 and unhybridized p orbitals. Fig. 2.1 shows a schematic diagram of the (111) surface of a diamond crystal that has just been cleaved. The cleaved top surface consists of dangling single bonds which are energetically unstable. It is easy to imagine that in order to reduce its energy this surface will reconstruct to a graphite-like structure containing a mixture of single and double bonds. Electron-stimulated

desorption studies show (Kubiak *et al.* 1990) that after exposure to atomic hydrogen a monolayer of reacted atomic hydrogen consisting of single C-H bonds will stabilize this diamond surface and thus prevent its reconstruction. Since the C-H bond is stronger than a C-C bond no carbon atom can easily displace the bound hydrogen atom from the surface. How can diamond growth proceed from here? Another hydrogen atom impinging from the surrounding gas phase can react with a surface hydrogen to form a hydrogen molecule. Because the H-H bond is stronger than the C-H bond this reaction will result in a vacant site. Since in most CVD diamond growth processes the ratio of hydrogen to carbon is of the order 99 to 1, it is more likely that another hydrogen atom will fill the vacant site. Occasionally, however, a carbon atom (or rather a CH_x or C_2H_x radical) will collide with the vacant site and form a C-C bond to propagate growth.

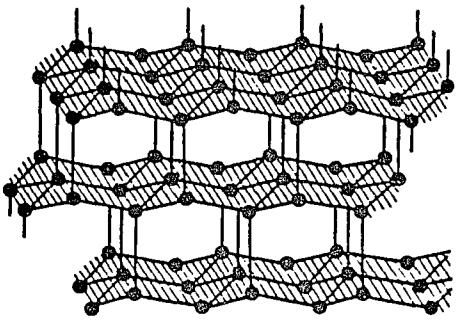

Figure 2.1 Cleaved diamond (111) surface showing dangling bonds.

Atomic hydrogen not only stabilizes the growing diamond surface and creates vacant sites, it also serves as a "solvent" for carbon. This behavior will be clearly demonstrated in the next chapter where we present predicted rates of evaporation of hydrocarbons. Experiments show that atomic hydrogen etches graphite and amorphous carbon much more rapidly than diamond. Setaka (1987) has reported etching rates of diamond, graphite and, glassy carbon in a hydrogen plasma under typical diamond growth conditions to be 0.006, 0.11, and 0.13 mg/(cm^2 h), respectively. Whether or not this

differential etching by atomic hydrogen is essential for CVD diamond growth has not been proven. It was suggested that the etching function of atomic hydrogen is not needed for CVD diamond growth. Instead, a formalism was proposed that relates molecular hydrogen at high temperatures to the suppression of the formation of graphite precursors (Frenklach 1989) in the gas phase. These graphite precursors are polycyclic aromatic hydrocarbons composed of benzene rings.

Atomic hydrogen has also been related to the reduction of the critical size of the diamond nucleus. In the presence of atomic hydrogen the surfaces of small diamond nuclei react with hydrogen and thereby greatly reduce their surface energy (Pate 1986). A stable nucleus consisting of only a few atoms is formed. One such nucleus is the adamantane molecule ($C_{10}H_{16}$) which has been proposed as an embryo for diamond growth (Matsumoto & Matsui 1983).

Yet another role that atomic hydrogen plays during the growth of low-pressure diamond is the generation of condensable carbon radicals. After the removal of a surface-bonded hydrogen atom a reactive site is created, as has been explained above. Only hydrocarbon radicals (or ions) can attach themselves to the surface carbon atom and form a C-C bond. Consequently, atomic hydrogen has to react with hydrocarbon molecules to generate the necessary radicals, e.g. $C_2H_2 + H \rightarrow C_2H + H_2$.

Chapter 3

Thermodynamic Approach to Diamond CVD

The chemical reactions between a vapor and a solid can yield a large number of products depending on the experimental parameters (e.g. temperature and pressure). Especially at elevated temperatures (such as are encountered in the hot filament assisted CVD of diamond where filaments are typically operated at ~2200°C) species which are not stable at ordinary temperatures may become quite prominent (e.g. H, C_2H, CH_3 ...). Increased mobility of the reactants, caused by increased temperature can lead to faster reaction rates which at low temperatures might be so slow that equilibrium can never be reached within reasonable time. K. Spear (1976) emphasizes in his treatise on high-temperature reactivity that 'equilibrium properties gain in importance over kinetic properties' when the temperature is increased. The chemical nature of a reaction and the extent to which it can occur are governed by thermodynamic principles which will be briefly discussed in the section below.

3.1 Thermodynamic Principles

A. Burcat (1984) differentiates between two kinds of properties: thermodynamic and thermochemical. The thermodynamic properties of any substance include the enthalpy H, the entropy S, and the the Gibbs free energy G, which is given by

$$G_T = H_T - T\,S_T \qquad (3.1)$$

Here T is the absolute temperature, and the subscript denotes that the various quantities are evaluated at temperature T. While the absolute values of these quantities are not very meaningful, it is the changes of G, H, and S in a chemical reaction that are at the center of chemical equilibrium calculations. According to Burcat (1984) ΔG, ΔH, and ΔS belong to the thermochemical properties, since they focus on the chemical reactions undergone by a substance. Hence, ΔH_T is the enthalpy change or the heat absorbed or released during the reaction, and ΔS_T is the change of entropy. Note that ΔH_{298} is also called the "heat of formation". It follows from the definition of G (Eq. (3.1)) that for any given isothermal, isobaric process

$$\Delta G_T = \Delta H_T - T\,\Delta S_T \qquad (3.2)$$

where

$$\Delta G_T = \Sigma\, G_T(\text{products}) - \Sigma\, G_T(\text{reactants}) \qquad (3.3)$$

When a chemical reaction refers to the production of a given compound from its constituent elements the increment in Gibbs free energy associated with this specific reaction is called the "Gibbs free energy of formation", and is typically denoted by ΔG_{Tf}. Although we will not distinguish here between ΔG_T and ΔG_{Tf}, we would like to remark that the values listed in the JANAF Thermochemical Tables (1971), for instance, correspond to the Gibbs free energies of formation of the various substances.

It should be noted that G, H, and S are not only functions of temperature but also depend on pressure, i.e. $G_T = G(T, P)$ etc. However, it can be shown that pressure effects on enthalpy and entropy of condensed phases are completely negligible (except at extremely high pressures); pressure effects on the enthalpy of a gas are negligible to the extent that the gas can be assumed ideal. The dependences of ΔH and ΔS on temperature are expressed as follows:

$$\Delta H_T = \Delta H_{298} + \Delta\ (H_T - H_{298}) \qquad (3.4)$$

$$\Delta S_T = \Delta S_{298} + \Delta\ (S_T - S_{298}) \qquad (3.5)$$

and

$$H_T - H_{298} = \int_{298}^{T_i} C_p(\alpha)\, dT \ + \ \Delta H_{T_i}(\alpha \rightarrow \beta) \ + \ ... \ + \int_{T_\kappa}^{T} C_p(\gamma)\ dT \qquad (3.6)$$

$$S_T = \int_{0}^{T_i} \frac{C_p(\alpha)}{T}\, dT \ + \ \frac{\Delta H_{T_i}(\alpha \rightarrow \beta)}{T} \ + \ ... \ + \int_{T_\kappa}^{T} \frac{C_p(\gamma)}{T}\, dT \qquad (3.7)$$

where $\alpha,...,\gamma$ represent the various phases of a substance that undergo phase transitions at $T_i,...,T_\kappa$ with enthalpy changes at the transformations of ΔH_{T_i}... . In cases where the ΔH_T and ΔS_T values for a process do not change greatly over limited temperature ranges of a few hundred degrees the temperature dependence of the expression (3.2) reduces to

$$\Delta G_T = \Delta H_{298} - T\ \Delta S_{298} \qquad (3.8)$$

The equations above (3.4-3.7) illustrate how ΔH_T and ΔS_T can be determined experimentally from calorimetric and specific heat measurements.

The sign of ΔG (from now on the subscript T will be omitted) determines in which direction a chemical reaction will proceed depending on the experimental conditions. A negative ΔG indicates that the forward direction from left to right is favorable, a positive value indicates that the reverse direction is favorable, and a zero value is a criterion that equilibrium has been obtained. At this point the concentrations of each specie remain constant.

The activity *a* of a substance is the ratio of its fugacity in a given state to its fugacity in a fixed "standard state". Fugacity corresponds to a "fictitious pressure"; it

plays the same role for real gases and solids as does the pressure for ideal gases. For ordinary pressures (few atmospheres or less) pressures or fugacities are essentially equal and will be treated as such from now on. The concept of a "standard state" provides a reference point from which to measure ΔG. For a gas the standard state is the ideal gas at 1 atm pressure and the temperature of interest, while for a condensed phase it is the pure substance under 1 atm external pressure and the temperature of interest. Hence the activity *a* of a gas is its pressure divided by its standard state pressure of 1 atm. The relationship of the Gibbs free energy ΔG to the thermodynamic activities of the reactants and products for a process is given by the equation

$$\Delta G = \Delta G^{o} + RT \ln Q \qquad (3.9)$$

where ΔG^{o} is the Gibbs free energy change needed to transform the reactant species from their standard state activities (unity) to their equilibrium state activities, R is the ideal gas constant, T is the temperature in K, and Q is the activity quotient

$$Q = \frac{\prod_{i=1}^{n} a(\text{product i})}{\prod_{i=1}^{n} a(\text{reactant i})} \qquad (3.10)$$

The equilibrium state for an isothermal, isobaric process was defined above by the condition that ΔG is equal to zero. In this case Q takes on the special equilibrium state value K and Eq. (3.8) yields the well-known relationship

$$\Delta G^{o} = - RT \ln K \qquad (3.11)$$

K is also called the equilibrium constant and is given by

$$K = \frac{\prod_{i=1}^{n} P_{eq}(\text{product i})}{\prod_{i=1}^{n} P_{eq}(\text{reactant i})} \qquad (3.12)$$

where the activity a_i of specie i has been replaced with its equilibrium partial pressure P_{eq} (in atm). With the use of Eq. (3.11) ΔG^o values can be easily obtained by measuring the equilibrium partial pressures of the volatile species in a chemical reaction via Knudsen effusion methods (see section 3.2) and values of ΔG^o and K have been tabulated as functions of temperature in the JANAF Thermochemical Tables (1971). For the reference state of an element it is customary to choose that form of the element which is the most stable or the most common at the temperature under consideration, i.e. the ΔG^o value (i.e. Gibbs free energy of formation) for that form of the element is identically zero.

3.2 Evaporation from Solids

Let us consider the process of converting a solid into vapor which can be achieved in two distinct ways. First by evaporation or more exactly sublimation, and second by a chemical reaction between the solid and another species to form gaseous products. (For a more detailed discussion of this subject we recommend an article entitled 'Evaporation from Solids' by R. Rosenblatt (1976)). To outline some of the basic principles of vaporization we assume for simplicity that the vapor consists entirely of atoms supplied by the solid. The reactions of solids with other gases, although more complex, are related and quite similar to direct evaporation, i.e. sublimation. We have to distinguish between the evaporation (a) at equilibrium, (b) into vacuum, and (c) at partial saturation (e.g. in a Knudsen cell).

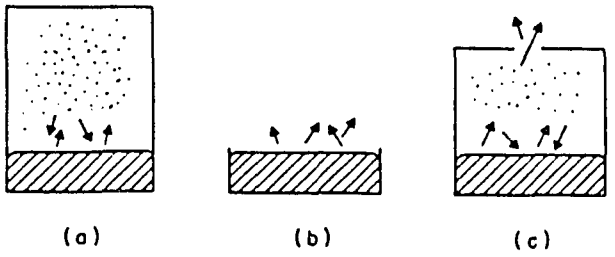

Figure 3.1 Evaporation of a solid (a) at equilibrium, (b) into vacuum, and (c) at partial saturation in a Knudsen cell.

In Fig. 3.1(a) the condensed phase and its vapor are in a closed container at constant temperature. When the sample and its vapor are at equilibrium the number of molecules evaporating in unit time will be equal to the number condensing in unit time and the net rate of vaporization will be zero. Kinetic gas theory provides an expression for the rate at which a gas is incident on a surface

$$I = \frac{P}{\sqrt{2\pi mkT}} \tag{3.13}$$

If the gas is a vapor in equilibrium with its solid, the equilibrium incident flux is

$$I_{eq} = \frac{P_{eq}}{\sqrt{2\pi mkT}} \tag{3.14}$$

Here P and P_{eq} are the vapor pressure and equilibrium vapor pressure respectively, m is the molecular mass, k is the Boltzmann constant, and T is the absolute temperature of the solid. Under equilibrium conditions we find for the rate at which the solid evaporates

$$R_{eq} = I_{eq} = \frac{P_{eq}}{\sqrt{2\pi mkT}} \tag{3.15}$$

This assumes that every vapor molecule which hits the surface sticks and is incorporated into the condensed phase. If the vapor is in equilibrium with the solid the kinetic theory of gases predicts that both incident and reemitted molecules are characterized by a random spatial distribution and a Maxwellian velocity distribution.

If the solid is evaporated at constant temperature in vacuum, as depicted in Fig. 3.1(b), such that no vaporizing molecules return to the surface, one can show that the rate of evaporation is given by

$$R_v = I_{eq} = \frac{P_{eq}}{\sqrt{2\pi m k T}} \tag{3.16}$$

Eq. (3.16) states that the spatial, velocity, and energy distribution of molecules evaporating from a surface into vacuum is identical to those striking that surface under equilibrium conditions. Evaporation into vacuum is also referred to as "free" evaporation. Evaporation rates at partial vapor saturation (between vacuum and equilibrium) can be determined with an arrangement shown in Fig. 3.1(c), where the degree of saturation is controlled by varying the orifice diameter.

In Eqs. (3.13-3.16) we have assumed i) that every molecule which strikes the surface condenses and ii) that no surface processes retard vaporization. If these requirements are not met (e.g. some molecules that are impinging on the surface may simply be reflected back into the gas phase) we can still use the foregoing formalism by introducing nonthermodynamic "equilibration" (or sticking) coefficients η and "accomodation" (or desorption) coefficients η'. The expressions for the incident flux and the rate of evaporation into vacuum then become

$$I = \eta \frac{P_{eq}}{\sqrt{2\pi m k T}} \tag{3.17}$$

$$R_v = \eta' \frac{P_{eq}}{\sqrt{2\pi m k T}} \tag{3.18}$$

Equilibration and accomodation coefficients are generally different from each other and can depend both on temperature and pressure. The temperature dependence of η is expected to be more complex than that of η' since the rate of condensation depends upon both the temperature of the solid and the energy states of the impinging molecules, while for evaporation the energy states of vaporizing molecules are determined entirely by the

temperature of the solid. The structure of the surface (e.g. its roughness) is expected to play an important role.

Eq. (3.18) which relates the free vaporization flux to the equilibrium pressure is a convenient way of describing the evaporation process. Since it involves only macroscopic quantities no detailed information about surface events (chemical reaction, migration, etc.) is necessary. In his article Rosenblatt (1976) also discusses other approaches based on microscopic models. For example, in absolute rate theory one considers the formation and migration of activated surface complexes to derive an expression for R_V. Although the latter model seems to give a more accurate description of vaporization processes it suffers from a lack of experimental data since activation energies are often not well-known for a large number of processes. We will take the first approach and use evaporation rates defined in terms of equilibrium pressures in the quasiequilibrium model which will be introduced below.

Most of the equations derived in the discussion above are applicable only to pressures where the mean free path in the gas phase is of the order of the sample dimensions or longer, i.e. the molecular flow region. If the vapor density is too high, the molecular density will not be uniform throughout the container and mass transport processes have be taken into account. For example a boundary layer near the surface through which vaporizing or condensing molecules must diffuse may build up at higher pressures. Also gas phase reactions can no longer be neglected.

In the foregoing discussion we have studied a special case of evaporation from a solid, its sublimation. If we introduce other species that can react with the solid to form various products and assume that processes similar to those described above occur during and after formation of product molecules, the previous arguments can be extended to include additional species. Eqs. (3.13) through (3.18) now refer to specie i that is incident on or desorbs from the surface and the vapor pressure P now corresponds to the

partial pressure P_i of specie i. Molecules that strike the surface no longer condense but "equilibrate" both thermally and chemically to the surface and other adsorbed species.

3.3 The Quasiequilibrium Thermodynamic Model for the C-H System

There seems to be a vast amount of reported observations, most of which have been discussed in chapter 2, on the effect of varying deposition parameters, such as substrate temperature, pressure, C-H ratios, etc. on the growth of solid carbon, i.e. diamond and graphite. Our goal is to bring some order into this "muddle" of experimental data and try to explain some of the observed trends with the aid of a simple thermodynamic model. The basic principles introduced in sections 3.1 and 3.2 will now be applied to one specific process, namely the reactions of hydrogen (both molecular and atomic) with a solid carbon surface in relation to CVD diamond growth. Two methods are commonly employed to determine the equilibrium composition of the gas phase: the first is minimizing the Gibbs energy (Eriksson 1971), the second involves solving a set of nonlinear equations which contain the equilibrium constants of all the species considered. The quasiequilibrium (QE) model, as developed by Batty and Stickney (1969), is based on the latter method.

At the heart of the QE model is the assumption that thermochemical equilibrium exists between the carbon sample and the vapor species, H_x, C_xH_y, *desorbed* from it. Of course the question arises whether it is meaningful or useful to apply a thermodynamic analysis to the non-equilibrium steady state deposition of diamond and graphite. An answer can only be supplied on the basis of comparisons between model predictions and experimental results. Since the growth rates of CVD diamond films can be very low, implying that the competition between deposition and etching of solid carbon may be due to local equilibrium conditions, it seems justified to use equilibrium thermodynamics at

least as a starting point. It should be noted that the QE model has been successfully applied to some gas-surface reactions earlier (Smith & Ghidini 1982). The first goal of this approach is the determination of the temperature-dependent evaporation rates for the system under consideration. Some of the possible reactions between solid carbon and hydrogen are

$$C(s) + 2\ H_2\uparrow \leftrightarrow CH_4\uparrow \quad \text{or} \quad 2\ C(s) + H_2\uparrow \leftrightarrow C_2H_2\uparrow \quad \text{etc.} \tag{3.19a}$$

$$C(s) + 4\ H\uparrow \leftrightarrow CH_4\uparrow \quad \text{or} \quad 2\ C(s) + 2\ H\uparrow \leftrightarrow C_2H_2\uparrow \quad \text{etc.} \tag{3.19b}$$

which can be generalized as follows:

$$x\ C(s) + \frac{y}{2} H_2\uparrow \leftrightarrow C_xH_y\uparrow \tag{3.20}$$

or

$$x\ C(s) + y\ H\uparrow \leftrightarrow C_xH_y\uparrow \tag{3.21}$$

if we distinguish between the reactions of molecular and atomic hydrogen with the solid carbon surface. Under equilibrium conditions the Gibbs free energy for reaction (3.20), for example, is given by

$$\Delta G^o(3.20) = \Delta G^o(C_xH_y) - \frac{y}{2}\Delta G^o(H_2) - x\ \Delta G^o(C(s)) = -\ RT \ln \frac{P_{eq}(C_xH_y)}{a_C P_{eq}(H_2)^{y/2}} \tag{3.22}$$

according to Eqs. (3.3), (3.11), and (3.12). Here $P_{eq}(C_xH_y)$ and $P_{eq}(H_2)$ are the equilibrium partial pressures (in atm) of C_xH_y and H_2, respectively. a_C is the activity of solid carbon which is equal to unity for both graphite and diamond. If C(s) refers to the graphitic form of carbon its Gibbs free energy of formation, $\Delta G^o(C(s))$, is by definition equal to zero, as is $\Delta G^o(H_2)$. In terms of the corresponding equilibrium constants $K(C_xH_y)$ Eq. (3.22) may be written as follows

$$K(C_xH_y) = \exp(-\Delta G^o(C_xH_y)/RT) = \frac{P_{eq}(C_xH_y)}{P_{eq}(H_2)^{y/2}} \tag{3.23}$$

If one wishes to express $K(C_xH_y)$ as a function of $P_{eq}(H)$ instead of $P_{eq}(H_2)$ one needs to know the following relationship

$$P_{eq}(H) = K(H)\ P_{eq}(H_2)^{1/2} \tag{3.24}$$

In addition we use the expressions derived in section 3.2 for the rates at which vapor species are incident on or evaporated from the carbon surface

$$I(C_xH_y) = \eta\ \frac{P(C_xH_y)}{\sqrt{2\pi mkT}} \tag{3.25}$$

and

$$R_{eq}(C_xH_y) = \eta'\ \frac{P_{eq}(C_xH_y)}{\sqrt{2\pi mkT}} \tag{3.26}$$

where m is the molecular mass of C_xH_y (in grams) and the meaning of η and η' has been explained before. The use of $P(C_xH_y)$ and $P_{eq}(C_xH_y)$ in Eqs. (3.25) and (3.26), respectively, reflects the key assumption of the QE model, namely that only the product is in thermochemical equilibrium with the carbon surface at temperature T. Now we are able to express all the evaporation rates $R_{eq}(C_xH_y)$ in terms of equilibrium constants $K(C_xH_y)$ and a single independent variable, $P_{eq}(H_2)$ or $P_{eq}(H)$, via Eqs. (3.23), (3.24), and (3.26). One gets

$$R_{eq}(C_xH_y) = \eta'\ K(C_xH_y)\ \frac{P_{eq}(H_2)^{y/2}}{\sqrt{2\pi mkT}} \tag{3.27}$$

or

$$R_{eq}(C_xH_y) = \eta'\frac{K(C_xH_y)}{K(H)^y}\ \frac{P_{eq}(H)^y}{\sqrt{2\pi mkT}} \tag{3.28}$$

To obtain the mixture of vapor species in equilibrium with the surface one needs to consider one more equation, namely the conservation of hydrogen atoms arriving at and leaving the surface

$$I(H) + 2\ I(H_2) = R_{eq}(H) + 2\ R_{eq}(H_2) + \sum_{x,y} y\ R_{eq}(C_xH_y) \tag{3.29}$$

where Σ represents the summation over all possible hydrocarbons. When all the rates R_{eq} are expressed in terms of $P_{eq}(H)$ and then substituted into Eq. (3.29), a polynomial of degree y_{max} in $P_{eq}(H)$ results; y_{max} is the maximum value of y of all the species C_xH_y considered. If we include, for example CH_4 and C_2H_4 but not C_2H_6, then $y_{max}= 4$. (When C_2H_6 is included its evaporation rate can be shown to be ~6 orders of magnitude smaller than that of CH_4). The total pressure in the system is one of the input parameters and its value fixes the left hand side of Eq. (3.29) via Eq. (3.25). The temperature of the incoming flux is equal to the temperature of the carbon sample. Since initially we do not know what the important products in the C-H system will be, a large number of vapor species (H, H_2, CH, CH_2, CH_3, CH_4, C_2H_2, C_2H_4, C_2H, C, C_2, C_3) are included in the calculations. The computations necessary to solve Eq. (3.29) are performed on the VAX which is installed in the Science building at City College. Generally we obtain four different roots for the quartic equation, two of which are real. The positive, real root is chosen for $P_{eq}(H)$. The values of $R_{eq}(C_xH_y)$ corresponding to this solution for $P_{eq}(H)$ are then determined according to Eq. (3.28) and are presented as functions of temperature below. We remark that equilibrium calculations yield the same results for $R_{eq}(C_xH_y)$ independent of whether the rates of evaporation are expressed in terms of $P_{eq}(H_2)$ or $P_{eq}(H)$.

3.4 Predictions of the Model: Evaporation and Deposition of Carbon

In Fig. 3.2 the predictions of the QE model for the rates of evaporation R_{eq} (in units of molecules $cm^{-2}\ s^{-1}$) of H, H_2, CH, CH_2, CH_3, CH_4, C_2H_2, C_2H_4, and C_2H from the surface of graphitic carbon are given as functions of temperature T (in K). These values of R_{eq} correspond to an incoming flux of pure hydrogen at a total pressure 36

torr (4800 Pa). At this point of the calculation we assume that all coefficients η and η' are equal to one. Up to about 600 K CH_4 is the most important reaction product, H_2 dominates from 600 to 2900 K and above 2900 K H_2 molecules dissociate into H atoms. Between 1700 and 2900 K C_2H_2 is the dominant hydrocarbon specie which will then transform to the C_2H radical at very high temperatures. The rates of evaporation of all the other hydrocarbons (CH, CH_2, CH_3, C_2H_4) are obviously unimportant. C, C_2, and C_3 have been included in the calculations but their concentrations are too small to be shown here. We note that there is a region (850-2500 K) where the production rate of hydrocarbons is small, or in other words the solubility of carbon in hydrogen is low. This is the temperature range of interest for the deposition of carbon and we will turn to this point now.

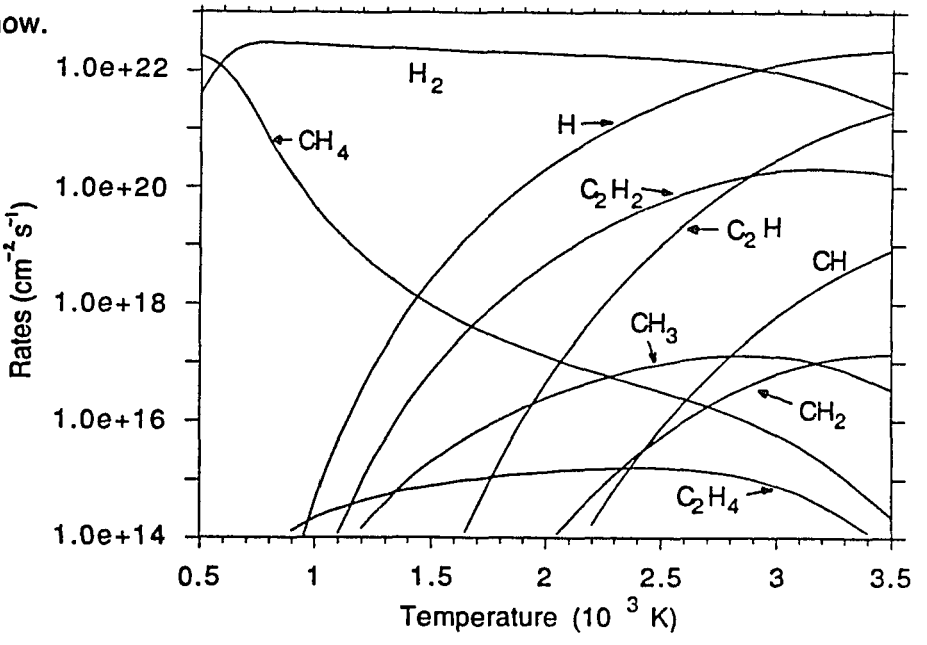

Figure 3.2 Predictions of the QE thermodynamic model for the rates of evaporation of gaseous species as functions of temperature T for the interactions of hydrogen with solid carbon. The total pressure is 36 torr.

So far we have only considered the etching of solid carbon by hydrogen via formation of volatile hydrocarbons C_xH_y. Since the purpose of this analysis is to gain insight into the deposition process of diamond or graphite we have to supply carbon atoms to the growth surface. This is achieved by adding a hydrocarbon specie (typically

CH_4 or C_2H_2) to the incoming flux of hydrogen and an additional term $\Sigma\, y\, I\,(C_xH_y)$ then appears on the left hand side of Eq. (3.29). To determine whether deposition or evaporation of solid carbon occurs we compare the flux of C atoms incident on the surface

$$I(C) = \sum_{x,y} x\ I(C_xH_y) \tag{3.30}$$

with the total flux of C atoms evaporating from the surface in the form of gaseous products C_xH_y

$$R_{eq}(C) = \sum_{x,y} x\ R_{eq}(C_xH_y) \tag{3.31}$$

and obtain an expression for the net rate of carbon deposition, namely

$$R_{dep}(C) = I(C) - R_{eq}(C) \tag{3.32}$$

Note that $R_{dep}(C) < 0$ is consistent with etching of solid carbon, if any is present, and that $R_{dep}(C) > 0$ indicates deposition.

The computer program developed for this thermodynamic analysis reads the $K(C_xH_y)$ values for a given temperature, finds the root $P_{eq}(H)$, calculates $R_{eq}(C_xH_y)$ and $R_{dep}(C)$ and then returns to the beginning of the program to repeat the computations for the next temperature. Temperature increments are 50 K between 500 and 2500 K and 100 K above 2500 K. If $R_{dep}(C)$ changes sign between T_i and $T_i+\Delta T$, a transition from etching to deposition of solid carbon, or vice versa, has occurred. The temperature T_b for which $R_{dep}(C) = 0$ is determined by linear interpolation. T_b constitutes one point of the phase boundary which separates regions where solid carbon is stable from regions where no condensed phase exists. The discussion of phase diagrams will be taken up below.

Figure 3.3 shows how the rates of evaporation R_{eq} of H, H_2, CH_4, C_2H_2, and C_2H and the rate of deposition $R_{dep}(C)$ vary with temperature when a mixture of 1% CH_4 in

H_2 at 36 torr reacts with a solid carbon surface. Since CH_4 is present in the incoming gas mixture deposition of solid carbon is possible when the incoming C flux exceeds the the flux of evaporating C atoms and the rates of deposition $R_{dep}(C)$ of both graphite and diamond are shown. The evaporation rates R_{eq} corresponding to graphite (solid lines) are essentially identical to the ones presented in the previous figure (Fig. 3.2). The dashed curves represent the evaporation rates of hydrocarbons over a diamond surface. As expected, the partial pressures of hydrocarbon species are higher for diamond than for graphite. We will return to this point later. For the gas mixture under consideration, corresponding to an incident C atom ratio $r_C = C/(C+H) = 4.9 \times 10^{-3}$, graphite will be deposited between 855 and 2560 K, while deposition temperatures for diamond range from 910 to ~2295 K. Evidently $R_{dep}(C) > 0$ for temperatures where the solubility of carbon in hydrogen is low, as has been pointed out before.

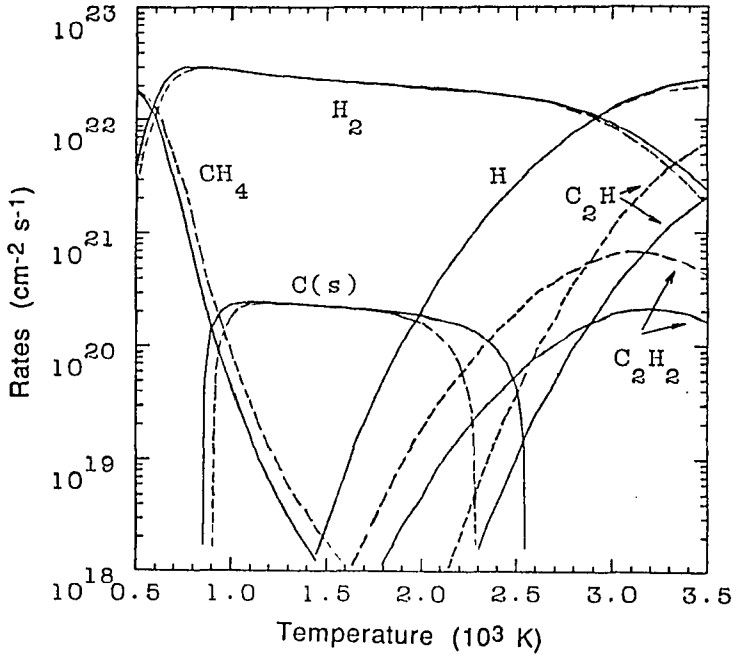

Figure 3.3 Predictions of the QE thermodynamic model for the rates of evaporation of gaseous species and the deposition for solid carbon (graphite and diamond) as functions of temperature T for the interactions of a 1% CH_4/H_2 mixture with solid carbon. The solid curves refer to graphite, whereas the dashed curves refer to diamond. The total pressure is 36 torr.

If the temperatures T_b where $R_{dep}(C) = 0$ are determined for different values of r_C while keeping the pressure constant we can create the phase diagram for the C-H system shown in Fig. 3.4. Both the phase boundary for graphite ('g') and for diamond ('d') have been included in this figure. The boundary separates the region where only gaseous products are stable from the region where a condensed phase is formed (to the right of the boundary). From the comparison of Figs. 3.3 and 3.4 we can infer that the lower branch of the phase boundary corresponds to the low temperature cutoff of $R_{dep}(C)$ due to the formation of CH_4, while the upper branch corresponds to the high temperature cutoff where etching of C occurs via formation of C_2H_2. It is apparent from Fig. 3.4 that for a pressure of 36 torr (4800 Pa) graphite can be deposited only for r_C values greater than 2×10^{-5} and then only for a limited range of temperatures. In other words, even when $r_C > 2 \times 10^{-5}$, the critical value, graphite is stable only if the substrate temperature falls within the graphite stability region. Diamond can be deposited only for r_C values greater than 5×10^{-5} and within a limited temperature range.

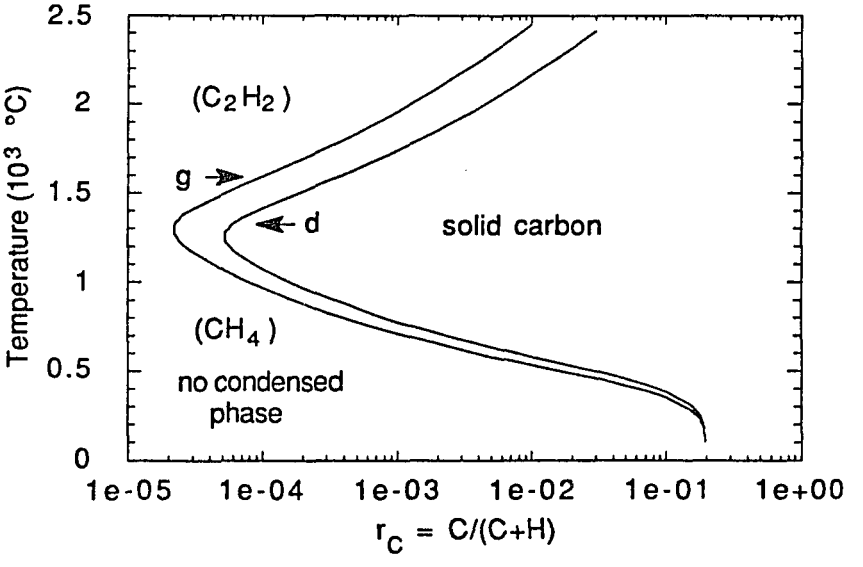

Figure 3.4 Predicted phase diagram for the C-H system for a total pressure of 36 torr. Phase boundaries between the regions where solid carbon exists and where no condensed phases exist are shown for both graphite (g) and diamond (d). CH_4 dominates in the gas phase below about 1400 °C, whereas C_2H_2 dominates at higher T.

Next we want to investigate how a variation in the total pressure can affect the C-H phase diagram. In Fig. 3.5 the phase boundary of graphite is presented for $P_{tot} = 1$, 36, and 760 torr. The dependence on pressure is quite drastic, especially for the lower branch, with increasing P corresponding to increased etching and a reduced stability region for solid carbon. Upon closer examination of Fig. 3.5 we see that the different curves almost coincide at high temperatures, i.e the phase boundary is essentially independent of pressure in this range. This behavior can be explained as follows. According to Eq. (3.27) the evaporation rate of CH_4, $R_{eq}(CH_4)$, is proportional to the *square* of the partial pressure of H_2, $P_{eq}(H_2)$, while the evaporation rate of C_2H_2, $R_{eq}(C_2H_2)$, is proportional to $P_{eq}(H_2)$. For example, doubling the total pressure will double $P_{eq}(H_2)$ and therefore $R_{eq}(C_2H_2)$, but the rate of CH_4 formation will increase by a factor of four. In other words an increase in P_{tot} will result in increased etching when CH_4 is the dominant product (mainly at lower temperatures), but no shift of the phase boundary is observed when C_2H_2 is produced (at high temperatures). It should be noted that pressure effects are quite similar for graphite and diamond. The results illustrated in Fig. 3.5 are consistent with those obtained by Knippenberg *et al.* (1967) for the case of the CVD of pyrolytic graphite.

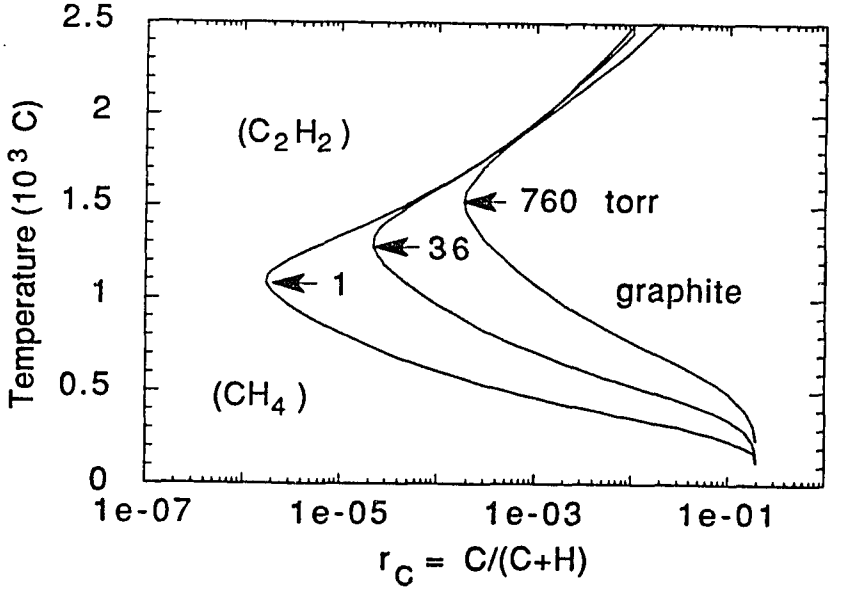

Figure 3.5 Predicted phase boundaries for graphite at total pressures of 1, 36, and 760 torr.

3.5 Graphite vs Diamond

Since we have already referred to a diamond surface in earlier sections of this chapter let us now examine how we can apply the above formalism to the evaporation and deposition of diamond. Where in the model do we have to specify the nature of the solid carbon surface? In Eq. (3.22) we set $\Delta G^{o}(C(s)) = 0$ assuming that a graphitic carbon surface is exposed to hydrogen. If the C surface corresponds to diamond we have to include ΔG^{o}(dia) or K(dia) in the calculations and Eq. (3.23) then yields for the case of diamond

$$K(C_xH_y) = K(\text{dia}) \frac{P_{eq}(C_xH_y)}{P_{eq}(H_2)^{y/2}} \qquad (3.33)$$

ΔG^{o}(dia) is the Gibbs free energy necessary to transform graphite into diamond at a given temperature, and K(dia) is the corresponding equilibrium constant. The thermodynamic data for diamond taken from Berman and Simon (1955) are valid at zero pressure and in the temperature range 0-1200 K only. However they have been extended to higher temperatures by linear extrapolation because appropriate data have not been found.

We remark that the Gibbs free energy of formation of diamond, ΔG^{o}(dia), is higher than the Gibbs free energy of formation of graphite, ΔG^{o}(graph), by about 0.7 kcal/mole under ambient conditions. There are two important implications of this result. Firstly, since $\Delta G^{o}(\text{dia}) > \Delta G^{o}(\text{graph})$ the equilibrium partial pressures of carbon-containing gases are higher over diamond than over graphite, as has been pointed out before in reference to Fig. 3.3. The equilibrium pressure, for example, of CH_4 over diamond at 1000 K is calculated to be approximately twice as high as the corresponding value for graphite. According to thermodynamics the carbon supersaturation σ_C, which for a given partial pressure of CH_4 is defined as $\sigma_C = \ln\{P(CH_4)/P_{eq}(CH_4)\}$ (Piekarczyk *et al.* 1989), is therefore always smaller over diamond than over graphite.

Secondly, we note that although ΔG^{o}(dia) > ΔG^{o}(graph) the difference is very small when compared, for example, to the heat of formation of diamond (ΔH^{o}(dia) = 450 kcal/mole). Under certain conditions when kinetic factors gain in importance this difference becomes negligible. A carbon layer deposited at a high rate under high supersaturation will generally contain a mixture of sp^3, sp^2, and sp hybridized C-C bonds. D. V. Fedoseev *et al.* (1984) argue that 'the problems in the synthesis of diamond in its metastability region do not concern the formation of diamond itself: they relate to the prevention of the appearance of the stable phase (graphite) which would otherwise block the diamond nuclei' once they are formed.

Let us take another look at Fig. 3.4 which depicts the predicted phase boundaries for both graphite and diamond at a pressure of 36 torr (4800 Pa). Clearly, the diamond stability region is found *inside* the region where graphite is stable, as is expected from thermodynamics. It has been emphasized above that the synthesis of diamond in its metastable region cannot be explained on purely thermodynamic grounds. But we have argued that under certain conditions there can exist kinetic factors that favor growth of diamond over graphite. Let us now attempt to identify some of those "kinetic factors".

3.6 The Role of Kinetic Factors

There is experimental evidence that diamond, in spite of its metastability at low pressures, is more inert towards gasification by atomic hydrogen or oxygen than graphite or amorphous carbon (Fedoseev *et al.* 1984). In Fig. 3.6 we plot the experimental results (labelled 'B & O') of Balooch and Olander (1975) who examined the reactions of atomic and molecular hydrogen with pyrolitic graphite, and the corresponding predictions of the QE model (labelled 'QE'). Shown is the apparent reaction probability $R(CH_4)/[2\,I(H_2)+I(H)]$ for methane as a function of inverse surface temperature. It is obvious that the experimentally observed etching of graphite

via production of CH_4 is strongly enhanced above the rate obtained from the QE model in the temperature range from 450 to 800 K. Consequently, the actual stability region of graphite is smaller than predicted in Fig. 3.4.

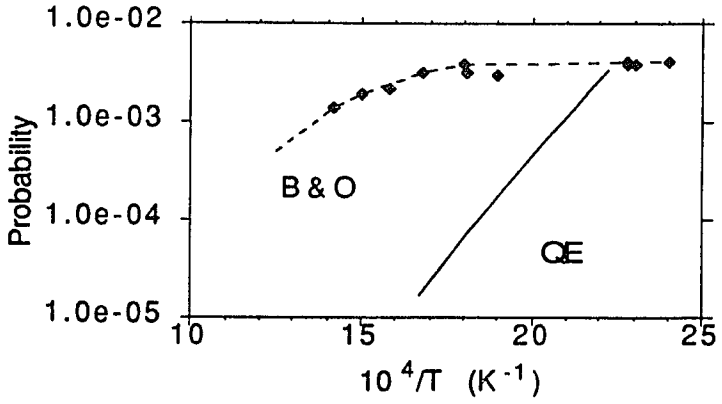

Figure 3.6 CH_4 reaction probability, $R(CH_4)/[2\ I(H_2)+I(H)]$, as function of inverse temperature. Shown are the experimental results of Balooch and Olander (1975), 'B & O', and the predictions of the QE model, 'QE'.

Now the question arises whether we should admit the failure of the QE model and attempt to formulate and solve a more sophisticated atomic kinetic model, or whether we should attempt to modify the QE model to include the observed (Balooch & Olander 1975) enhanced etching of graphite by hydrogen. Recalling that we chose the QE thermodynamic model because of its simplicity and the small number of adjustable parameters, we feel it is worth to continue the present study and incorporate some kinetic factors into the model. Also one should not forget that despite its simplicity the QE model has been successfully employed to identify the important vapor species and condensed phases in the C-H system and their dependences on system variables (pressure, temperature,...). The only nonthermodynamic parameters in this analysis are the sticking (or equilibration) and desorption (or accomodation) coefficents η and η', respectively. Although it is not possible at this point to determine conclusively which kinetic factors cause the experimentally observed enhanced etching of graphite by hydrogen, possible candidates include: i) a desorption coefficient $\eta'_{H_2}(g)$ for H_2 on graphite less than unity which

would inhibit the production of H_2 and consequently enhance the formation of CH_4, or ii) H atoms tightly bound to the graphite surface which would hinder the recombination of H atoms to form H_2 and thereby also promote the production of CH_4. Clearly, further experimental work is necessary to identify the dominant kinetic factor(s).

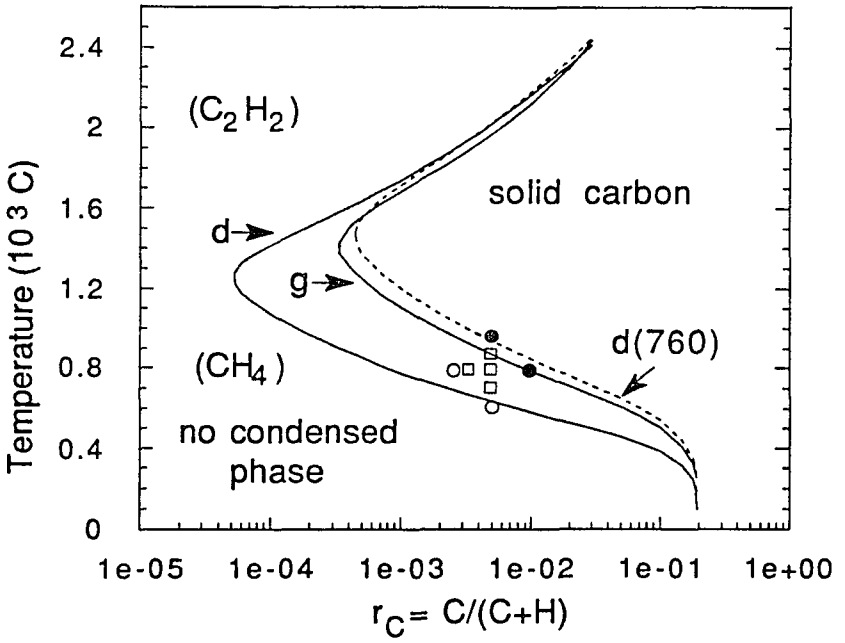

Figure 3.7 Predicted phase diagram for the C-H system modified to include the enhanced etching of graphite by hydrogen. Also shown are the experimental results of Matsumoto *et al.* (1982). Open squares refer to the observation of well-defined diamond particles, open circles correspond to small, poorly-defined diamond particles, and filled circles represent large particles apparently covered with graphitic deposits. The curve labelled 'd(760)' corresponds to the phase boundary for diamond at 760 torr.

We tentatively decide in favor of $\eta'_{H_2}(g)$ as *the* kinetic parameter responsible for the enhanced etching of graphite. In Fig. 3.7 we present the predictions of the now modified thermodynamic model together with the experimental results of Matsumoto *et al.* (1982) who investigated the growth of diamond particles from CH_4/H_2 mixtures via hot filament assisted CVD at a total pressure of about 36 Torr. In order to arrive at a possible explanation for the results of Matsumoto *et al.* (1982) we choose a value of

$\eta'_{H_2}(g)$= 0.2, which is well within the range of values (0.03-1) needed to explain the results of Balooch and Olander (1975). It can be seen that the stability region of graphite now lies *within* that of diamond, which is unchanged from Fig. 3.4. The data points included in Fig. 3.7 are described as follows. The open squares represent well defined diamond particles and they lie inside the region where only diamond is predicted to be stable. Open circles correspond to small poorly defined particles and they are found near the boundary for etching. Large, ball-like structures apparently covered with graphite (filled circles) fall in or close to the region where graphite is stable. Matsumoto *et al.* (1987) reported that diamond growth at 760 torr required up to 10% CH_4 in H_2, in agreement with the predicted shift of the phase boundary at high pressures. For comparison the calculated etch-growth boundary of diamond at 760 torr is included in Fig. 3.7.

To conclude this section let us now summarize the predictions of the QE thermodynamic model which we modified to include the observed (Balooch & Olander 1975) enhanced etching of graphite by hydrogen. Firstly, the model can reliably identify the important species in the diamond growth environment. They are the same as the species measured in a hot filament reactor (Celii *et al.* 1988) although at lower concentrations than predicted. Secondly, the existence of the C-H phase diagram with its stability regions for diamond and graphite is used to explain why the CVD of diamond films from hydrocarbon/hydrogen mixtures is possible under the conditions presently used. Thirdly, we have verified and explained the observed tendencies associated with a variation of the growth parameters. For example, an increase in the carbon atom fraction r_C requires a decrease in substrate temperature in order to prevent the appearance of graphite in the deposited films. If for a given r_C value the substrate temperature is raised too much, graphitic inclusions in the deposit will dominate. On the other hand, substrate temperatures must not be decreased to too low a value or there will be no growth. Since increasing the pressure expands the etching region this

requires an increase in the carbon atom fraction for a given temperature or an increase in both r_C and T.

3.7 Extensions of the QE Model

In this section we shall discuss how the QE thermodynamic model can be applied to more complicated systems. We begin with the reactions of a solid carbon surface (graphite or diamond) with oxygen and hydrogen and will then turn our attention to the study of the C-H-F system.

3.7.1 The C-H-O System

CVD diamond films have been successfully grown from a variety of C-H-O mixtures and there have been numerous reports in the literature about the effect of oxygen on diamond growth (see the summary in chapter 2). It has been demonstrated that small amounts of oxygen improve the quality of the deposited films and extend the range of substrate temperatures suitable for diamond growth to lower values (Liou *et al.* 1989, 1990). Diamond growth rates can increase or decrease depending on the amount of oxygen added (Johnson *et al.* 1990). We attempt to apply the QE thermodynamic model to the C-H-O system and hope to gain insight into the processes that govern the etching or deposition of graphite and diamond.

Apart from the addition of one more equation, namely the conservation of oxygen atoms arriving at and leaving the carbon surface, we follow the same approach as outlined above. In addition to the hydrocarbon species C_xH_y there are now products such as H_2O, CO, COH etc. The following 24 reaction products have been included in the calculations: H, H_2, CH, CH_2, CH_3, CH_4, C_2H_2, C_2H_4, C_2H, O, O_2, CO, CO_2, C_2O, C_3O_2, OH, H_2O, HO_2, CH_2O, CHO, C_2H_4O, C, C_2, C_3. The rates of evaporation of all the species

considered, $R_{eq}(C_xH_yO_z)$, are expressed in terms of their equilibrium constants and the partial pressures of H or H_2, $P_{eq}(H)$ or $P_{eq}(H_2)$, and O or O_2, $P_{eq}(O)$ or $P_{eq}(O_2)$. Eqs. (3.27) or (3.28) are then replaced by

$$R_{eq}(C_xH_yO_z) = \eta' \, K(C_xH_yO_z) \frac{P_{eq}(H_2)^{y/2} \, P_{eq}(O_2)^{z/2}}{\sqrt{2\pi mkT}} \tag{3.34}$$

or

$$R_{eq}(C_xH_yO_z) = \eta' \, \frac{K(C_xH_yO_z)}{K(H)^y \, K(O)^z} \frac{P_{eq}(H)^y \, P_{eq}(O)^z}{\sqrt{2\pi mkT}} \tag{3.35}$$

where the meaning of the various quantities has been explained above. The expression for the conservation of hydrogen is the same as before except that the species $C_xH_yO_z$ replace the species C_xH_y. The conservation of oxygen atoms is given by

$$I(O) + 2\,I(O_2) + \sum_{x,y,z} z \; I(C_xH_yO_z) = R_{eq}(O) + 2\,R_{eq}(O_2) + \sum_{x,y,z} z \; R_{eq}(C_xH_yO_z) \tag{3.36}$$

The conservation of hydrogen and oxygen constitutes a pair of nonlinear equations in two unknowns $P_{eq}(O_2)$ and $P_{eq}(H_2)$ (or $P_{eq}(O)$ and $P_{eq}(H)$) whose solutions are determined via the Newton-Raphson method*. After finding the solutions, the evaporation

---

* The Newton-Raphson method is a routine which finds the roots x_i, i=1, 2,..., N, of N nonlinear equations

$$f_i(x_1, \ldots, x_N) = 0; \quad i = 1, 2, \ldots, N.$$

Since our problem involves only two such equations we will concentrate on N=2 in the following discussion. For a more general treatment of root finding we suggest the book by Henrici (1960). If we define $\mathbf{X} = (x_1, x_2)$ then, in the neighborhood of $\mathbf{X}$ each function f_1 and f_2 can be expanded in a Taylor series

$$f_1(\mathbf{X} + \delta\mathbf{X}) = f_1(\mathbf{X}) + \frac{\partial f_1}{\partial x_1}\delta x_1 + \frac{\partial f_1}{\partial x_2}\delta x_2 + O(\delta\mathbf{X}^2) = 0$$

with the same expression for f_2. By neglecting the terms beyond linear, we obtain a pair of linear equations for the corrections $\delta\mathbf{X}$ that move each function closer to zero simultaneously, namely

$$J_{11}\,\delta x_1 + J_{12}\,\delta x_2 = -\,f_1 \quad \text{and} \quad J_{21}\,\delta x_1 + J_{22}\,\delta x_2 = -\,f_2$$

rates of the different species are determined and the net deposition rate of solid carbon is again the difference between the incoming and outgoing fluxes of carbon atoms (Eq. (3.32)). The distinction between graphite and diamond is based upon the choice of $\Delta G^o(C(s))$, as has been explained above.

In Fig. 3.8 the predictions of our QE thermodynamic model for the rates of evaporation of H, H_2, CH_4, C_2H_2, C_2H, H_2O and CO from the surface of solid carbon are presented as functions of temperature T from 500 to 3500 K. These values correspond to incoming fluxes from a gas mixture with a C/O atomic ratio of 3, i.e. CH_4 (3%), H_2 (97%) and $O_2/(CH_4+H_2)$ = 0.5%, and a total pressure of 25 torr (3330 Pa). It should be noted that CO is an important specie for all temperatures higher than ~700 K. Other species such as O, O_2, OH etc. have been included in the computations but their rates of evaporation are insignificant in comparison to the ones shown. The dashed line refers to the rate of deposition of graphite, the only form of solid carbon considered in this diagram. Deposition temperatures range from ~1020 to 2390 K.

When the C/O ratio of the incident flux is less than or equal to one, the model predicts that all the incoming CH_4 reacts with O_2 to form CO for temperatures greater than ~900 K. Under these conditions no solid carbon will be deposited. This becomes quite clear in the predicted phase diagrams in Fig. 3.9 where graphite is stable only to the right of the boundary. It is illustrated how the etch-growth boundary shifts to higher r_C = C/(C+H) values when increasing amounts of oxygen (0, 0.5, 1, and 1.5%) are

---

where J_{ij} is the Jacobian, i.e. $J_{ij} = \frac{\partial f_i}{\partial x_j}$.

After solving these equations for the corrections $\delta \mathbf{X}$, new values for x_1 and x_2 are obtained as follows

$$x_1(\text{new}) = x_1(\text{old}) + \delta x_1 \quad \text{and} \quad x_2(\text{new}) = x_2(\text{old}) + \delta x_2$$

and the process is iterated until f_1 and f_2 have converged.

added to a C-H mixture at 25 torr. This decreased stability of graphite, which corresponds to an increased solubility of carbon in the gas phase, results from the etching by oxygen via formation of CO.

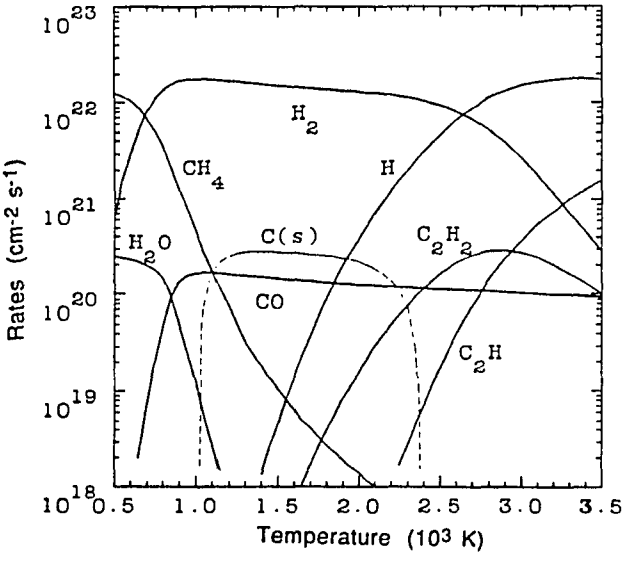

Figure 3.8 Predictions of the QE thermodynamic model for the rates of evaporation of the vapor species in the C-H-O system as functions of temperature T. These evaporation rates correspond to incoming fluxes of CH_4 (3%), H_2 (97%), and $O_2/(CH_4+H_2)$ = 0.5% at 25 torr. The dashed curve refers to the rate of deposition of graphite, the only form of solid C considered here.

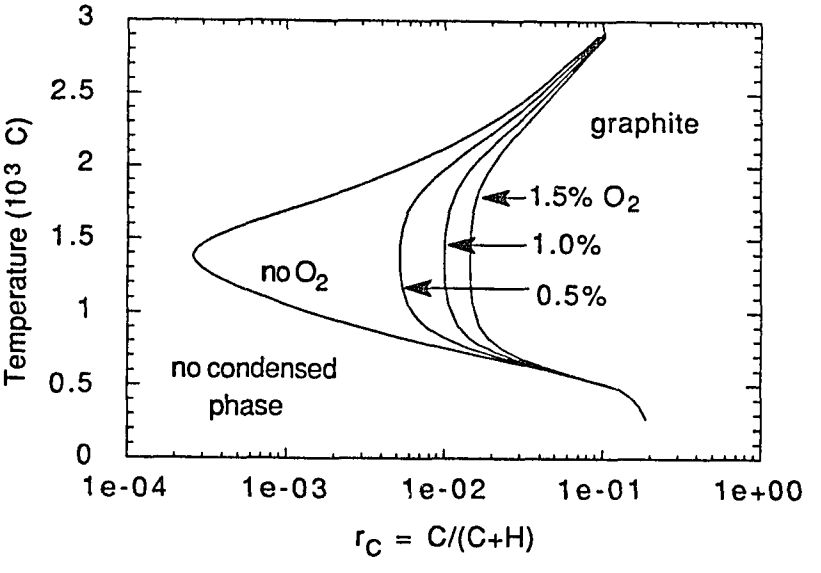

Figure 3.9 Predicted phase boundaries for graphite in the C-H (no O_2) and C-H-O (0.5, 1, and 1.5% O_2) phase diagrams for P_{tot} = 25 torr. r_C is the carbon atom fraction.

The comparison between experimental results and predictions of the QE thermodynamic model for mixtures of CH_4/H_2 with small amounts of O_2 will be postponed until chapter 6. Instead we will apply the QE model to yet another example of the C-H-O system, namely the oxyacetylene welding torch with gas mixtures containing large amounts of oxygen.

In chapter 2 the oxyacetylene torch was mentioned as one of the techniques employed to deposit polycrystalline diamond films in the ambient atmosphere. In Fig. 3.10 we present the predicted rates of evaporation for H, H_2, CH_4, C_2H_2, C_2H, H_2O, CO_2 and CO, as well as the rate of deposition of graphite, the only form of solid carbon shown. The total pressure is set to 760 torr (1.013×10^5 Pa) and the incident fluxes of O_2 and C_2H_2 are chosen in a ratio 1:1. At temperatures below ~900 K hydrogen preferentially reacts with oxygen to produce H_2O at the expense of forming CH_4. The remaining oxygen atoms are tied up in CO_2. Graphite can be deposited for temperatures up to ~1600 K but it is apparent that the rate of deposition of graphite as well as the rates of evaporation of H_2O and CO_2 drop rapidly when CO starts to dominate.

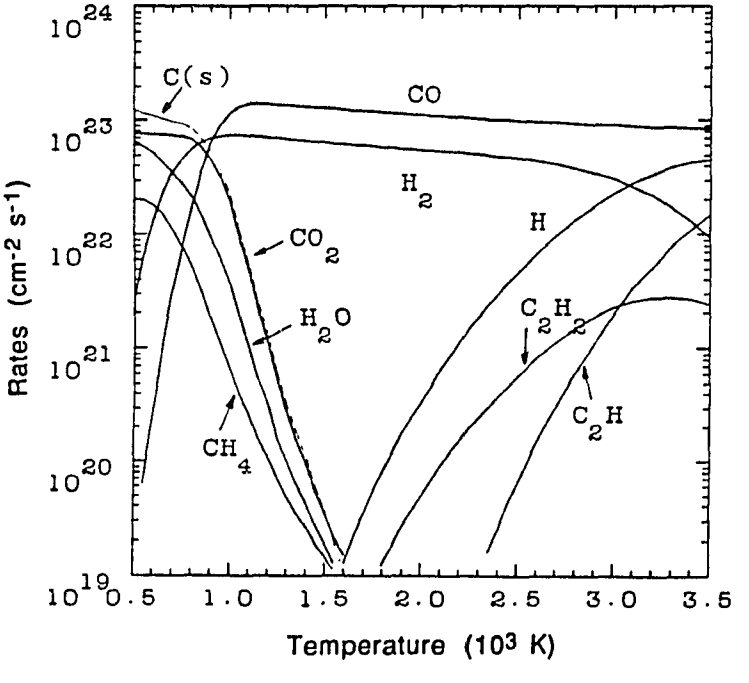

Figure 3.10
Predictions of the QE thermodynamic model for the rates of evaporation and deposition for graphite via the oxyacetylene torch as functions of temperature T. These rates correspond to a stoichiometric gas mixture consisting of equal amounts of O_2 and C_2H_2 at 760 torr.

Although not shown in Figs. 3.8 and 3.10, the QE thermodynamic model predicts that the rates of evaporation of carbon-containing species such as CO, CH_4, C_2H_2 and other hydrocarbons are higher for diamond than for graphite, due to the higher Gibbs free energy of formation of diamond (see discussion above). As long as $T < 900\,K$ the rate of evaporation of CO_2 is also higher for diamond but it falls below that for graphite when the reaction $C(s) + CO_2 \leftrightarrow 2\,CO$ starts to dominate in the forward direction for either form of carbon.

The predicted stability regions of graphite and diamond are shown in the phase diagram for the oxyacetylene torch in Fig. 3.11. Note that here solid carbon is stable only to the left of and below the boundary. When R = O/C is less than unity, deposition of C via the oxyacetylene torch is possible over a wide range of temperatures while the stability region of C shrinks considerably when $R \geq 1.0$ due to the production of CO. Since no effort has been yet to identify the kinetic factors which are clearly necessary to explain the growth of diamond in its metastable region via the oxyacetylene torch, the stability region of diamond lies within that of graphite.

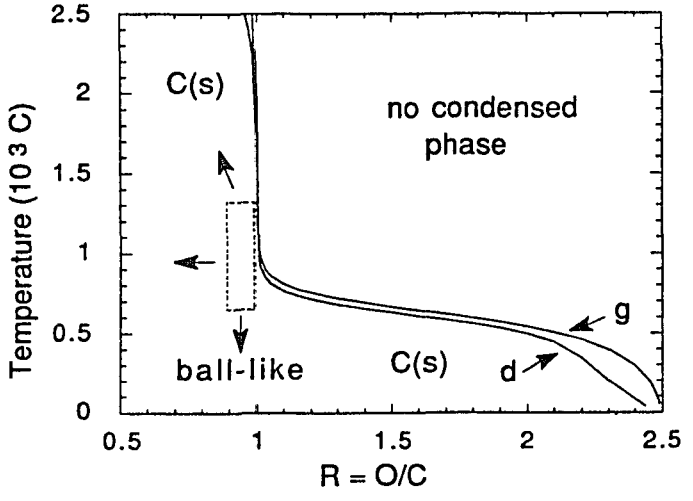

Figure 3.11 Predicted phase diagram for the oxyacetylene torch. Also included are the experimental observations of R. Wang (to be published) who reported growth of high quality diamond within the enclosed region. Above and below the indicated temperature range and for O_2/C_2H_2 ratios smaller than 0.89, ball-like structures were obtained. No growth of solid carbon (either graphite or diamond) was possible for $R \geq 1$.

Also included in Fig. 3.10 is a summary of the experimental observations of R. Wang, a visiting scientist from the P. R. of China who has carefully investigated the oxyacetylene torch (to be published). He observed growth of well-defined diamond particles or polycrystalline films for substrate temperatures between ~650 and ~1320°C (±50°C) and O/C ratios ranging from 0.89 to 0.99. Above and below this temperature range and for ratios smaller than 0.89, ball-like structures are deposited. These results are consistent with the observations of Hirose *et al.* (1988). R. Wang noted that with his experimental setup no growth occurred for $R \geq 1.0$ independent of the substrate temperature. This result which seems to be in disagreement with the QE model, which predicts low temperature growth for O/C ratios up to 2.5, might be related to the disappearance of the flame feather where growth typically occurs. Another rather puzzling experience reported by R. Wang is the dependence of the experimental results on the acetylene/acetone ratio in the gas cylinder. Commercially available acetylene is shipped dissolved in acetone in order to prevent violent decomposition under high pressure. Further work is necessary to explain these observations.

3.7.2 The C-H-F System

The most recent breakthrough in diamond CVD came in September 1990 when Patterson *et al.* (1990) reported the successful growth of diamond films from carbon-hydrogen-halogen mixtures at atmospheric pressure. In their apparatus which has already been more carefully described in chapter 2, the reacting species flow along a heated monel tube into which a suitable substrate has been placed. No gas activation is provided although the heated monel tube may be important. Typical gas mixtures employed were 0-5% CF_4 in H_2 or 0-5% CH_4 in F_2. In order to predict which gaseous species will be present and what the effect of fluorine on the deposition of solid carbon will be, our QE thermodynamic model has been extended to the C-H-F system. The

formalism describing the reactions of the solid carbon surface (graphite or diamond) with hydrogen and fluorine is analogous to the C-H-O system, and the following predictions result. The predicted rates of evaporation for HF, CF, CF_2, CF_3, CF_4, H_2F_2, CHF_3, C_2F_4, H, and C_2H from a graphite surface, the only form of carbon considered, are depicted in Fig. 3.12 as functions of temperature from 500 to 3500 K. The incident gas mixture consists of 5% CH_4 in F_2 at 760 torr. It is observed that throughout the whole temperature range essentially all of the incoming hydrogen reacts with fluorine to form HF except at very high T where some H and C_2H are being formed. CF_4 is the dominant product between 500 and 2600 K; above 2600 K atomic fluorine and other fluorocarbons, such as CF_2, CF_3, and CF become important. Additional species such as H_2F_2, CHF_3 and C_2F_4 have been included for completeness only. We remark that no solid carbon will be deposited for this choice of parameters.

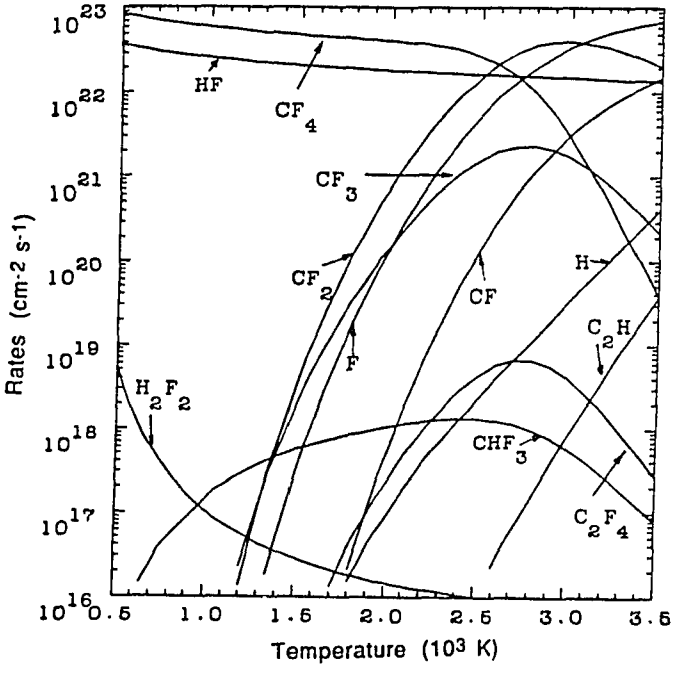

Figure 3.12 Predictions of the QE thermodynamic model for the rates of evaporation of the vapor species in the C-H-F system as functions of temperature T. These evaporation rates correspond to gas mixture consisting of 5% CH_4 in F_2 at 760 torr. Note that no solid carbon can be deposited for this choice of parameters.

The predicted phase boundaries for graphite in the C-H-F phase diagram are presented in Fig. 3.13 for P_{tot} = 76 and 760 torr. Note that according to equilibrium thermodynamics no growth of graphite is possible for less than 25% CH_4 in F_2 in contrast to the results obtained by Patterson *et al.* (1990). However in the QE model we assume that the reacting species are activated and that all chemical reactions are possible. What this shows is that activation of the reacting species for the C-H-F system is unnecessary and actually undesirable when low CH_4/F_2 ratios are used.

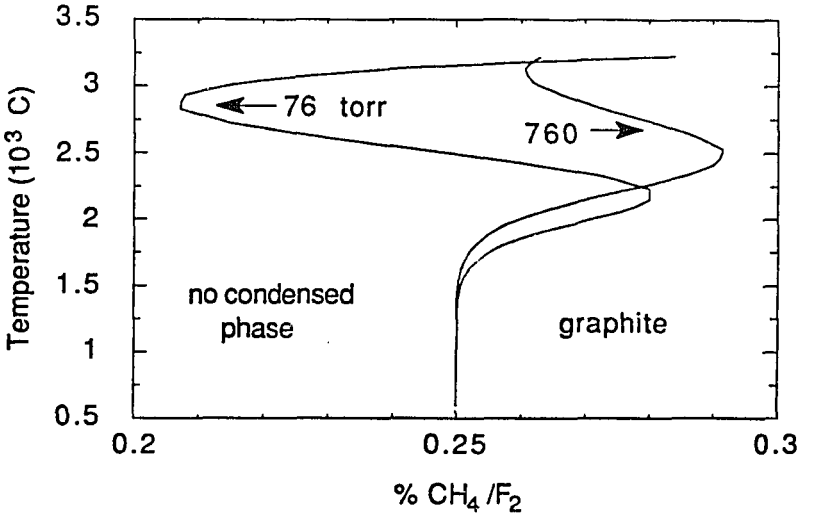

Figure 3.13 Predicted phase boundaries for graphite in the C-H-F phase diagram for P_{tot} = 760 and 76 torr.

3.8 Conclusions

We have modified the QE model of Batty and Stickney (1969) to include the observed (Balooch and Olander 1975) enhanced etching of graphite by hydrogen and have thus been able to both clarify and even explain qualitatively the CVD of diamond films under the conditions presently employed. With the aid of our model we can identify the important gaseous species in the diamond growth environment and explain how the deposition of diamond varies with the available experimental parameters (pressure,

temperature,...). The model has been extended to examine the possible reactions between a solid carbon surface (graphite and diamond) with hydrogen and either oxygen or fluorine and important conclusions can be made.

One point that needs to be addressed is the activation of the reacting species. Why is it necessary and how do we incorporate it into the model? Our point of view is that gas activation is necessary to drive chemical reactions to their completion. This has been clearly demonstrated by Patterson *et al.* (1990) for the C-H-F system. Diamond deposition was possible for CF_4/H_2 ratios much smaller than predicted by our model *because* the reactants were not activated. Therefore only a small fraction of the incoming fluorine acted as an etchant for solid carbon.

After having demonstrated the success of the model let us now turn our attention to its limitations. As has been pointed out before most of the expressions derived in section 3.2 are not valid under high pressure conditions. Gas phase reactions become quite prominent and should therefore be incorporated. Another point concerns the nature of the impinging species. Since the reacting gases are typically activated before they come in contact with the substrate we expect a large number of excited or fragmented molecules to take place in the chemical reactions. In other words we face the impossible task of finding realistic values for the sticking coefficients of impinging species which are not even identified. Yet another complication arises from the fact that dangling bonds at the growing diamond surface are stabilized by hydrogen atoms. In the model, however, it is assumed that the impinging molecules strike the bare graphite or diamond surface rather than another complex. This means we have to find sticking coefficients of the impinging species that also depend on the composition (purity) of the surface, in addition to all the other dependences. In spite of all these limitations we will continue applying the model to the analysis of diamond CVD as long as no better model is developed.

Chapter 4

Experimental Setup and Procedures

In the first section of this chapter the High Vacuum (HV) reaction chamber used in our experiments and the subsidiary apparatus (pumps, gauges, controllers, ...) are described. In later sections we shall also discuss the sample preparation and experimental procedures, as well as the characterization of the deposit.

4.1 Experimental Setup

Figure 4.1 shows a schematic drawing of the HV system with its 5 6-inch-diameter ports. One port is closed by a 7056 glass window and thus allows direct view of the center of the chamber. The main body of the chamber and the gas delivery system are made of non-corrosive stainless steel. The setup is that of a flowthrough reactor where the gases enter typically at a rate of 100 sccm (standard cubic centimeters per minute). When the total pressure inside the chamber is at 25 torr the residence time of gas molecules is calculated to be about 200-300 seconds.

The preliminary pumpdown of the chamber is accomplished with a Veeco VS-9 pumping station consisting of a Veeco EP2-AB air-cooled diffusion pump (DP) and a Welch 1402 mechanical pump (MP). The DP is also fitted with a liquid nitrogen (LN) trap to reduce backstreaming of oil and condensable vapors (mainly water). When reactive gases (such as H_2) were used during the experiments the pumps and cold trap

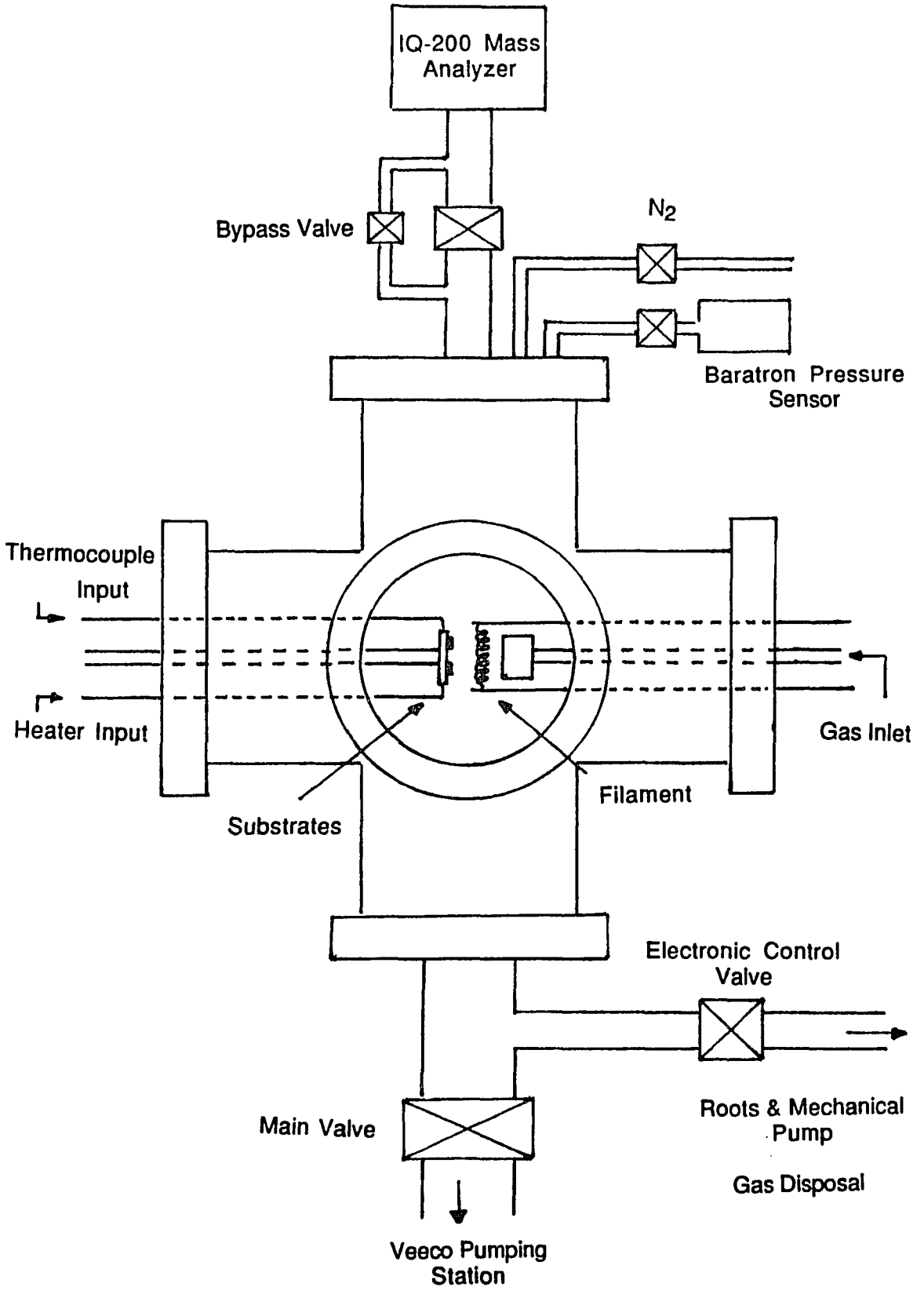

Figure 4.1 Schematic presentation of HV system.

were isolated and a separate pumping system was used. Evacuation was then performed by a Leybold-Heraeus WS150 Roots pump (RP) which is backed by a Leybold-Heraeus Trivac D8A mechanical pump with an additional exhaust filter to trap oil vapor. To minimize backstreaming of oil and condensable vapors from the MP to the RP we introduced nitrogen at a pressure of ~100 mtorr between the the two pumps. After exiting from the chamber and the pumps, reactive gases were disposed through a hood. Although not used in this work provisions were made to neutralize reactive gases, such as SiH_4, before discharging them into the environment.

The VS-9 pumping system contains six high vacuum valves and is supplied with a Veeco RG-3A ionization and thermocouple gauge control circuit. The main body of the chamber reactor can be isolated from the Veeco pumping station via a manually operated main valve and from the RP via an electronic MKS throttling valve. The system is equipped with five different pressure gauges whose ranges of operation vary from 1000 down to 10^{-8} torr: a Varian 563 ionization gauge tube (Bayard-Alpert type) at the entrance of the DP, a thermocouple (TC) gauge between DP and MP, another TC gauge between electronic control valve and RP, and one TC gauge between RP and MP. On top of the chamber there is also a MKS 315BD Baratron capacitance manometer which is part of a pressure control unit described below.

Since the hot-filament assisted CVD growth of diamond films is a lengthy process, typically lasting 6-8 hours, it is important to keep the process parameters constant during deposition. The pressure in the system is maintained by an MKS control system consisting of a pressure sensor (Baratron), a temperature controlled transducer which converts pressure to an electrical signal (MKS 270B and 272), a controller (MKS 252A), and a control valve (MKS 253A). Its operation rests on the following principle: The controller takes the DC transducer signal and compares it to the setpoint. Any error between actual and setpoint signal is amplified by the controller and fed back to the valve which is then positioned in such a manner as to drive the actual pressure level to the

required level. By varying the pumping speed it is therefore possible to keep the pressure in the reaction chamber constant (to within ~0.1 torr).

The flow control system which can deliver four different gases into the reaction chamber simultaneously consists of electronic mass flow meters (MKS 1258B) in conjunction with control circuitry (MKS 260, 260 PS-3, and 261). The principle of operation is identical to that of the pressure control circuit. Deviations between actual and required flow rate will drive the controlling valve to a position where deviations are eliminated. Although the flow controllers are calibrated for N_2 only, it is possible to measure the flow of different gases by choosing appropriate gas correction factors. These factors take into account differences in specific heat, density and molecular structure of various gases. Individual flow rates can range from 0 to 100 sccm with an estimated accuracy of ±0.1 sccm. No more than three different gases were used at one time, H_2 (99.99%), CH_4 (99.97%) or C_2H_2 (99.6%), and O_2 (99.6%); all supplied by Linde.

Attached to the top port of the chamber, and separated from it by a manual Varian polyimide sealed valve, is an Inficon Leybold-Heraeus IQ 200 "residual gas analyzer". The analyzer is equipped with a 20 l/s Varian Vaclon pump which can achieve pressures below 10^{-8} torr, and its control unit. Since operation at high pressures is not possible, a bypass valve allows its use even when the pressure is high in the chamber. The analyzer consists of a sensor and an electronics unit which operates the sensor. Its operation is based on the following principle: In the sensor, gas molecules from the residual atmosphere are ionized by bombarding them with electrons from a heated filament. These ions will then be analyzed in an electrostatic quadrupole which acts as a filter for one specific mass. Ions that pass through the filter are collected on a detector (Faraday cup or electron multiplier) and the resulting ion current is converted to a peak corresponding to the masses of the ions present. When gas molecules are ionized usually more than one kind of ion will result. For example water vapor, H_2O, will

produce H_2O^+, OH^+, O^+, and H^+ ions. The array of peaks produced by a single substance is called a fragmentation pattern. Patterns of common molecules have been tabulated.

The magnitude of a signal representing a particular mass is characteristic of the number of ions produced and therefore of the concentration of molecules of the substance under consideration. However it must be realized that there are limitations on the quantitative relationship between ion current and molecular concentrations. Since different kinds of molecules exhibit different ionization cross sections (heavy large molecules are easier to ionize than light small ones), the sensitivity of the instrument is a function of mass. In addition, there can be interactions between the spectrometer itself (e.g. hot filament) and reactive gases (e.g. O_2) which may lead to faulty results. To correct measured signals for mass discrimination, relative ion gauge sensitivities ($S/S(N_2)$) have been tabulated. Starting with known gas compositions we have determined relevant gauge sensitivity factors for the gases of this present study.

It will be shown later in chapter 6 that the presence of oxygen, even in small amounts, can have significant effects on the performance of the hot filament in the reactor. It is therefore essential to eliminate all uncontrolled sources of oxygen such as leaks and water vapor adsorbed on the chamber walls. Prior to running an experiment the chamber was baked at ~200 ^oC for 12-24 hours. This bakeout is accomplished with the use of Thermolyne flexible electrical heating tapes which are wrapped around the main body of the chamber.

One crucial parameter in the CVD growth of diamond is the temperature of the substrate (see chapter 2). If gas activation is achieved by a hot filament, its temperature is another important parameter. Measurement of the substrate temperature was carried out with a thermocouple embedded in the substrate holder which will be described below.

The measurement of the filament temperature involved the use of two pyrometers, a disappearing filament (Pyrometer Instrument, Micro-Optical pyrometer,

λ=0.65 μm) and a two-color pyrometer (IRCON Modline Plus, R series, λ_1=0.97 μm, λ_2=1.08 μm). The working temperature ranges are from 700-3200 °C and 900-2400 °C for the disappearing and the two-color pyrometer, respectively. In order to understand the principles of operation and to illustrate why this technique was chosen a short digression is necessary.

The disappearing filament pyrometer is essentially a low power telescope with a red filter (usually centered at 0.65 μm). The filament of a vacuum lamp is mounted in the focal plane. To measure the temperature of a glowing object it is viewed through the telescope and by varying the lamp current the filament can be made to glow with the same brightness as the target, or in other words the filament "disappears" into the target. The lamp current can be calibrated as a function of target temperature by using a blackbody of known temperature as a reference. Although the pyrometer is thus calibrated in terms of blackbody temperature it can be used for non-blackbodies as well, provided the target's spectral emissivity ε is known. With the aid of Planck's law for blackbody radiation one can derive a relationship between the "brightness" temperature T_b, indicated by the pyrometer, the "true" temperature T_t of the target, and the spectral emissivity ε:

$$\frac{1}{T_t} - \frac{1}{T_b} = \frac{\lambda}{C_2} \ln \varepsilon \qquad (4.1)$$

where $C_2 = hc/k_B = 1.438$ cm K and ε is a function of λ and T. T_b represents the fact that the radiation in a small interval at λ from a blackbody at temperature T_b is equal to that from a non-blackbody of emissivity ε at temperature T_t.

The two-color pyrometer utilizes the "color" of a glowing object to measure its temperature. The color temperature T_c of a non-blackbody is the temperature at which a blackbody needs to be operated so that its radiation will match the *visual color* of the source under investigation (Harrison 1960). By taking the ratio of powers radiated

from an incandescent body at two adjacent wavelengths λ_1 and λ_2 ($\lambda_1 < \lambda_2$), one obtains the following expression for T_c:

$$\frac{1}{T_t} - \frac{1}{T_c} = \frac{\ln \varepsilon_1/\varepsilon_2}{C_2\,(1/\lambda_1 - 1/\lambda_2)} \qquad (4.2)$$

where ε_1 and ε_2 are the emissivities at the wavelengths λ_1 and λ_2, respectively. In the visible region of the spectrum ε is a slowly decreasing function of wavelength for most common materials so that the ratio $\varepsilon_1/\varepsilon_2$ is very close to unity. It is therefore justified to approximate T_c by T_t. This method offers an elegant solution for measuring the temperature of a body whose spectral emissivity is not known. In addition, pyrometry allows measurements which do not interfere with the setup inside the chamber and guarantees fast, accurate temperature determination. By utilizing a disappearing filament and a two-color pyrometer simultaneously, we were able to determine the spectral emissivity of a hot filament in the reaction chamber by using Eq. (4.1) and thereby obtain important results concerning its interaction with the reactant gases. These interactions will be discussed in more detail in chapters 5 and 6.

The substrates on which the diamond films were deposited were mounted on the top surface of a round 2.75" diameter molybdenum plate and held in place by a molybdenum mask. A schematic drawing of the substrate holder is shown in Fig. 4.2. Heating of the substrates to ~800 °C is accomplished by an ARI Aerorod heater which cannot be operated at temperatures exceeding 1000 °C. Because of this limitation it was essential to keep heat losses due to conduction and radiation at a minimum. The design of the sample holder required as little material and as small an area as possible.

The heater is wound in a spiral and sandwiched between two Mo plates. Grooves in the top (~1.5 mm thick) and bottom (~1 mm thick) plates help accommodate the heater and guarantee excellent thermal contact between the heater and the plates. Alternating current from a VARIAC transformer (General Radio Co.) is supplied to the heating

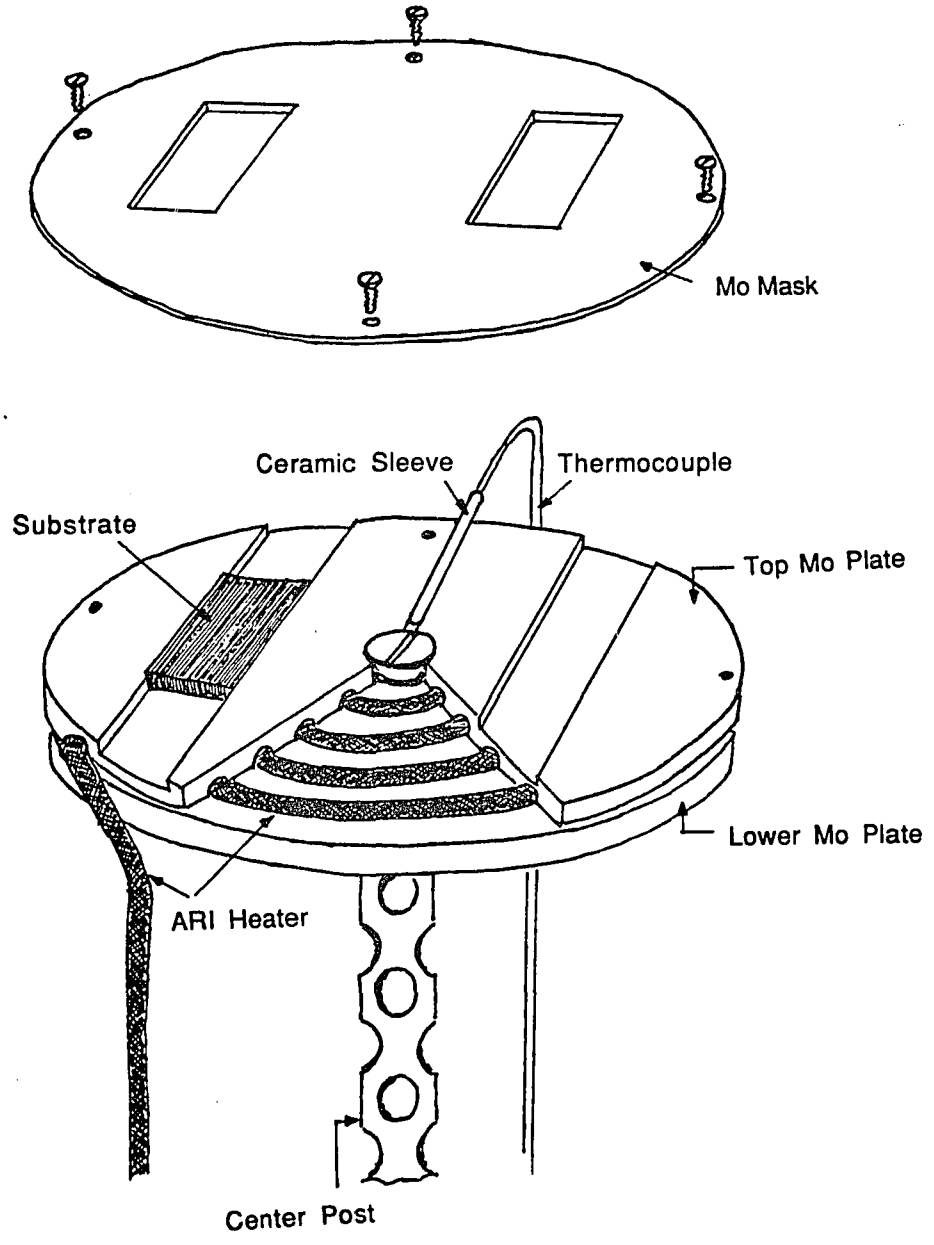

Figure 4.2 Schematic drawing of substrate holder assembly with cutaway showing heater.

element. The support for the holder assembly is made from a piece of 1/4" SS tubing with holes to eliminate excess material and improve thermal isolation. Two substrates with typical dimensions of 0.75"x 0.5"x (0.012-0.016") can be accomodated next to each other (~0.5" apart) on the top surface of the holder. When the mask which has two rectangular openings, slightly smaller than the substrates, is screwed down on the holder, the substrates are held in place tightly and are in excellent thermal contact with the heatable Mo plate. Between the two substrates there is a recessed shielded chromel-alumel thermocouple, isolated electrically by a ceramic sleeve. It was used to determine the temperature of the substrate. Substrate holder, thermocouple, and heater are attached to an 8" SS Conflat flange which provides both mechanical support and electrical contact and are introduced into the chamber from the side.

Inserted into the chamber from the opposite side and thus facing the substrates are the filament fixtures and gas inlet. Fig. 4.3 shows a sketch of the arrangement. The filaments used were made either from 0.010" tungsten (99.9%) or 0.010" rhenium (99.97%) wire. A regulated DC power supply (6274B Hewlett Packard) working in constant current mode provided direct current of up to 15 A for resistive heating. Filaments were formed into coils (~1/8" dia) whose number of turns depended on the type of experiment executed and were suspended vertically in the reaction chamber. For filament studies (see chapters 5 and 6) they consisted of 3-4 turns, while for diamond deposition they could have as many as 12 turns. The filaments were spot-welded to tungsten rods (99.95%, 0.040" dia, ~2.5" long), roughly 2.25" apart, which are then extended by 1/4" copper rods. The gas mixture used in this study entered through a piece of 1/4" SS tubing whose diameter is widened to ~1.5" by a SS funnel. During initial experiments on W filaments gases entered the chamber on the top so that the direction of gas flow was parallel to the filament. Later the direction of gas flow was changed to the present arrangement depicted in Fig. 4.3. Now gases impinge perpendicu-

larly on the filament and the substrate. Note that our experimental results were found to be independent of the direction of gas flow.

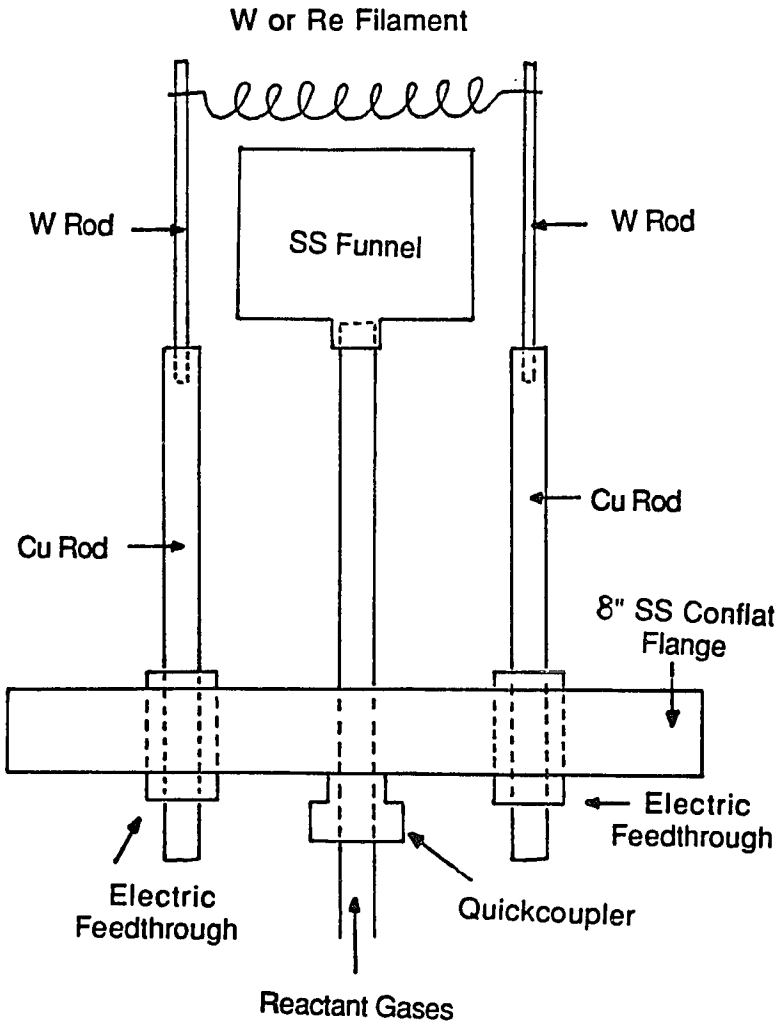

Figure 4.3 Schematic drawing of filament fixtures and gas inlet.

4.2 Substrate Preparation

Silicon was one of our most common substrate materials for diamond deposition, but molybdenum and clear fused quartz also worked. Si substrates were scribed from 2" dia single crystal wafers polished on one side (Texas Instruments). We examined lightly B-doped, both (111) oriented (ρ = 0.015-0.025 Ωcm) and (100) oriented (ρ = 0.015-0.020 Ωcm) crystals.

In chapter 2 we discussed the importance of substrate treatment on diamond deposition. It was pointed out that in order to increase the number of diamond nucleation sites and shorten the induction period, scratching of the substrate is essential. Initially our Si substrates were scratched on a grinding wheel with 6 μm Dupont diamond compound (diamond-oil suspension) for 45-60 minutes. However, this process did not always result in a uniformly scratched substrate surface. At a later stage the Si samples were scratched by hand for ~10 min with the diamond paste applied to a cotton swab. This way microscratches distributed uniformly throughout the substrate could be observed. After scratching the Si substrates they were cleaned ultrasonically in HPCL acetone for ~10 min and then in distilled, deionized water for 5 min. The next step of the cleaning procedure consisted of a gentle boil in transene-100 (Transene Company) for 5 min followed by repeated rinses in boiling distilled, deionized H_2O. Finally the Si samples were dipped into transene-100 at room temperature and were either allowed to dry or were blown dry with nitrogen gas. Since transene-100 is completely volatile it does not leave any residue and is, in that respect, much purer than water.

When molybdenum was chosen as substrate material, 0.75"x0.5" pieces were cut from 0.001" foil (99.9%, A. D. Mackay). Some were scratched with steel-wool or sandpaper, most remained unscratched. The cleaning was essentially identical to the Si substrates, except for the boiling and dipping in transene-100. Clear fused quartz

substrates were scratched with sandpaper and cleaned in the same fashion as Si samples. After this treatment substrates were ready for mounting on the top face of the Mo holder.

4.3 Running the Experiment

Once the substrates were prepared and mounted on the substrate holder, they were introduced into the chamber which was then sealed and evacuated. Since the DP requires fore pressures below ~10^{-3} torr the MP was used for the initial pumpdown starting at 1 atmosphere; the DP and cold trap were isolated. To achieve further evacuation, both DP and MP were pumping via the cold trap line while the roughing line was shut off. It should be noted that water vapor was the main residual gas in the chamber limiting the vacuum. To drive water molecules off the inside walls bakeout was necessary. The stage of water vapor removal could be tested by monitoring the mass #17 (OH^+) and #18 (H_2O^+) peaks of the mass analyzer described above. Fig. 4.4 shows a mass spectrum which was taken after bakeout and with a full LN trap at a final system pressure of 1.2×10^{-7} torr. The #17 and #18 peaks indicate that there was still some water vapor in the chamber, while the ratio of peaks #28 (N_2^+) and #32 (O_2^+) is consistent with the composition of air and thus reveals a small leak.

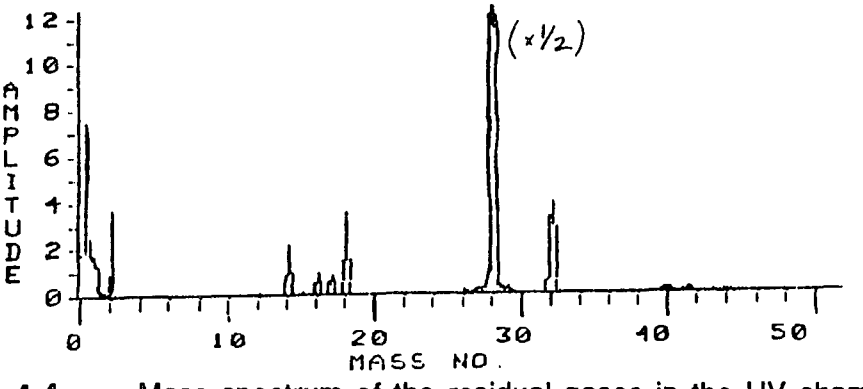

Figure 4.4 Mass spectrum of the residual gases in the HV chamber after bakeout and with a full LN trap at a final pressure of 1.2×10^{-7} torr. The #17 (HO^+) and #18 (H_2O^+) peaks correspond to water vapor, while the ratio of peaks #28 (N_2^+) and #32 (O_2^+) is consistent with the composition of air and thus reveals a small leak.

The present experimental study consists of two parts: filament studies and diamond film deposition. Depending on where our emphasis lies the steps following the above experimental procedure will vary. First, we examine the interactions between hot filaments (W and Re) and gas mixtures that are typical for the diamond growth environment. We have shown (Sommer & Smith 1990b, c) that filaments can serve as high temperature substrates for the deposition of graphitic carbon and that the presence of solid carbon on the filament surfaces will impair their activity. Second, these results are applied to the growth of diamond films via hot-filament-assisted CVD.

4.3.1 Filament Studies

For these experiments the substrate holder assembly was absent from the chamber and the filaments were in the form of short coils, as was pointed out before. Voltage leads were spot-welded to either side of the coiled portion of the filament. The purpose of a four-terminal arrangement (two current and two voltage leads) is to eliminate contributions from leads or contacts to the measured resistance.

Filaments are initially heated to 2400 °C for W and 2200 °C for Re in vacuum and/or pure H_2, and then cooled to room temperature. Before H_2 is allowed into the chamber the main valve is closed and the MKS pressure control system (section 4.1) put into operation. When heated in the presence of H_2, steady state conditions, i.e. constant flow rate (~99 sccm) and pressure, are established before the temperature cycle is performed. The thermal treatment serves several purposes: firstly, contaminants are evaporated from the filament surface, secondly, it helps to stabilize the electrical resistance of the wire at its minimum value, probably due to a recrystallization process (Jansen *et al.* 1989), and thirdly, it is used for calibration of the two-color pyrometer as will be explained below.

Our version of two-color pyrometer (R-series) is furnished with a so-called "e-slope" control, a dial which allows tuning of the measurement circuits to the characteristics of the material under consideration (e.g. type of material and appearance of surface). Values range from 0.8 to 1.15, where unity refers to both a gray- or blackbody. Every time the material is changed, the e-slope of the new material must be determined and the dial reset accordingly. Since the properties of W have been studied extensively, in particular its spectral emissivity $\varepsilon(\lambda,T)$ is well known as a function of temperature and wavelength (DeVos 1954), the two-color pyrometer can be calibrated easily for W. For Re we assume a constant emissivity of ~0.42 (Krikorian *et al.* 1969). If the brightness temperature is measured with the disappearing filament pyrometer and the appropriate value chosen for ε, the "true" temperature T_t can be determined from the expression in Eq. (4.1). The e-slope is then changed until the digital temperature readout from the two-color pyrometer agrees with the value obtained for T_t. Note that the reading from the disappearing filament pyrometer has to be corrected for absorption losses in the glass viewport. Care is taken to ensure that the two pyrometers are aimed at the same portion of the glowing filament, mainly the central region. The e-slope settings for W filaments range from 1.04 to 1.06, for Re filaments they spread from 1.08 to 1.10. We estimate that our temperature measurements are accurate to within ± 20 C°.

After these initial temperature cycles a carbon-containing gas is allowed to flow into the chamber at a constant rate (1 sccm CH_4 or 0.5 sccm C_2H_2 for W, and 1 sccm C_2H_2 for Re) along with 99 sccm H_2, and the filaments are typically carburized at 1900 °C. The stage of carburization is monitored by measuring the resistance of the coiled portion of the filaments. Figure 4.5 shows how the resistance R of a W filament changes as a function of time. Owing to the increase in R, the current through the wire has to be lowered continuously in order to keep the temperature constant. During this conversion of W to W_2C (Moustakas 1989) the filaments expand and deform, no longer holding their

original shape. Surface cracks along the filament axis develop. If the filaments bend, the two-color pyrometer has to be adjusted in order to keep the fill factor for its aperture constant. It is assumed that carburization is essentially complete once R reaches a steady value. W filaments require a carburization time between ~40 and 60 min and their resistances increase by 100%. That this treatment results in a complete conversion of the W to W_2C is confirmed by resistance measurements at room temperature (Barnes 1929). Since Re does not form a carbide, the resistance of Re filaments saturate after approximately 15 min and the increase in R is about 15%.

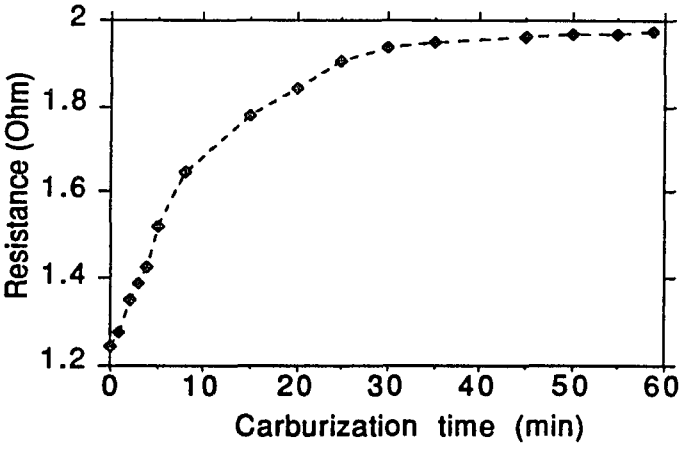

Figure 4.5 Change in the resistance R of a W filament during carburization in a 1% CH_4/H_2 mixture. When R saturates, the conversion of W to W_2C is essentially complete.

Following carburization, the "true" filament temperature, as measured by the calibrated two-color pyrometer, is raised in steps of 25 or 50 C° up to 2400-2500 °C for W and 2300 °C for Re, at which point the temperature path is reversed and the filament cooled to room temperature in steps of 25 or 50 C°. The gas mixture ratio (e.g. CH_4/H_2) is then typically changed and the heating and cooling cycle described above is repeated. During each temperature cycle the following quantities are carefully measured: The current I flowing through the filament, the voltage drop V across the coiled portion of the filament, the partial pressures of the relevant gases in the reaction

chamber (H_2, CH_4, C_2H_2, and in the presence of oxygen also H_2O, CO, O_2, and CO_2), and of course the temperature of the filament (T_b and T_t). The resistance R = V/I, the power consumption P = V I, and the spectral emissivity ε (via Eq. 4.1) can then be easily determined.

4.3.2 Diamond Deposition

When our goal was to grow diamond films, two substrates, typically one Si and one Mo sample, were prepared and mounted as described in the preceding section. Prior to deposition, the pressure inside the chamber is reduced to approximately $2x10^{-7}$ torr by carrying out the above evacuation procedure. Then a constant flow of H_2 (97-99 sccm) is established and the pressure inside the chamber maintained at a preset value (typically 25 torr). Alternating current is supplied to the ARI heater and the temperature of the substrates, T_s, monitored via the thermocouple output. When $T_s \approx 600$ °C the carbon-containing gas is introduced into the reaction chamber at a constant rate (0.5-1.5 sccm C_2H_2 or 1-3 sccm CH_4) and the filament is slowly heated to the desired temperature (2000-2300 °C) and condition (e.g. no graphitic carbon on its surface). Due to irradiation by the hot filament and energy carried towards the substrates by gas molecules, T_s will increase and it is necessary to adjust the heater current until T_s reaches the desired value. Actually, when the filament is at 2300 °C, the minimum substrate temperature attainable (without substrate cooling) lies near 700 °C. The time at which both filament and substrate temperatures have stabilized is defined as the starting point of the deposition process.

The first indications of a growing film typically appeared after ~3-4 hours on the Si samples and correspond to a change in their spectral emissivity. Deposition times stretched from 6 to 8 hours during which the process parameters were checked

periodically (every 30-45 min). Owing to the radiation from the hot filament, the walls of the reaction chamber reach temperatures well above 100 °C.

Upon completion of the deposition process, the valve to the carbon source is closed and the substrate heater turned off. Then the temperature of the filament is decreased slowly to avoid abrupt contraction and thereby prolong the lifetime of the filament. After closing the valve to the H_2 cylinder, the entire system, consisting of chamber and gas delivery lines, is pumped out via the gas disposal system. When the system pressure is in the low militorr range, the exhaust control valve is closed and the main valve to the DP and cold trap line opened. Finally, the Roots pump and backing pump are turned off and backfilled with nitrogen to atmospheric pressure. Backfilling with N_2 prevents water and other condensable vapors from entering the pumps where they adhere to vanes or impellers and impair the performance of the pumps. Generally, the gas delivery system is sealed off and kept under vacuum when not in use.

4.4 Characterization of Deposit

After deposition the chamber is allowed to cool to room temperature, usually overnight, before it is backfilled with nitrogen to atmospheric pressure. As soon as the samples are removed, the chamber is sealed off and evacuated to keep contamination from the laboratory environment at a minimum.

After 6-8 h of deposition, the substrates are typically coated with a "greyish" looking film, and sharp boundaries between masked and exposed areas are clearly visible. In the optical microscope (UNITRON TMD 1783) at a magnification of x400, the deposit is identified as consisting of single particle populations whose densities depend on the growth parameters (mainly T_s and r_C=C/(C+H)). However, to obtain more information about the structure of those single particles, a higher magnification is required. Before the deposit can be characterized in the scanning electron microscope

(SEM) the backsides of the substrates are glued onto small (0.5" dia) aluminum stubs with conducting silver paint. Then the samples have to be coated with a thin layer of gold (~100 Å) in order to prevent electrical charge from accumulating on the electrically insulating diamond particles and thereby producing distortion of the images. Up to four samples at one time can be examined in the SEM (Zeiss) which is installed in the science building at City College.

SEM pictures can reveal critical information about the quality of the deposited diamond particles/films. For example, cauliflower-type particles are known to include significant amounts of graphitic carbon. Even when deposited particles seem to exhibit well-defined crystal habits, SEM studies are not conclusive, since these particles could still contain some sp^2-bonded carbon. To completely eliminate any doubts about the quality of the film, it should be examined by Raman spectroscopy. Raman spectra were measured at room temperature with the 4880 Å line of an argon ion laser in a 90^o scattering geometry (i.e. incident at an angle of 45^o) and at relatively low power (~100 mW) on the samples. Since access to the Raman spectrophotometer was limited, only three of our samples were examined.

Chapter 5

Activity of Tungsten and Rhenium Filaments in C-H Mixtures

5.1 Introduction

In chapter 2 we presented some of the techniques which have been successfully employed to grow low pressure diamond from the vapor phase, hot filament-assisted CVD being one of them. The function of the filament is to thermally decompose the source gas molecules into reactive radicals, mainly atomic hydrogen. The importance of atomic hydrogen for successful diamond growth has been discussed before. That hydrogen can be dissociated by hot W filaments was demonstrated by Langmuir and Mackay (1914) at the beginning of this century. In a series of experiments we have analyzed the behavior of W and Re filaments in a carbon-containing environment, such as found in the diamond growth chamber, and have obtained important information concerning their activity. We will provide evidence that a hot filament loses its activity, i.e. its ability to activate the reactant gases, when graphitic carbon is present on its surface. As a matter of fact, we propose that the results of Celii and Butler (1989) who reported significant changes in the H atom signal near a hot filament with varying CH_4/H_2 ratio and filament temperature can be understood in this way. It will also be shown that the results of our experimental study can be interpreted in terms of the thermodynamic quasiequilibrium model for the C-H system which has been discussed in detail in chapter 3.

5.2 Experimental Results and Discussion

In this section we shall present the results of our experimental study which entailed measuring the filament resistance R, spectral emissivity ε, power consumption, and partial pressures in the reaction chamber as functions of filament temperature in various CH_4/H_2 and C_2H_2/H_2 mixtures. In addition, we shall offer explanations for the observed behavior. The experimental procedures and equipment utilized here have been described in great detail in the previous chapter. A few remarks concerning the partial pressures of gases present in the chamber are appropriate. Since H_2 is the main constituent (~99%) of the gas composition in the chamber its partial pressure should remain approximately constant, once the system pressure has attained its preset value. Fluctuations in the partial pressures of CH_4 and C_2H_2 caused by small variations in the total pressure can therefore be greatly reduced if these partial pressures are normalized with respect to that of hydrogen. It is important to recognize that the gas composition measured in the mass analyzer at the top of the chamber is not necessarily identical to the gas composition in the vicinity of the glowing filament. In particular, radicals, such as H, CH_3, or C_2H cannot be expected to reach the analyzer. However, any variations in the gas composition with changing filament temperature do in fact reflect the impact of the filament.

Before we begin our discussion we would like to quickly review the sequence of experimental steps taken. Every filament experiment starts with a temperature cycle in vacuum and/or pure H_2, followed by the carburization process in a C-H mixture. Then the C/H ratio is changed and the T cycle repeated. Since filaments can be expected to behave differently in vacuum or pure H_2 as compared to their operation in CH_4/H_2 or C_2H_2/H_2 mixtures, the two cases will be presented separately below.

5.2.1 Operation in Vacuum and Pure H_2

Figure 5.1 shows the power consumption measured for a W filament both in vacuum up to 2400 °C and in pure H_2 up to 2300 °C at a pressure of 25 torr. Re filaments show very similar behavior. In vacuum, essentially all of the power generated in the filament is radiated to the surroundings. Heat loss due to conduction through the filament supports is negligible. This is confirmed by the observation of a nearly linear relationship between the filament power P and T^4, in accordance with Planck's radiation law ($P = \varepsilon\sigma T^4$). From Fig. 5.1 it is also apparent that additional power is necessary to maintain the filament at a given temperature in pure H_2. The difference in power consumption between vacuum and H_2, $\Delta P = P(H_2) - P(\text{vacuum})$, takes into account all the energy dissipation processes, such as convection, electronic excitations, and dissociation, which are solely due to the presence of the gas. When ΔP is plotted as a function of T in Fig. 5.2, it can be seen that above about 1700 °C a strong increase in power consumption is observed. This is due to the exponentially activated thermal dissociation of H_2 by the filament (Langmuir & Mackay 1914). These results are consistent with a recent careful study by Jansen *et al.* (1989) who also examined the rate of H_2 dissociation for different heater configurations. They found that thin wires were more efficient than sheets.

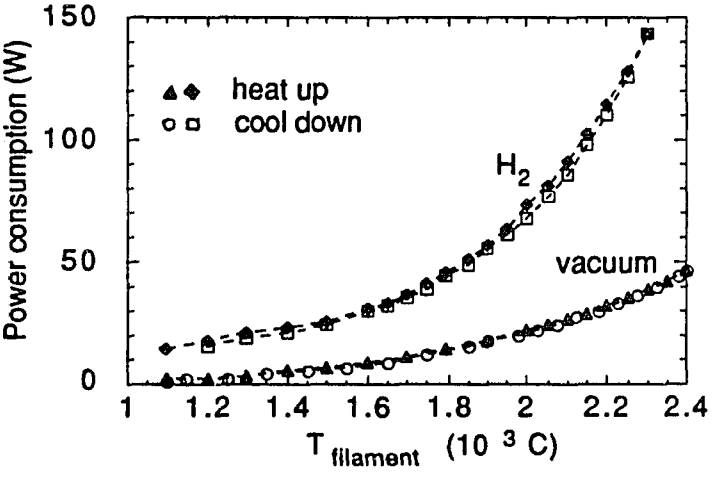

Figure 5.1
Electrical power consumption in a W filament both in vacuum and in 25 torr of H_2 as a function of filament temperature.

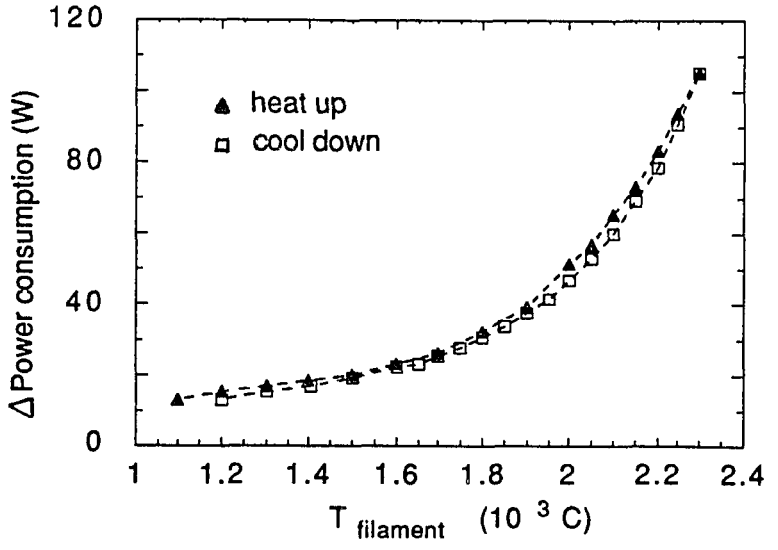

Figure 5.2 Difference $\Delta P = P(H_2)-P(vacuum)$ between the electrical power consumption in H_2 at 25 torr and vacuum for a W filament as a function of filament temperature.

5.2.2 Operation in CH_4/H_2 and C_2H_2/H_2 Mixtures

The behavior of W and Re filaments changes drastically when operated in CH_4/H_2 and C_2H_2/H_2 mixtures as compared with their operation in pure H_2. Since most of the arguments used to explain our experimental results will be valid for both types of filaments (W or Re), we will first focus on the behavior of W filaments and will later point out the important differences observed for Re filaments.

TUNGSTEN FILAMENTS

The variations of ε, R, power consumption, and CH_4 and C_2H_2 partial pressures with filament temperature for 1.5% C_2H_2/H_2 at 9 torr are shown in Fig. 5.3[(a)-(d)] for a W filament. From these experimental results we can deduce that there exist two different regimes of filament operation corresponding to surface-related and gas phase reactions, respectively. These two regimes of operation will be discussed separately below.

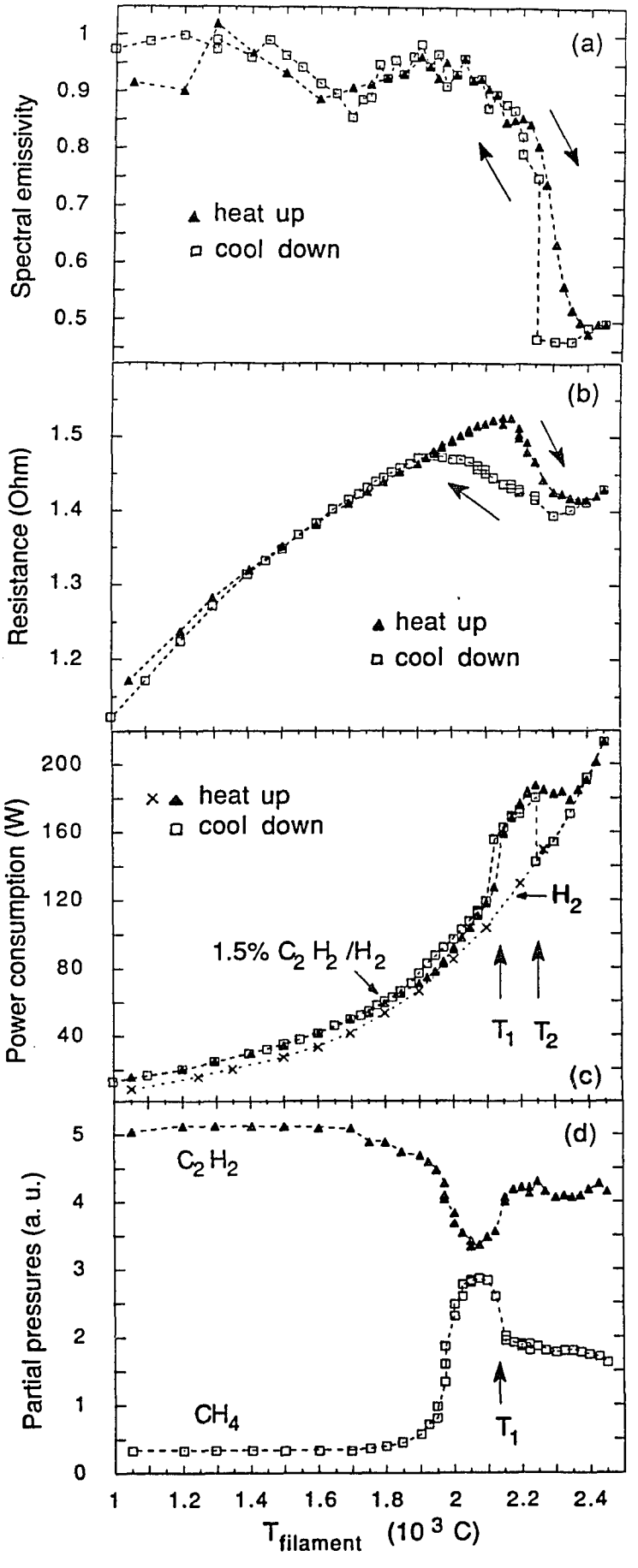

Figure 5.3
Temperature dependences for a W filament of
(a) filament emissivity ε,
(b) filament resistance R,
(c) power consumed in filament, and
(d) partial pressures of CH_4 and C_2H_2 in the reaction chamber. These results correspond to 1.5% C_2H_2/H_2 and P = 9 torr.

a) Surface-related Reactions

After the W filaments have been carburized at 1900 °C in 0.5% C_2H_2/H_2 (or 1% CH_4/H_2) a value of ε between 0.9 and 1 is observed (Fig. 5.3(a)) which is consistent with the presence of a rough layer of graphitic carbon on the filament surface (Toulukian *et al.* 1972). Surface cracks which developed during carburization appear brighter than the rest of the filament. Since these cracks are very small their brightness cannot be matched readily with the disappearing filament pyrometer. We estimate that they have emissivities which are approximately 0.1 higher than the rest of the filament. When T is raised to above 2200 °C in 1.5% C_2H_2/H_2, ε begins to decrease (Fig. 5.3(a)) and at about 2350 °C reaches a value of ~0.5, which is slightly higher than the emissivity of either W or W_2C (~0.45). Since the two-color pyrometer was calibrated for a smooth filament surface, the e-slope setting can be expected to be somewhat different for a rough surface. One should therefore keep in mind that this roughness may affect the emissivities measured here. Based on the above results we infer that a transition to etching of carbon on the filament surface occurs at T ≈ 2200 °C and that the surface of the filament is essentially carbon-free by 2350 °C. This transition can also be observed in Fig. 5.3(b) where the filament resistance actually decreases between 2200 °C and 2350 °C. In addition to removing the graphitic carbon from the surface, etching thus also leads to a partial decarburization of the filament.

When the power consumption in the filament is plotted vs temperature (Fig. 5.3(c)) the transition to a carbon-free surface is again observed. Between 2250 °C and 2350 °C the power dissipated in the filament is seen to decrease with increasing T. This observation is consistent with the decrease in emissivity mentioned above which is caused by the removal of carbon from the surface. According to Planck's radiation law less power is necessary to maintain the filament at a given temperature when ε drops. Abrupt changes with temperature are also observed in the gas phase composition, as can be seen for the CH_4 and C_2H_2 partial pressures, normalized to that of H_2, shown in Fig.

5.3(d). These changes correspond to the conversion of CH_4 to C_2H_2 and occur at a temperature T_1 = 2150 °C. We suggest that these changes are associated with the appearance of active, carbon-free regions on the filament surface. These changes at T_1 = 2150 °C are also reflected by jumps in the filament power consumption which can be seen in Fig. 5.3(c). When regions of the filament surface become carbon-free the activity of the filament increases dramatically and more power then has to be provided in order to decompose the source gases. When the substrate holder was placed about one cm from the filament, the substrate temperature rose significantly (~60 °C) right after the jump in the filament power. This sudden increase in substrate temperature resulted from the energy liberated (which is the binding energy of H_2) by the recombination of hydrogen atoms on the surface of the substrate and serves as additional, albeit indirect, evidence for the enhanced activity of the filament. We note that for 1.5% C_2H_2/H_2, the temperature T_1 = 2150 °C for the jumps in power and partial pressures is somewhat lower than the temperature T_2 = 2250 °C for the onset of the emissivity change. This behavior is typical for W filaments.

When the filament is cooled from 2450 °C to room temperature in steps of 25 or 50 C°, hysteretic behavior is observed (see Fig. 5.3a-c) and the transition back to a carbon-covered surface is shifted to a somewhat lower temperature. Since the filament was partially decarburized towards the end of the heating cycle, carbon atoms will first diffuse back into the bulk before they can accumulate on the filament surface. Hysteresis is typically more severe when the filament is heated in a mixture of 1% CH_4/H_2 or 0.5% C_2H_2/H_2. Due to the smaller arrival rate of carbon at the surface it takes even longer to recarburize the filament. It is probable that we did not wait long enough to achieve complete equilibrium between the gas phase and the filament bulk as the temperature was lowered. In a separate experiment we were able to demonstrate that hysteresis diminishes or even disappears when the temperature cycle is reversed at a

lower temperature, such that excess decarburization of the filament is prevented in the first place.

Figure 5.4 shows how the partial pressures of CH_4 and C_2H_2 vary with filament temperature when the reactant gas mixture consists of 3% CH_4/H_2 at 9 torr. Some conversion of CH_4 to C_2H_2 begins at temperatures as low as 1800 °C. Abrupt changes are observed at T_1 = 2150 °C which is the same temperature as observed for 1.5% C_2H_2/H_2. Thus, it appears that the transition from deposition to etching of carbon on the filament surface is independent of the hydrocarbon used and depends only on the C/H ratio of the reactant gas mixture. We would like to stress that the directions of the changes observed in Fig. 5.3(d) and Fig. 5.4. are in agreement with the QE model which predicts that the production of C_2H_2 is favored over CH_4 at 2150 °C (Figs. 3.2 or 3.3).

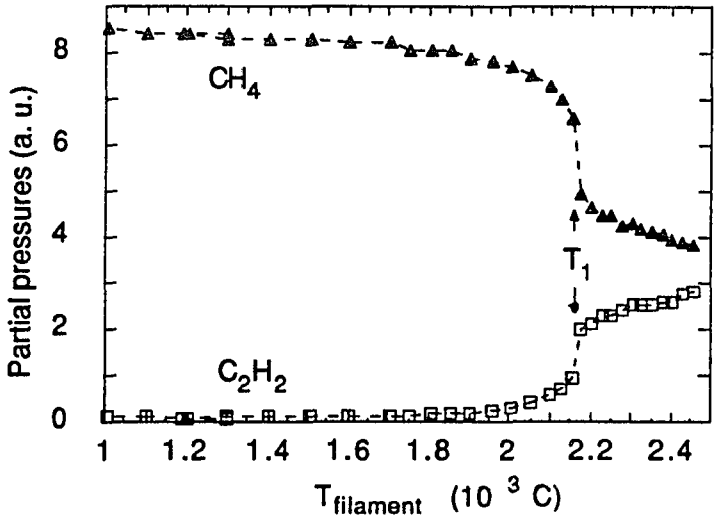

Figure 5.4 Dependences of CH_4 and C_2H_2 partial pressures on increasing W filament temperature for 3% CH_4/H_2 and P = 9 torr.

All of the changes presented so far can be interpreted in terms of the thermodynamic model discussed in chapter 3. Indicated on the C-H phase diagram in Fig. 5.5 are the transition temperatures T_1 which correspond to the jumps in filament power consumption and in partial pressures of CH_4 and C_2H_2. Results are shown for W

filaments (0.7, 1, and 1.5% C_2H_2/H_2 and 2 and 3% CH_4/H_2 at 25 torr; 1.5% C_2H_2/H_2 and 3% CH_4/H_2 at 9 torr) and for Re filaments (0.5, 1, and 1.5% C_2H_2/H_2 and 3% CH_4/H_2 at 25 torr). Values of T_1 obtained for the same r_C (e.g. 1.5% C_2H_2/H_2 and 3% CH_4/H_2 with $r_C \approx 0.0145$) coincide and so are shown by a single symbol. The observation that the same experimental values of T_1 are obtained for 9 and 25 torr, as is apparent from Fig. 5.5, confirms the prediction that in the high temperature regime (T > 1600 °C) the etching-growth boundary of solid carbon is indeed independent of pressure. This is not true when the temperature T_2 at which the emissivity changes abruptly is compared for 9 and 25 torr, as was done at an earlier stage (Sommer & Smith 1990b). One has to realize, however, that sometimes it may be difficult to decide which value to assign to T_2. Results of measured transition temperatures T_1 have been summarized in Table 5.1.

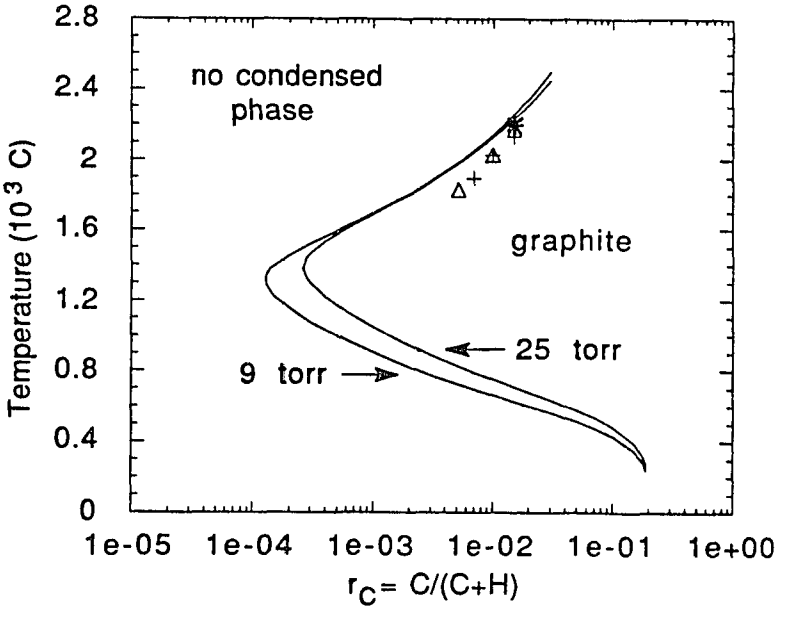

Figure 5.5 Predicted phase boundaries for graphite in the C-H phase diagram for P = 9 and 25 torr. r_C is the carbon atom fraction. Also shown are experimental points corresponding to the temperatures T_1 where jumps in both the power consumption and the CH_4 and C_2H_2 partial pressures were observed. Crosses and triangles refer to the results obtained for W and Re filaments, respectively (see text). The star refers to the temperature where Celii and Butler (1989) measured an abrupt change in the H atom signal near a heated filament for 3% CH_4/H_2 at 25 torr.

Table 5.1 Transition temperatures T_1 for W and Re filaments in various CH_4/H_2 and C_2H_2/H_2 mixtures at 9 and 25 torr. (T_1 is the temperature where jumps in the power consumption and CH_4 and C_2H_2 partial pressures occur).

Pressure	C_xH_y/H_2		T_1 (Tungsten)	T_1 (Rhenium)
25 torr	CH_4/H_2	1.0%	-	-
		2.0%	2000 °C	2025 °C
		3.0%	(2175±25) °C	-
	C_2H_2/H_2	0.5%	-	1825°C
		0.7%	1900 °C	-
		1.0%	(2025±25) °C	(2025±25) °C
		1.5%	(2150±25) °C	(2200±25) °C
9 torr	CH_4/H_2	3.0%	2150 °C	-
	C_2H_2/H_2	1.5%	2125 °C	-

Obviously, the experimental results obtained here for T_1 depend on the carbon fraction r_C in a manner which is consistent with the predictions of the thermodynamic model. On the other hand, the observed phase boundary separating the regions of growth and etching of graphite on the filament surface lies below the predicted curve. A possible explanation for this behavior may be given in terms of thermal diffusion, i.e. the Soret effect. To understand why this is a plausible argument, a short review of the Soret effect is necessary.

According to D. E. Rosner (1980) 'thermal diffusion is important in mass transfer situations whenever both large molecular weight disparities and large temperature gradients coexist.' In other words, when the temperature of a gas mixture is not uniform, then its composition is also not uniform. The driving force is such that heavy

molecules diffuse *down* the temperature gradient, i.e towards colder regions. The above criteria are clearly met in the present situation where the molecular weight of either CH_4 or C_2H_2 is much larger than that of H_2 and where filament temperatures are much higher than wall temperatures. As a result, hydrocarbon molecules are expected to be depleted from the gas phase in the vicinity of the hot filament. Such a depletion will lead to a lower carbon fraction r_C near the filament and will thus favor etching at the expense of the deposition of graphite, in agreement with the results shown in Fig. 5.5.

Also included in Fig. 5.5 is the result of Celii and Butler (1989) for the temperature at which an abrupt change in the H atom signal near a W filament was observed for 3% CH_4/H_2 at 25 torr. Their result is consistent with the results obtained here, confirming that production of H atoms can be enhanced by using filaments with carbon-free surfaces.

Although all filaments show qualitatively identical behavior when operated in different gas mixtures, there exist quantitative differences, in particular with respect to the magnitude of the power jump. It has been observed that the *change* in power consumption at temperature T_1 does depend on the total pressure and the carbon ratio r_C. The magnitudes of the jumps in dissipated power (per unit length) which occur at temperatures T_1 have been summarized for W filaments at 9 and 25 torr and for Re filaments at 25 torr and are plotted vs r_C in Fig. 5.6. It is clear from this figure that the changes in dissipated energy at T_1 increase both with carbon fraction and total pressure. These results can be explained as follows.

While for 1.5% C_2H_2/H_2 (or 3% CH_4/H_2) the power jump occurs at $T_1 \approx 2150$ ^oC, for 0.7% C_2H_2/H_2 it is observed around 1900 ^oC. However, at 1900 ^oC the dissociation of H_2 has barely set in, as can be inferred from Fig. 5.2. The sudden transition from a non-reactive, carbon-covered to a reactive, partially clean filament surface at T_1 is therefore hardly noticeable. Very often, no power jump was observed for 1% CH_4/H_2 or 0.5% C_2H_2/H_2 mixtures. Since T_1 increases with r_C (see Fig. 5.5) and the

thermal dissociation of H_2 is exponentially activated, the magnitude of the power jump grows rapidly with increasing carbon ratio. An increase in the total pressure is equivalent to a larger number of gas molecules striking the filament surface per unit time, according to Eq. (3.13). When the filament becomes reactive at temperature T_1, more molecules will be available for dissociation and more energy can be transferred to the gas. We would like to remark that the magnitudes of power jumps also depend on the total length of the filament. This observation is not obvious from Fig. 5.6, since the magnitudes of power jumps have been stated per unit length. As the filament becomes longer the surface area in contact with the surrounding gas increases and the absolute number of molecules impinging on the surface will become larger.

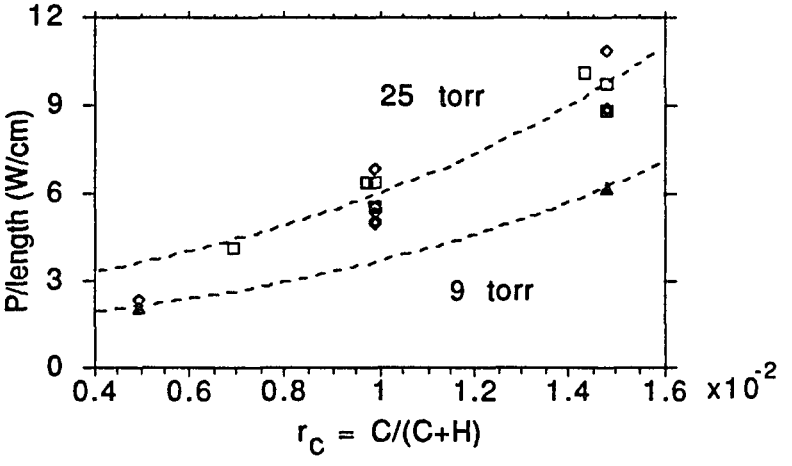

Figure 5.6 Changes in electrical power consumption (per unit length) occurring at temperatures T_1 as functions of carbon atom fraction r_C for P = 9 and 25 torr. The results correspond to W (squares and triangles) and Re (diamonds) filaments heated in various CH_4/H_2 and C_2H_2/H_2 mixtures.

b) Gas Phase Reactions

Upon closer examination of Fig. 5.3(d) it becomes clear that additional important changes are occurring in the CH_4 and C_2H_2 partial pressures for filament temperatures below T_1. We note that between 1700 °C and about 2050 °C conversion of C_2H_2 to CH_4 takes place which is consistent with the results of Wu *et al.* (1990). Since in this

temperature range the filament is carbon-covered and therefore, as we claimed before, non-reactive, these changes must occur in the gas phase surrounding the filament. Additional evidence supporting this viewpoint is presented in Fig. 5.7 where it can be seen that at a higher pressure of 25 torr, conversion of C_2H_2 to CH_4 starts well below 1700 °C for 1.5% C_2H_2/H_2. Since the number of molecular collisions increases with pressure, the probability of gas phase reactions increases also. According to the predictions of our thermodynamic model, reactions producing CH_4 are expected only below ~1200 °C. It seems likely that C_2H_2 molecules are dissociated at or near the surface of the hot filament and that the resulting hydrocarbon fragments (C or CH) then diffuse to regions of lower temperature where CH_4 is formed.

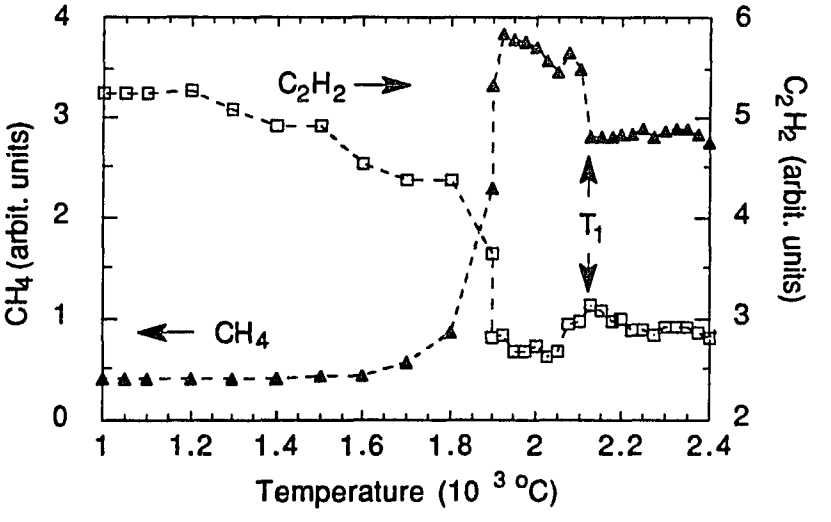

Figure 5.7 Dependences of CH_4 and C_2H_2 partial pressures on increasing filament temperature for 1.5% C_2H_2/H_2 and P = 25 torr.

RHENIUM FILAMENTS

Let us now turn our attention to Re filaments. We will describe and explain their behavior in various gas mixtures and will point out similarities and important differences as compared to W filaments. In Fig. 5.8(a) we present the temperature-dependences of the emissivity ε for an initially carbon-covered Re filament in pure H_2

and in a 1.5% C_2H_2/H_2 mixture at 25 torr. When the filament is heated in pure H_2, ε drops rapidly from ~0.8 to ~0.4 over a very narrow temperature range, starting at $T_2 \approx 1750$ °C. In the 1.5% C_2H_2/H_2 mixture ε also starts to decrease at approximately 1800 °C, but the Re surface in this case does not reach ε~0.4 until a much higher temperature, close to 2200 °C. Between $T_2 = 1750$ °C and 2200 °C dark and bright patches coexist on the filament surface, corresponding to regions of low (~0.4) and high (~1.0) ε. Typically, the temperature profile of the filament is quite uniform over the coiled part but falls off towards the ends due to heat conduction to the clamps. When the filament temperature is increased, small regions of low ε appear just above $T_2 = 1800$ °C. These regions then spread from the center outward until they comprise the entire filament surface at about 2200 °C. This behavior has been observed previously (Pallmer *et al.* 1980) for Re and is consistent with an inhomogeneous surface consisting of carbon-free (ε~0.4) and carbon-covered (ε~1.0) regions. In this case we are not able to use the disappearing filament pyrometer for temperature measurements since the brightness of the Re surface is ill-defined. Also, the two-color pyrometer readings of T_t cannot be trusted in this region and so it is not possible to use Eq. (5.1) to obtain even an average ε. For this reason, experimental results have been omitted in Fig. 5.8 between ~1800 and ~2200 °C.

In order to explain these observations, we propose that as the filament temperature is increased to T_2, carbon present on the surface of the Re filament begins to diffuse into the bulk. This is in agreement with the Re-C phase diagram (Elliot 1965) which indicates that the solubility of C in Re (~4-6 atomic %) increases with T in this range. In pure H_2 the surface carbon diffuses rapidly into the bulk and a low ε surface is generated quickly (see Fig. 5.8(a)). On the other hand, in the 1.5% C_2H_2/H_2 mixture surface carbon is replenished by dissociated C_2H_2 molecules and the transition to a surface with low ε extends up to 2200 °C. Finally, at 2200 °C the etching of surface

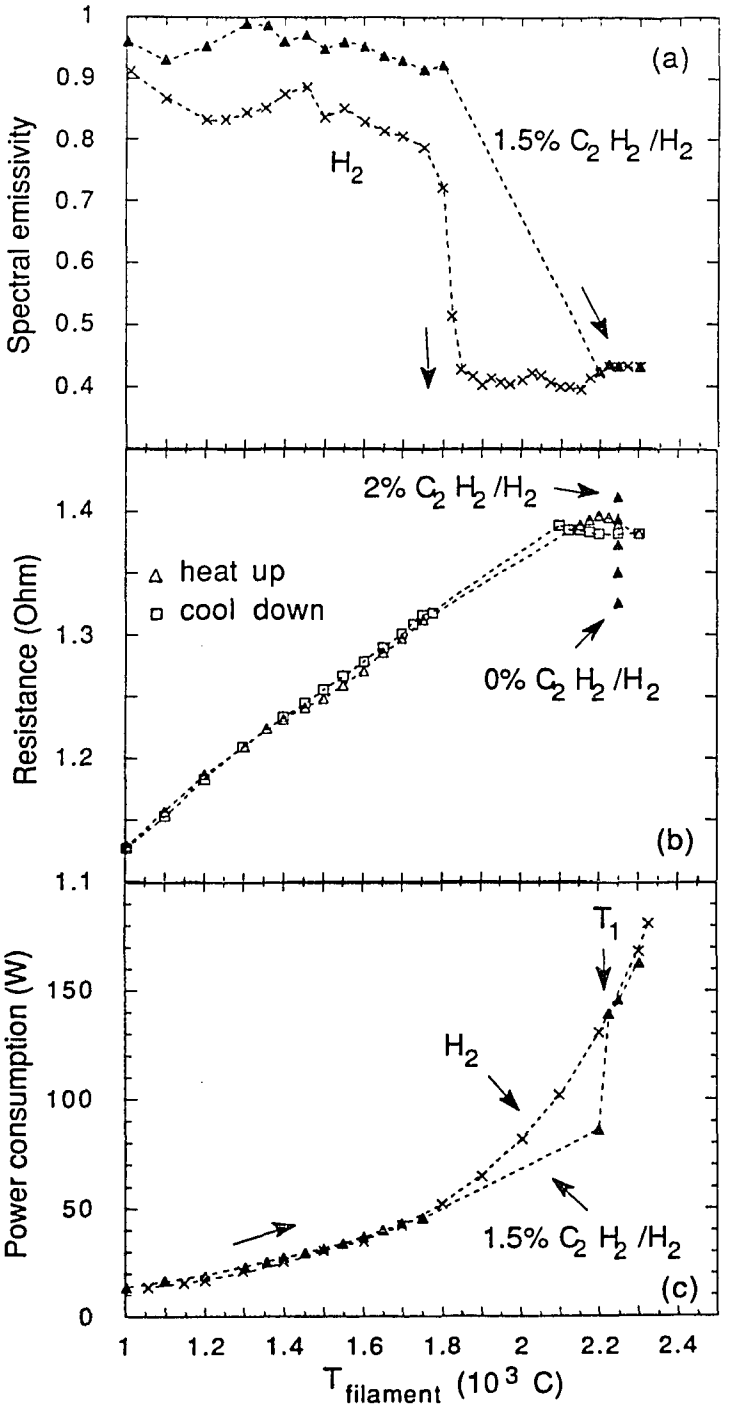

Figure 5.8 (a) Spectral emissivities of initially carbon-covered Re filaments in H_2 and 1.5% C_2H_2/H_2 at 25 torr as functions of increasing filament temperature. (b) Resistance of a Re filament in 1.5% C_2H_2/H_2 at 25 torr as a function of filament temperature. Also shown are values of R (solid triangles) at T = 2250 °C corresponding to C_2H_2/H_2 ratios of 0, 0.5, 1, 1.5, and 2%. (c) Power consumptions in a Re filament both in H_2 and 1.5% C_2H_2/H_2 at 25 torr as functions of increasing filament temperature.

carbon by atomic H dominates the deposition of carbon and the Re surface reaches a state with low ε. Ignoring all other features in Fig. 5.8(c) we focus on the jump in dissipated filament power near 2200 °C. This temperature is indeed equivalent to the temperature T_1 obtained for a W filament in a 1.5% C_2H_2/H_2 mixture (Fig. 5.3(c)). For $T > T_1$ Re filaments are seen in Fig. 5.8(b) to decarburize in the same manner as was observed for W filaments. We would like to add that the temperature dependences of the CH_4 and C_2H_2 partial pressures in the reaction chamber are almost identical to the ones depicted in Fig. 5.3(d), and have therefore been omitted.

The similarities that exist between Re and W filaments are remarkable. The temperature-dependences of their resistances R (Figs. 5.3(b) and 5.8(b)) and of the CH_4 and C_2H_2 partial pressures, the temperatures T_1 for the jumps in power and partial pressures (Fig. 5.5), and the magnitudes of the power jumps (Fig. 5.6) show very similar behavior for both types of filaments. There are, however, some differences between W and Re filaments. Deviations concerning their emissivities have already been pointed out above. Below we will analyze the power consumptions for W and Re in more detail.

Upon comparison of Figs. 5.3(a) and 5.8(a) we note that the transition from high ε to low ε occurs over a narrower temperature range for carbon-covered W filaments than for Re. Since W filaments have been completely carburized, i.e. saturated with carbon, at the outset of the experiment, further diffusion of carbon from the surface into the bulk is unlikely. Instead, as proposed above, removal of carbon from the surface of the W filament is accomplished via etching by atomic hydrogen.

Let us now take a closer look at Fig. 5.8(c), where the power consumption for a Re filament is shown in pure H_2 and in a 1.5% C_2H_2/H_2 mixture at 25 torr, and compare it with the equivalent figure for W, Fig. 5.3(c). If the power consumption in H_2 is used as reference, since there the filament activity is not limited by surface carbon,

we can draw interesting conclusions about the energy dissipated in a hydrocarbon-hydrogen mixture for both types of filaments.

When the filament temperature is raised in a 1.5% C_2H_2/H_2 mixture at 25 torr to slightly below T_1 for W, or slightly below T_2 for Re, a layer of graphitic carbon will be present on the filament surfaces and the emissivities will be higher (ε~1.0) than in H_2 (ε~0.45). Therefore more energy will be radiated to the surroundings. On the other hand, the presence of carbon on the surfaces severely limits the activity of the filaments so that less energy will be transferred to the gas. As a net result the power consumption in the C_2H_2/H_2 mixture tends to be about equal to the power consumption in pure H_2. For $T_1 < T < T_2$, W filaments are reactive *and* have an emissivity close to unity (only small patches are C-free). This leads to a power consumption which is much higher than in pure H_2. Between T_2 and T_1 Re filaments have emissivities which are dropping continuously, but they have not regained a reactive state yet. Consequently, Re filaments consume less power as compared to their operation in pure H_2. When $T > T_2$ for W, or $T > T_1$ for Re, the surface carbon has completely disappeared, resulting in ε~0.4, and the filaments are reactive. The same amount of energy is then dissipated in C_2H_2/H_2 mixtures and H_2. The main difference between W and Re filaments with respect to their emissivities and power consumption hence manifests itself in the position of T_2 with respect to T_1: while for Re T_2, the temperature at which ε starts dropping rapidly, lies *below* T_1, the temperature at which the power jump occurs, for W T_2 is found to lie *above* T_1.

It is somewhat surprising that the Re filaments remain inactive for $T_2 < T < T_1$, which is the region where its surface is "patchy". Even though there exist regions with low ε on the Re filament surface for $T < T_1$, apparently the concentration of carbon remaining on the surface is high enough to block the active sites for dissociation of the reactant molecules. Only when etching by atomic H dominates, leading to a significant reduction of the carbon on the surface, can these active sites be kept free of carbon. That

the properties of refractory metal surfaces are extremely sensitive to surface contamination has been demonstrated previously by Bettler *et al.* (1974). They examined the surface self-diffusion of W atoms in the presence of carbon on the W surface. Below a critical temperature T_c this self-diffusion process becomes severely limited which has been attributed to C atoms at special surface sites. Only when the temperature is raised above the critical value will the C atoms leave the surface.

Another interesting observation concerns the emissivity of Re filaments after carburization. While W filaments are carbon-covered with ε~1.0 following carburization in C_2H_2/H_2 mixtures, typically at 1900 °C, Re filaments maintain a low ε~0.4 under the same conditions. We propose that once the bulk of a Re filament is carburized to a level of 4-6 at. % , the active sites on the filament surface are quickly blocked so that any further decomposition of C_2H_2 leading to a surface layer of carbon with ε~1.0 is suppressed. We note, however, that a surface layer of carbon can be produced on Re when carburization occurs below T_2, i.e. at 1700 °C in pure C_2H_2 at 0.25 torr.

In a separate experiment we examined the resistance R of a Re filament and its dependence on the C_2H_2/H_2 ratio for $T > T_1$. The outcome of this study will be presented below. First, the filament is heated to 2250 °C in a 1.5% C_2H_2/H_2 mixture at 25 torr and the resistance R allowed to saturate. When the C_2H_2/H_2 ratio is now lowered, R will stabilize at a new, lower value. As a matter of fact, the resistance of the Re filament, and hence the level of carburization, can be *reversibly* changed by varying the carbon fraction, with higher values of R corresponding to higher C_2H_2/H_2 ratios. Values of R corresponding to 0, 0.5, 1, 1.5, and 2.0% C_2H_2/H_2 mixtures have been included in Fig. 5.8(b). The above behavior indicates that there exists a dynamic balance between the following quantities: 1) the carbon fraction r_C in the gas phase, 2) the concentration of carbon in the filament bulk, and 3) the concentration of carbon on the filament surface. It should be noted that at T = 2250 °C the filament surface can have different appearances, from C-free to "patchy" and then to C-covered, depending on the C_2H_2/H_2

ratio. For example, the Re filament can be completely decarburized in pure H_2 in a few minutes. On the other hand, a surface layer of carbon can exist on the filament surface when the C_2H_2/H_2 ratio is high enough. This behavior is consistent with the predictions of our thermodynamic model (see Fig. 5.5).

5.3 Conclusions

Since thermally activated diamond CVD remains popular among scientists it is essential to understand filament-related processes in the deposition chamber. In particular, one wants to know when the filaments are most effective in generating reactive radicals. We have shown that the activity of the W and Re filaments, i.e. their ability to dissociate the reactant gases, can be demonstrated most clearly by measuring the filament power consumption and partial pressures of CH_4 and C_2H_2 in the reaction chamber. All of these quantities undergo sharp jumps at the same well-defined temperature, T_1, which is essentially independent of the type of filament (W or Re), hydrocarbon (CH_4 or C_2H_2), or pressure (9 or 25 torr), but which do depend on the carbon fraction r_C of the reactant mixture. We have demonstrated that the jumps in power consumption and partial pressures are related to transitions between deposition and etching of carbon on the filament surface, and that the observed transition temperatures T_1 can actually be predicted by our thermodynamic model. Filament resistance measurements which are used to monitor the level of carburization of the filaments indicate that decarburization begins for $T > T_1$. Emissivity measurements reveal the presence of solid carbon on the filament surfaces. Dramatic changes in ε are observed when the removal of surface carbon sets in at temperature T_2. T_2 does in general not coincide with T_1 and differs for W and Re filaments, reflecting the different solubilities of C in W, W_2C, and Re. Evidence for gas phase reactions and for the importance of thermal diffusion (the Soret effect) have also been presented. Our results

are also consistent with the observations of Celii and Butler (1989). On the basis of our measurements we suggest that the optimum conditions for filament-assisted diamond deposition will require that the filament surface is free of carbon and hence most active. To monitor the carbon-coverage and activity of the filament surface, all one has to do is simply measure filament resistance, emissivity, and power consumption.

It is clear from the experimental results presented above that Re filaments have an important advantage over W filaments for use in the CVD of diamond. When W reacts with C to form W_2C, its volume and shape changes significantly, and it becomes very brittle. Re is clearly superior since it does not form a carbide and is therefore less fragile. It expands only slightly and holds its shape. Jansen *et al.* (1989) have developed techniques to overcome the problem of volume expansion, e.g. by using straight wires mounted under tension. Since Re filaments typically outlast W filaments by many hours of operation, the higher costs of Re can be easily offset.

Chapter 6

Activity of Tungsten Filaments in C-H-O Mixtures

6.1 Introduction

There have been numerous reports in the literature recently about the effect of adding oxygen to the diamond growth environment. It has been demonstrated that improvements in the growth of diamond films for both the hot-filament and microwave-assisted CVD techniques can be achieved with a variety of oxygen-containing gases, either separately (CH_3OH/H_2, CO/H_2, etc.) or added to the CH_4/H_2 mixture (see chapter 2). Higher growth rates and growth of diamond at lower temperatures have been reported (Chang *et al.* 1988, Liou *et al.* 1990). Some of the effects attributed to the presence of oxygen which could help explain the above observations include: 1) a strong increase in the mole fractions of atomic hyrdogen and other radicals, such as OH (Mucha *et al.* 1989), 2) a change in the characteristics of a carbon surface through the formation of an oxide complex (Cao & Back 1985), 3) the removal of non-diamond carbon from the substrate surface, and 4) the reduction of hydrocarbon mole fractions by converting them to (mainly) CO and H_2 (Kawato & Kondo 1987, Harris & Weiner 1989, Sommer & Smith 1990c, 1991). Unfortunately, our experimental arrangement does not allow the direct measurement of radical concentrations or a detailed surface

analysis, but we can obtain important information about the effect of O_2 on both the gas composition in the diamond deposition chamber and the activity of the filament.

From our thermodynamic analysis of the C-H-O system which has been introduced in chapter 3, we know that oxygen does have a significant influence on the C-H phase diagram. Calculated rates of evaporation and deposition of solid carbon for different C-H-O mixtures as well as the corresponding phase diagrams have been presented in section 3.7.1. We have predicted and verified experimentally, as will be shown below, that oxygen reacts readily with solid carbon to form (mainly) CO, thus leading to a reduced stability region of solid carbon. The results of our experimental study which has focused on the interactions of a W filament with various C-H-O mixtures will be presented and discussed in the following section.

6.2 Experimental Results and Discussion

In the preceeding chapter we have demonstrated that with simple measurements of filament resistance R, spectral emissivity ε, and power consumption one could gain crucial information about the activity of W and Re filaments heated in various C-H mixtures. To determine the effect of oxygen on filament activity, W filaments have now been heated to 2300 ^{o}C in mixtures of 3% CH_4/H_2 with varying amounts of O_2 (0.5, 1.0, and 1.5%) at a pressure of 25 torr. The experimental setup used in this extended study is identical to the one described in chapter 4. Since the experimental procedures also remain unchanged, they will only be briefly summarized: Each filament experiment consists of an initial temperature cycle in vacuum and/or flowing hydrogen, followed by a carburization process and repeated heating/cooling cycles in varying gas mixtures. During each T cycle the resistance R, spectral emissivity ε, power consumption, and partial pressures of the stable gases (H_2, CH_4, C_2H_2, O_2, CO, and H_2O) in the reaction chamber have been carefully monitored.

It will become clear that most of the arguments which have been used to explain the behavior of filaments in C-H mixtures (chapter 5) also apply to their behavior in C-H-O mixtures, and so they will not be presented again in great detail. For example, results concerning filament resistances will be omitted from the following discussion since they look almost identical in C-H and C-H-O mixtures. One should keep in mind, however, that resistance measurements can provide useful information about the level of carburization of the filament, as we have learned in the previous chapter. We would like to add that this discussion will be limited to the use of W filaments in $CH_4/H_2/O_2$ mixtures, but that Re filaments have been found to show essentially the same behavior.

Figure 6.1[(a)-(c)] illustrates how the spectral emissivity ε of W filaments varies with temperature in a gas mixture consisting of 3% CH_4/H_2 and 0, 0.5, 1, and 1.5% O_2. When filaments are heated in a mixture of 3% CH_4/H_2 with no oxygen present (Fig. 6.1(a)), a value of ε between 0.9 and 1.0 is observed for temperatures up to 2250 ^oC which is consistent with the presence of a layer of graphitic carbon on the filament surface. When T is increased above 2250 ^oC, ε begins to decrease rapidly and at about 2350 ^oC reaches a value of ~0.5. This is identical to the behavior shown in Fig. 5.3(a) where a W filament had been heated in a 1.5% C_2H_2/H_2 mixture. Again, surface roughness may affect the emissivities measured here. Upon addition of 0.5% O_2 to the 3% CH_4/H_2 mixture this decrease in ε is again observed, but it begins at a somewhat lower temperature, 2150 ^oC. A low ε value is established above 2300 ^oC. It is apparent from Fig. 6.1(c) that between 2050 and 2150 ^oC this same transition from a high (~1.0) to a low (~0.55) ε also occurs for a mixture of 1% O_2 and 3% CH_4/H_2. These results indicate clearly that a transition from deposition to etching of carbon takes place on the filament surface and that this transition is shifted towards lower temperatures when O_2 is added to the mixture.

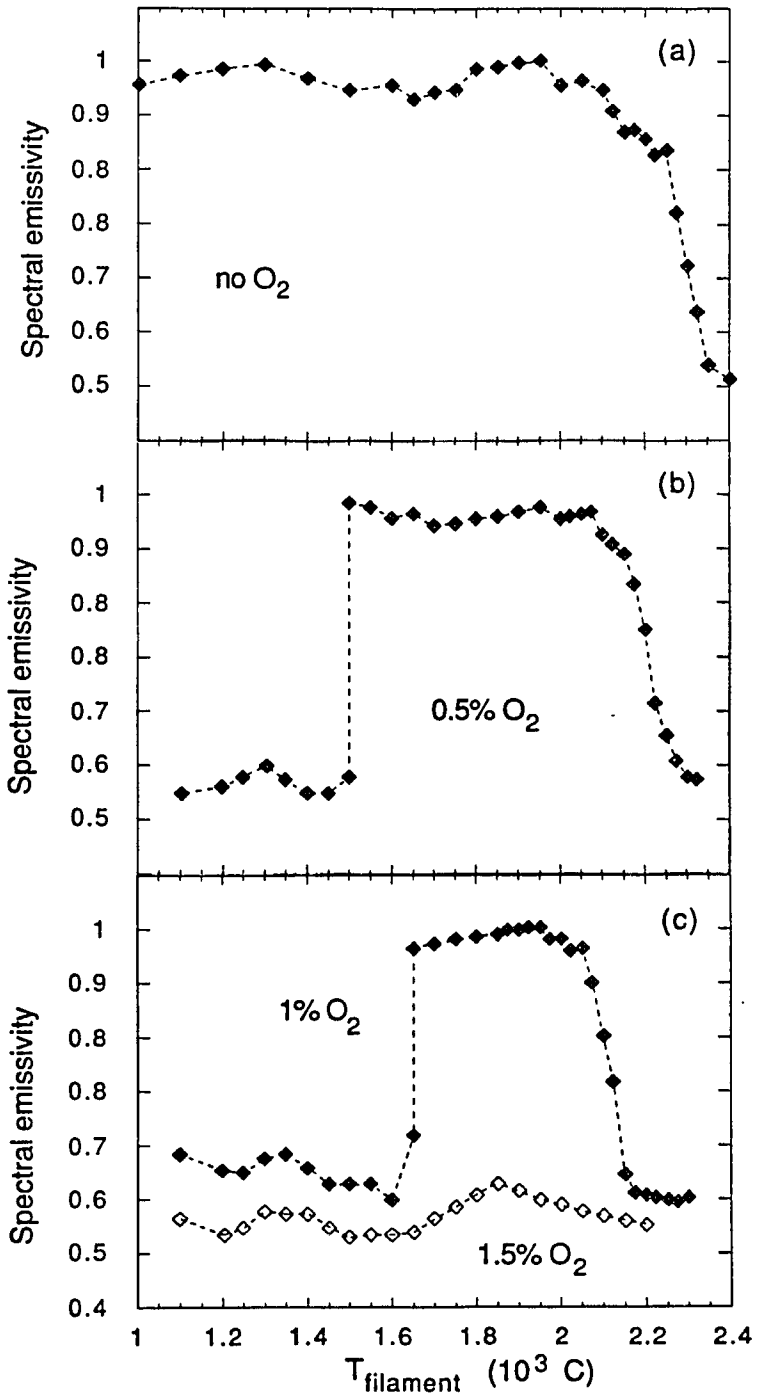

Figure 6.1 Spectral emissivities as functions of increasing filament temperature for a W filament in a mixture of 3% CH_4/H_2 at 25 torr and varying amounts of O_2: (a) 0%, (b) 0.5%, (c) 1 and 1.5% O_2.

It is important to note that additional transitions in ε are observed at temperatures of ~1500 and ~1600 ^{o}C in Figs. 6.1(b) and 6.1(c), respectively. Below these temperatures the thermally-activated dissociation of CH_4 molecules is incomplete and only a small fraction of the incoming CH_4 molecules deposit carbon atoms on the filament surface. Since oxygen is very reactive towards carbon, any carbon that is present on the filament surface will be rapidly removed via the formation of CO. Only when the filament temperature is high enough to dissociate sufficient CH_4 and when all of the incoming oxygen has been completely converted to CO can a layer of graphitic carbon form on the filament surface. When 1.5% O_2 is mixed with 3% CH_4/H_2, the emissivity remains at a low value (~0.55) throughout the whole temperature range (Fig. 6.1(c)) which is consistent with a C-free filament surface. This mixture results in a C/O ratio equal to unity and our thermodynamic model predicts that no solid carbon can be deposited in this case. The above results indicate that there exists a competition between the deposition of carbon from CH_4 and its subsequent removal as CO via etching by O_2 which determines whether the filament surface is carbon-covered or free of carbon. In this case (Fig. 6.1(c)), sufficient oxygen is available to keep the filament surface clean even when all the incoming CH_4 is dissociated. This behavior will be encountered again in Fig. 6.5.

When the power consumption in the W filament is plotted vs. temperature for a mixture of 0.5% O_2 and 3% CH_4/H_2 in Fig. 6.2 we notice, ignoring the feature at 1500 ^{o}C for now, the striking resemblance with Fig. 5.3(c), which is the equivalent figure in the absence of oxygen. In analogy to C-H mixtures (chapter 5) we propose that the large jump in the filament power consumption for $T_1 \approx 2050$ ^{o}C is due to the appearance of C-free patches on the filament surface. When regions of the filament surface become "clean", the activity of the filament increases dramatically and more power has to be supplied for the activation of the reactant gases. Note that essentially the same value for T_1 was obtained when a Re filament was heated in a mixture of 0.5% O_2 and 3% CH_4/H_2.

Starting at a temperature $T_2 \approx 2175^oC$ the power dissipated in the filament actually decreases with increasing temperature. This decrease is related to the decrease in ε (Fig. 6.1(b)) and the removal of carbon from the surface. As in chapter 5, this behavior can be explained on the basis of Planck's radiation law: When ε drops, less energy is radiated to the surroundings and less power is therefore necessary to maintain the filament at a given temperature. Although this investigation has been limited to W filaments, we know from other experiments (chapter 5) that, while T_1 is typically less than T_2 for W filaments, the opposite is true when Re filaments are used.

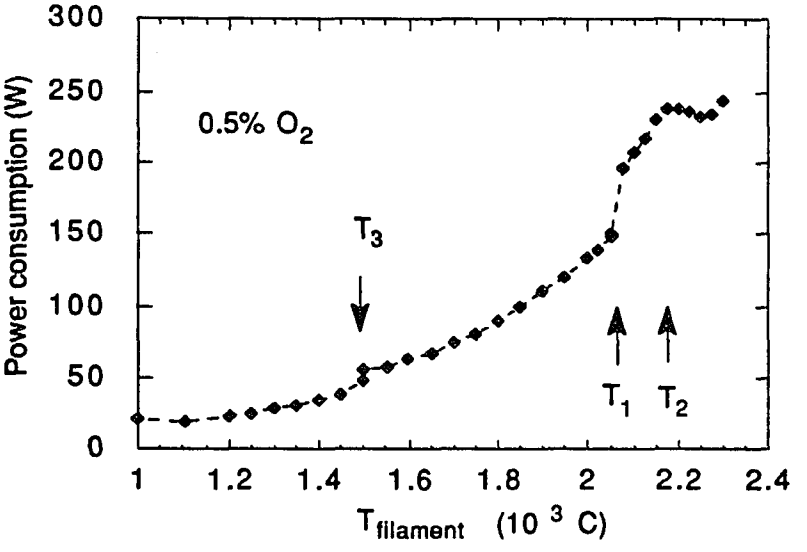

Figure 6.2 Electrical power consumption in a W filament as a function of increasing filament temperature in a mixture of 3% CH_4/H_2 and 0.5% O_2 at 25 torr.

Let us now take a closer look at the additional feature in Fig. 6.2. An abrupt increase in the dissipated power occurs at a temperature $T_3 = 1500\ ^oC$. This is consistent with the increase in ε observed in Fig. 6.1(b) at the same temperature which is caused by the formation of a carbon layer on the surface. Once again, Planck's law can offer an explanation for the observed behavior: When ε rises, more power has to be supplied to the filament to keep it at a given temperature.

The transition temperatures T_1 corresponding to the jumps in power consumption are indicated on the C-H and C-H-O phase diagrams in Fig. 6.3. The results shown were obtained for W filaments in mixtures of 3% CH_4/H_2 with 0.5% O_2 (square) and without O_2 (circle). Also included is the result for Re filaments (cross) in a mixture of 3% CH_4/H_2 and 0.5% O_2, obtained in a different experiment. There are two interesting observations that we wish to address: firstly, it can be seen that experimental transition temperatures fall slightly below those predicted by the quasiequilibrium thermodynamic model. As in chapter 5, this behavior will be attributed to thermal diffusion (the Soret effect) which tends to deplete heavier molecules, such as hydrocarbons and oxygen, from the gas phase near the hot filament. Secondly, we note that transition temperatures are shifted to lower values when oxygen is added to C-H mixtures, in agreement with model predictions. An explanation of this shift will be attempted below in terms of a reduced "effective" C/H ratio.

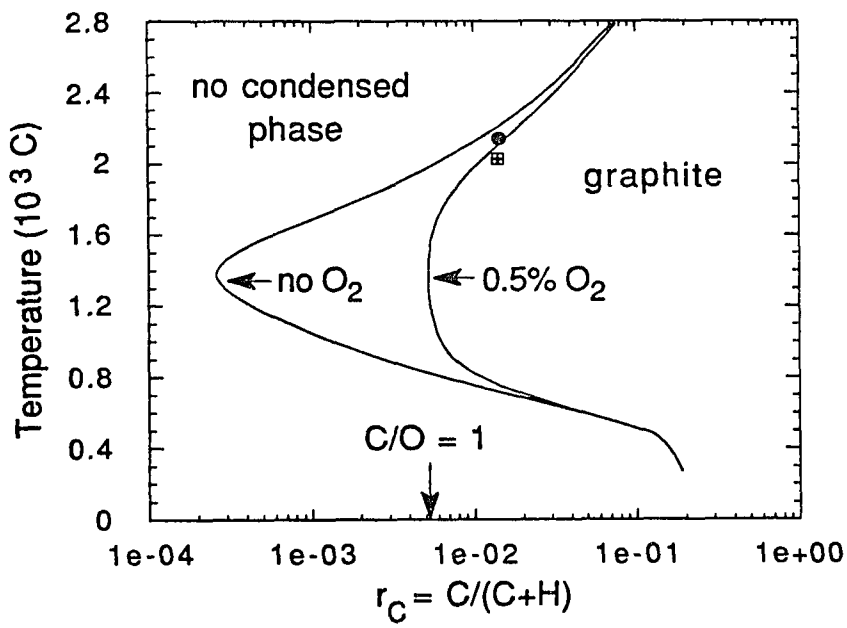

Figure 6.3 Predicted phase boundaries for graphite in the C-H (no O_2) and C-H-O (0.5% O_2) phase diagrams for P = 25 torr. r_C is the carbon atom fraction. Also shown are the experimental points corresponding to the temperatures where jumps in both the power consumption and the CH_4 and C_2H_2 partial pressures were observed. These results were obtained for W filaments in mixtures of 3% CH_4/H_2 without O_2 (circle) and with 0.5% O_2 (square), and for Re filaments in mixtures of 3% CH_4/H_2 with 0.5% O_2 (cross).

Before we focus on the gas composition inside the reaction chamber, we would like to emphasize once more that the partial pressures of the gases measured in the mass analyzer cannot be expected to be identical to the ones in the vicinity of the filament. However, any variations occurring in the gas composition are in fact caused by the changing filament temperature. Figure 6.4[(a)-(d)] shows the partial pressures of CH_4, C_2H_2, CO, H_2O, and O_2, normalized to that of H_2, as functions of increasing filament temperature for varying amounts of oxygen (0, 0.5, 1.0, and 1.5%) in the 3% CH_4/H_2 reactant gas mixture. In the absence of oxygen (Fig. 6.4(a)) the filament surface is C-covered below ~2250 °C and is reactive only above 2175°C. The slow conversion of CH_4 to C_2H_2 is in agreement with thermodynamic predictions (chapter 3) and must be due to gas phase reactions occurring in the vicinity of the filament. When the filament surface starts to become free of carbon (at T_1 = 2175°C), its ability to dissociate the reactant gases can be seen to increase. This behavior has already been explained in chapter 5.

In a mixture of 0.5% O_2 and 3% CH_4/H_2 (Fig. 6.4(b)) the filament is covered with carbon between 1500 and ~2150 °C (Fig. 6.1(b)) and becomes reactive at T_1 = 2050 °C. Below 1500 °C the partial pressures of O_2 and CH_4 are seen to decrease with increasing temperature while the partial pressures of CO and H_2O increase. We suggest that CH_4 molecules are dissociated on the clean filament surface and that the resulting carbon atoms are rapidly removed by the incoming oxygen through the formation of CO. When all the incoming oxygen has been converted to CO (and some H_2O), the partial pressures of CO and H_2O level off and the filament becomes carbon-covered for T > 1500 °C. The same general trends in the variation of the gas composition with temperature as outlined above are observed in Fig. 6.4(c) for 1% O_2 and Fig 6.4(d) for 1.5% O_2. However, the temperature range over which the filament is covered with nonreactive carbon has shrunk for 1% O_2 (1600-2050 °C, Fig. 6.1(c)) and the sharp changes observed for 0.5% O_2 have been washed out. Fig. 6.4(d) shows the changes in gas composition when the filament is heated in a mixture of 1.5% O_2 and 3% CH_4/H_2. We

know from above (Fig. 6.1(c)) that its surface is "clean" and reactive for all temperatures. Between 1100 and 1400 °C almost all of the oxygen is converted to H_2O. Above about 1500 °C CO is the dominant product and the partial pressures of CH_4 and H_2O are seen to drop at the same rate above ~1300 °C. Essentially no C_2H_2 is being produced in the reaction chamber.

It is interesting to note that the partial pressure of C_2H_2 decreases steadily with increasing additions of oxygen [Fig. 6.4(a)-(d)]. At sufficiently high temperatures and in the absence of oxygen, carbon will dissolve in H_2 to form C_2H_2. When oxygen is present, however, carbon preferentially binds to oxygen and the formation of C_2H_2 is therefore suppressed. The partial pressure of CH_4 is also expected to be suppressed but this cannot be observed due to the continuous flow of CH_4 into the chamber. For a mixture of 1.5% O_2 and 3% CH_4/H_2 essentially all the C_2H_2 has disappeared. This mixture corresponds to the interesting case mentioned above where the C/O ratio equals one.

We would like to remark that in contrast to these experimental observations, our quasiequilibrium thermodynamic model is not able to predict the suppression of hydrocarbons in the presence of oxygen. Since the solid carbon surface in the model constitutes an unlimited source of carbon, the predicted rates of evaporation of species C_xH_y are only limited by the amount of hydrogen available, but never by the amount of carbon.

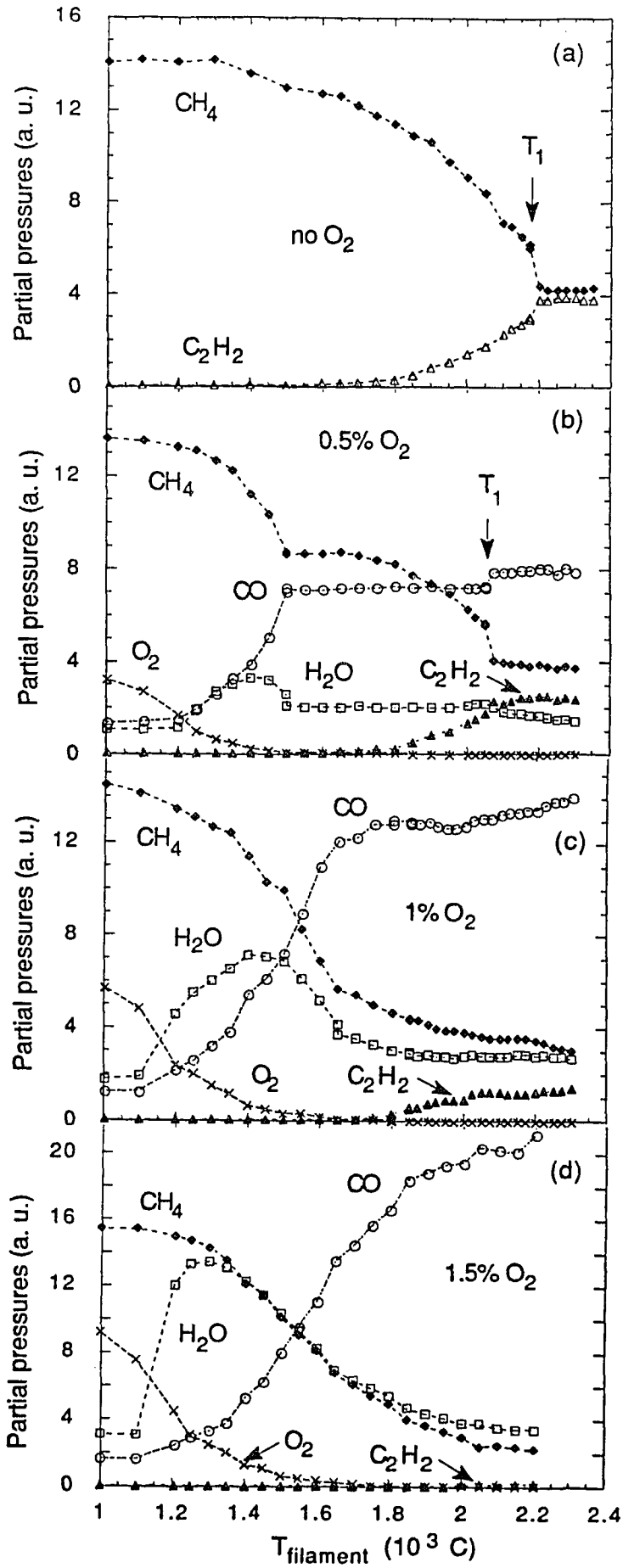

Figure 6.4
Partial pressures of stable gases (CH_4, C_2H_2, CO, H_2O, and O_2) in the reaction chamber as functions of increasing W filament temperature at 25 torr in a mixture of 3% CH_4/H_2 and varying amounts of O_2: (a) 0%, (b) 0.5%, (c) 1%, and (d) 1.5% O_2. All partial pressures have been normalized to that of H_2 and are shown on the same scale.

The series of experiments described above serve as a probe for the high temperature etch-growth boundary in the C-H-O phase diagram. The transition from deposition to etching with increasing temperature and fixed C/H and O/H ratios corresponds to the crossing of the phase boundary along the vertical axis. In a separate experiment we have shown that the phase boundary can also be traversed horizontally by increasing the C/H ratio for a given temperature and O/H ratio. To demonstrate this, a W filament has been heated in a mixture of 1% O_2 in H_2 to a temperature of 2050 °C and CH_4 has slowly been added to the reactant gas mixture. The variations of filament resistance R and gas composition in the chamber with increasing CH_4 concentration are depicted in Fig. 6.5(a) and 6.5(b), respectively.

As long as C/O is less than one, the resistance R stays essentially constant, indicating that no carbon has entered the filament. R is observed to rise sharply when C/O~1 (to within experimental accuracy). To understand why carburization of the W filament does not start immediately after the introduction of CH_4, let us examine the changes in the gas composition. It is clear from Fig. 6.5(b) that without any carbon, all of the incoming oxygen is converted to H_2O (no O_2 is observed). However, as soon as CH_4 is added to the O/H mixture the partial pressure of H_2O is seen to decrease while the partial pressure of CO increases at about the same rate. Note that although the flow rate of CH_4 is increased steadily, its partial pressure barely changes. We suggest that all the incoming CH_4 molecules deposit C atoms on the hot (2050 °C) filament surface but that the C atoms are removed by oxygen before they can diffuse into the filament. When C/O~1 the partial pressures of CO and H_2O saturate which confirms that the incoming oxygen can no longer remove all the carbon from the filament surface and that the excess C deposited on the surface can now diffuse into the bulk to form W_2C.

We would like to add a few comments related to the foregoing experiment. The same procedure as described above was carried out again but this time with the substrate holder assembly inserted into the chamber. The filament was heated to 2050 °C and CH_4

was added to the 1% O_2/H_2 gas mixture. As before, the resistance R remained constant initially but then increased drastically at the onset of carburization. It was found that now this increase in R occurred for a slightly lower C/O ratio (~0.9). When the substrate holder was heated to ~850 °C the transition to carburization was observed for C/O~0.8. This behavior seems to imply that the substrate holder assembly acts as an additional source of carbon which determines the "actual" C/O ratio. Since graphitic or amorphous carbon deposits have been detected regularly on the substrate heater, thermocouple, and other fixtures after diamond deposition processes, it is likely that additional C is introduced into the chamber in this way. Heating the substrate holder will increase the mobility of surface C atoms and lead to higher reaction rates between C and the incoming oxygen.

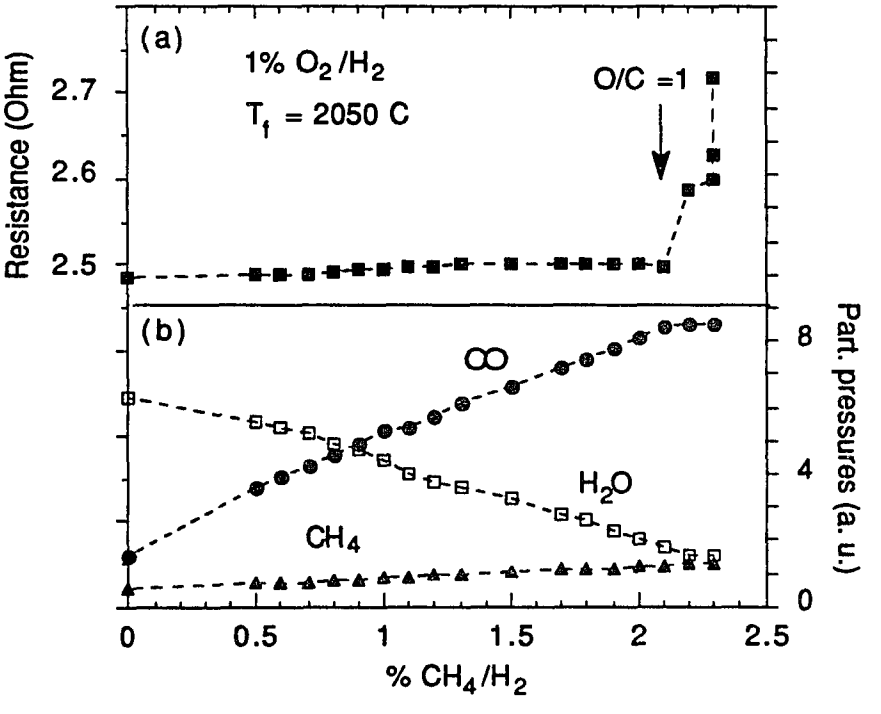

Figure 6.5 (a) Resistance of a W filament heated at 2050 °C in a mixture of 1% O_2 in H_2 at 25 torr as a function of increasing CH_4 concentration in the incoming reactant gas mixture. (b) Dependences of partial pressures of CH_4, H_2O, and CO on increasing CH_4 concentration in the incoming reactant gas mixture.

When we plotted the transition temperatures T_1 corresponding to the jumps in power consumption earlier in this section, we pointed out that, upon addition of oxygen to C-H mixtures, these transition temperatures were shifted to lower values (Fig. 6.3). A possible explanation for this result will be presented below.

We have compared the behavior of W filaments in mixtures of 3% CH_4/H_2 and 0.5% O_2 with their behavior in mixtures of 2% CH_4/H_2 (and no O_2) and have found that the temperatures T_1 at which the jumps in power consumption occur, as well as the temperatures T_2 at which the emissivity ε starts dropping, are essentially identical for these two mixtures. This observation was also confirmed when the operations of W filaments in mixtures of 3% CH_4/H_2 with 1% O_2 and 1% CH_4/H_2 were compared with one another. Note that the feature at T_3 described above is characteristic of $CH_4/H_2/O_2$ mixtures and so is only observed in the presence of oxygen. In chapter 5 we have shown that the transition temperatures T_1 decrease with the reactant carbon ratio r_C = C/(C+H). Based on these results it becomes clear that a mixture of 3% CH_4/H_2 should have a higher transition temperature T_1 than a mixture of 3% CH_4/H_2 and 0.5% O_2, which actually behaves like a 2% CH_4/H_2 mixture. But why do a 2% CH_4/H_2 and a 3% CH_4/H_2 with 0.5% O_2 mixture show almost identical behavior? We will attempt to answer this question by presenting some rather vague and simplified arguments.

According to Frenklach and Feigelson (1989) the addition of small amounts of oxygen to the inlet stream of hydrocarbon mixtures results in practically stoichiometric oxidation of carbon in the vicinity of the hot filament. Due to its stability at high temperatures, CO cannot be dissociated thermally and so appears to be chemically inert in a hot-filament reactor. (Its conversion to CO_2 is negligible). This is consistent with the results of Hayashi *et al.* (1990) who reported that diamond growth from CO/H_2 mixtures was impossible via thermally activated CVD, but that diamonds could be deposited by microwave-plasma techniques. If we assume that CO, once formed, does not take part in chemical reactions, we can, to a first approximation, exclude it from

further considerations. With respect to C-H-O mixtures in a hot-filament environment, it seems that an "effective" reactant ratio, which is responsible for deposition of solid carbon, is defined by:

$$r_C(\text{effective}) = r_C\ (1 - O/C) \qquad (6.1)$$

where $r_C = C/(C+H)$.

The meaning of this expression can be interpreted as follows. To obtain an effective ratio r_C one has to subtract from the incoming C flux the fraction of C that will react with the available oxygen to form CO. Solid carbon can then be deposited only from the amount of incoming C which has not been "passivated" by oxygen through the formation of CO. Hence the factor (1-O/C) determines the effective reactant ratio. For example, a mixture of 3% CH_4/H_2 and 1.5% O_2 results in r_C(effective)=0, i.e. no carbon is available for deposition, in agreement with our experimental observations. These arguments are consistent with those presented in a recent article by Frenklach and Wang (1991) in which they simulated the surface and gas-phase chemical kinetics of diamond deposition. They compared the theoretical predictions obtained for a (2.3 vol% CH_4)-(1.0 vol% O_2)-H_2 mixture with those for a (0.3 vol% CH_4)-H_2 mixture, and found that the species concentrations and deposition characteristics were very close to each other in the two cases.

The statement above that CO cannot be thermally dissociated and thus is chemically inert in a hot-filament environment is obviously an oversimplification. It does not take into account reactions where CO might act as a catalyst to promote or accelerate other reactions. For example, Mucha *et al.* (1989) suggest that there exist CO complexes on the substrate surface that provide additional pathways for the production of atomic hydrogen which can then in turn remove non-diamond carbon from the substrate.

6.3 Conclusions

In a simple experiment which has focused on the interactions of W filaments with various C-H-O mixtures, we have determined the effect of oxygen on filament activity. It has been demonstrated that filaments show very similar behavior when operated in C-H and C-H-O mixtures. However, a feature which does not appear in the oxygen-free case is the transition from a C-free to a C-covered filament surface at a temperature T_3. (For W filaments $T_3 < T_1 < T_2$). This behavior which is characteristic of $CH_4/H_2/O_2$ mixtures has been related to the incomplete dissociation of CH_4 molecules at low temperatures and the high affinity of oxygen towards carbon. The addition of oxygen to CH_4/H_2 mixtures also shifts transitions from deposition to etching of carbon on the filament surface to lower temperatures, in agreement with the predictions of our quasiequilibrium thermodynamic model (Fig. 6.3). An explanation for this result has been given in terms of a reduced C/H fraction. In fact, we have not only confirmed that oxygen reduces the effective C/H ratio, we have also provided a quantitative statement, $r_C(\text{effective}) = r_C(1\text{-}O/C)$. When filaments are heated in gas mixtures with O/C ratios equal to unity, i.e. $r_C(\text{effective})=0$, no solid carbon is detected on the filament surface, in agreement with theoretical predictions. We have verified experimentally the reports of Kawato & Kondo (1987) and Harris & Weiner (1989) that the addition of oxygen leads to a suppression of the partial pressures of the hydrocarbons (CH_4 and C_2H_2) in favor of the partial pressure of CO.

It has been demonstrated that growth/etching boundaries in the C-H-O phase diagram can be traversed both vertically by changing T and horizontally by changing r_C. In addition, we have detected "hidden" sources of carbon, such as the substrate holder assembly, which can contribute significantly to the actual C/H or C/O ratios. The shift in transition temperatures to lower values is of great practical importance for hot-filament diamond CVD since the filament can be operated at lower temperatures and still

be maintained in a reactive state. Practical applications of the results of our filament studies for the growth of diamond films in C-H and C-H-O mixtures will be reported in the next chapter.

Chapter 7

Hot Filament-Assisted CVD of Diamond

7.1 Introduction

In chapter 3 we have demonstrated that with a simple quasiequilibrium thermodynamic model one can predict the effects of varying the substrate temperature T_S, the reactant gas ratio r_C, and the system pressure P on the CVD phase diagram for the C-H (and C-H-O) system. When the enhanced etching of graphite by atomic hydrogen (Balooch & Olander 1975) is taken into account, a narrow window appears in the modified C-H phase diagram where diamond can be grown selectively (Fig. 3.7). Since gas activation is an essential ingredient for successful diamond deposition (chapter 2) we have analyzed the performance of hot filaments in the typical diamond growth environment (chapters 5 and 6). Based on these experimental observations we have concluded that, in order to dissociate source gas molecules effectively, filaments must be operated in a temperature regime where their surfaces are active, i.e. free of graphitic carbon deposits. After having discussed all the important aspects of CVD diamond growth in the previous chapters we shall finally turn to our diamond deposition experiments.

The organization of this chapter is as follows: In the experimental study whose results will be presented below, we shall first verify some of the previously reported observations (summarized in chapter 2), such as the importance of substrate surface treatment, the effects of changing T_S, r_C etc. Since the tendencies which accompany variations in the growth parameters can be extracted from the C-H phase diagram this

study will also serve as a test for the predictions of our quasiequilibrium thermodynamic model. In addition, we shall attempt to establish a link between the condition of the filament, i.e. its reactivity, and the quality of the deposited diamond. Unfortunately, as will be explained below, this turns out to be more challenging than anticipated. Furthermore, we shall examine whether the addition of oxygen does indeed improve the quality of the deposited diamond and lead to higher growth rates.

7.2 Experimental Results and Discussion

We shall now present the results of our experiments in which diamonds were deposited under a variety of growth conditions. A detailed description of the experimental setup and procedures, including substrate pretreatment, has been given in chapter 4. Briefly, the experimental steps that have been carried out are the following. Two substrates, typically single crystal Si and Mo foil, are first heated to ~600 °C in 25-30 torr of pure H_2 before the carbon-containing gas (CH_4 or C_2H_2) is introduced into the chamber. The filament (W or Re) which has been carburized prior to deposition is then heated to the desired temperature and condition (e.g. C-free surface). Once the substrate and the filament temperatures have reached their final values, deposition of diamond may begin.

The distance between the substrates and a newly installed filament is typically between 1 and 1.5 cm, but this distance can become uncontrolled when W filaments change their shapes after carburization. Very often, portions of the filament bend towards the substrates while others bend away from them, leading to ill-defined growth conditions. Also, we would like to remark that throughout this chapter T_s will be the substrate temperature as measured by the thermocouple. Due to the positioning of the thermocouple in the substrate holder, however, the temperature at the substrate surface may be somewhat higher than the measured value.

7.2.1 Effect of Surface Treatment on Diamond Deposits

Table 7.1 contains a list of 17 different samples together with a summary of the experimental conditions under which they have been deposited. SEM micrographs of samples 1 and 2 are shown in Fig. 7.1. Although the deposition parameters were the same for these two substrates (0.5% C_2H_2/H_2, T_s≈800 °C, P=30 torr), their surface pretreatments differed greatly from one another. While the Si substrate in Fig. 7.1(a) had been scratched with diamond paste prior to deposition, no efforts had been made to pretreat the substrate in Fig. 7.1(b). It is obvious from Fig. 7.1(a) that, even after 7.5 hours of deposition, the substrate is not totally covered but that single particles are distributed more or less uniformly throughout the surface. We shall see later, in Fig. 7.2, that the deposit can be identified as consisting of multiply-twinned microcrystals, ~1-2 μm in diameter. In Fig. 7.1(b) it can be observed that diamond particle populations formed only along a microscratch which probably resulted from the handling of the substrate during mounting. Sample 3, from Table 7.1, was deposited on Mo foil which had been roughened with steel wool prior to deposition. When viewed in the SEM, dense clusters of particles comprising almost the entire substrate surface are detected. Due to the high nucleation rate, individual particles must have coalesced rapidly and so their morphologies can no longer be discerned.

Figure 7.2 shows another micrograph of sample 1 taken at a higher magnification of x20000. The SEM image reveals interesting details concerning the morphologies of the deposited microcrystals. The particle labeled 'A' in the picture exhibits nearly perfect five-fold symmetry while particle 'B' has essentially the same basic symmetry but with a gap between two edges. Similar structures have been identified by Matsumoto and Matsui (1983) who examined vapor grown diamond particles via scanning electron microscopy, reflection electron diffraction, and transmission electron loss spectroscopy. Particles with nearly perfect pentagonal symmetry have been described as

Table 7.1 Summary of Deposition Conditions

Sample #	Substrate (a)	C_xH_y/H_2 + $O_2/(C_xH_y+H_2)$	T_s (°C)	P (torr)	T_f (°C)	filament (b)	ε (c)	Deposit (d)
1	Si+	0.5% C_2H_2	800	30	2150	R	low	Δ, □
2	Si-	0.5% C_2H_2	800	30	2150	R	low	Δ, □
3	Mo+	0.5% C_2H_2	800	30	2150	R	low	Δ, □
4	Si+	1% CH_4	800	30	2150	R	low	Δ, □
5	Si+	1% CH_4	700	25	2125	R	low	Δ, □
6	Si+	0.7% C_2H_2	720	25	1850	NR→R	high	Δ, □
7	Si+	1.5% C_2H_2	700	25	2300	R	low	O
8	Si+	1.5% C_2H_2	800	25	2300	R	low	O
9	Si+	1% C_2H_2	720	25	2300	R	low	O,□
10	Si+	1% C_2H_2	720	25	2050	NR→R	high	O,□
11	Si+	1% C_2H_2	720	25	2100	R	high	O,□
12	Si+	3% CH_4	700	25	2200	R	low	O
13	Si+	3% CH_4 + 0.5% O_2	700	25	2125	R	high	O,□
14	Si+	3% CH_4 + 1.0% O_2	700	25	2125	R	low	Δ, □
15	Si+	3% CH_4 + 1.5% O_2	700	25	2125	R	low	Δ, □
16	Si+	3% CH_4 + 1.8% O_2	700	25	2125	R	low	no growth
17	Si+	3% CH_4 + 0.5% O_2	650	25	2125	R	high	Δ, O

(a) scratching of substrate: '+' = yes, '-' = no

(b) filament surface: 'R' = reactive, 'NR' = non-reactive

(c) emissivity ε of filament surface: 'high' ≈ 1.0, 'low'≈ 0.45

(d) deposit morphology: Δ, □ = (111), (100) faces; O = spherically-shaped particles

five-fold twins in which the misfit angle of 7° 20' has been equally accommodated in the five twins or in the twin boundaries. It is apparent from Fig. 7.2 that the dominant crystal habits are square (100) and triangular (111) planes, which is consistent with the observations summarized in section 2.5. However, while (111) faces tend to be affected by parasitic nucleation, most (100) faces are seen to remain free of defects. This behavior has been explained by Spear (1989) in terms of different growth mechanisms for different crystal orientations (section 2.5). The structures that are present in sample 1 are recognized as: cubo-octahedrons bounded by 8 (111) and 6 (100) planes, icosahedrons consisting of 20 (111) planes, and so called "decahedral-Wulff-polyhedrons" (Matsumoto & Matsui 1983) with 5 (100) and 10 (111) planes. A schematic illustration of these geometric structures is provided in Fig. 7.3.

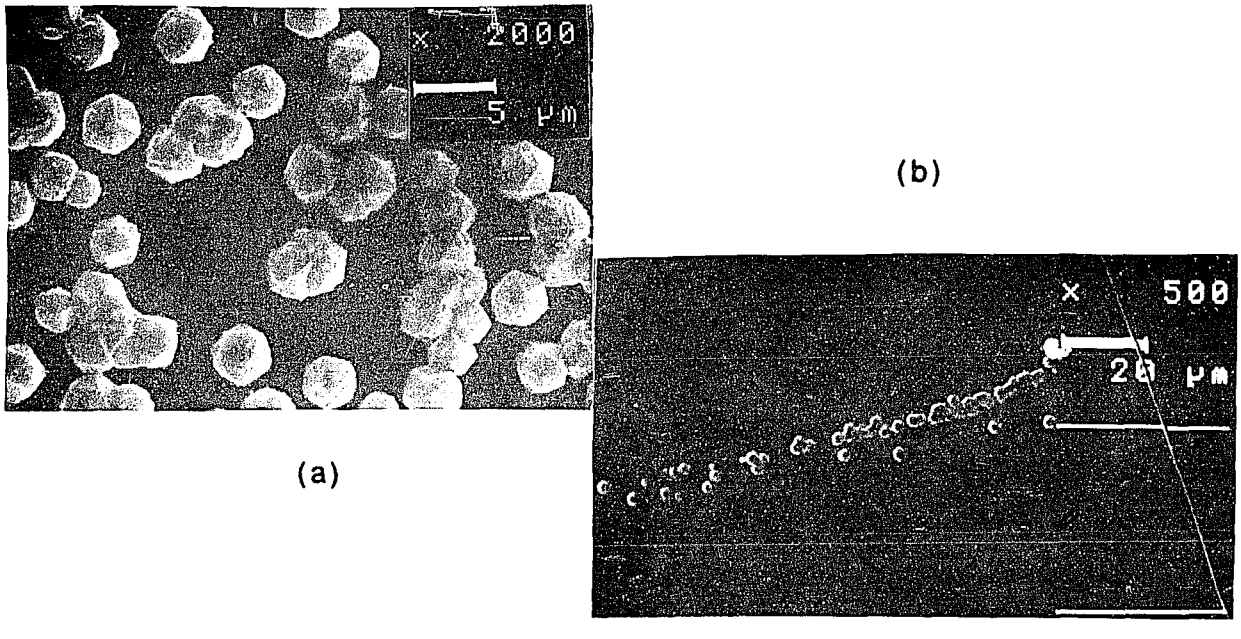

Figure 7.1 SEM micrographs of diamond particles deposited onto (a) scratched and (b) unscratched Si substrates under the following growth conditions: 0.5% C_2H_2/H_2, T_s = 800 °C, P = 30 torr, T_f = 2150 °C. These micrographs correspond to samples 1 and 2 of Table 7.1, respectively.

A B

Figure 7.2 SEM micrograph of diamond particles deposited onto scratched Si under the following growth conditions: 0.5% C_2H_2/H_2, $T_s \approx 800$ °C, P = 30 torr, $T_f = 2150$ °C (sample 1).

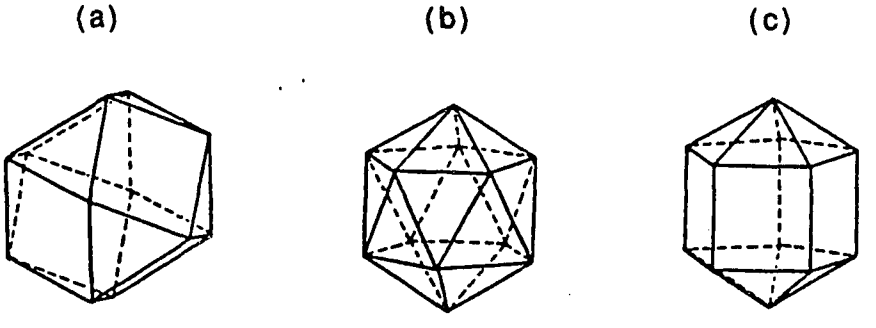

Figure 7.3 Schematic drawings of (a) a cubo-octahedron, (b) an icosahedron, and (c) a "decahedral-Wulff-polyhedron" (Matsumoto and Matsui 1983).

We would like to make a short remark concerning sample 4 of Table 7.1. The diamond particles grown from a mixture of 1% CH_4/H_2, which results in the same r_C value as 0.5% C_2H_2/H_2, look identical to the ones presented in Fig. 7.2. This confirms that diamond growth is independent of the hydrocarbon source. When included in the C-H phase diagram in Fig. 7.4 the experimental conditions for samples 1, 2, 3 and 4 fall in the region were diamond formation is favored over graphite, and so this experiment serves to verify the predictions of our QE thermodynamic model.

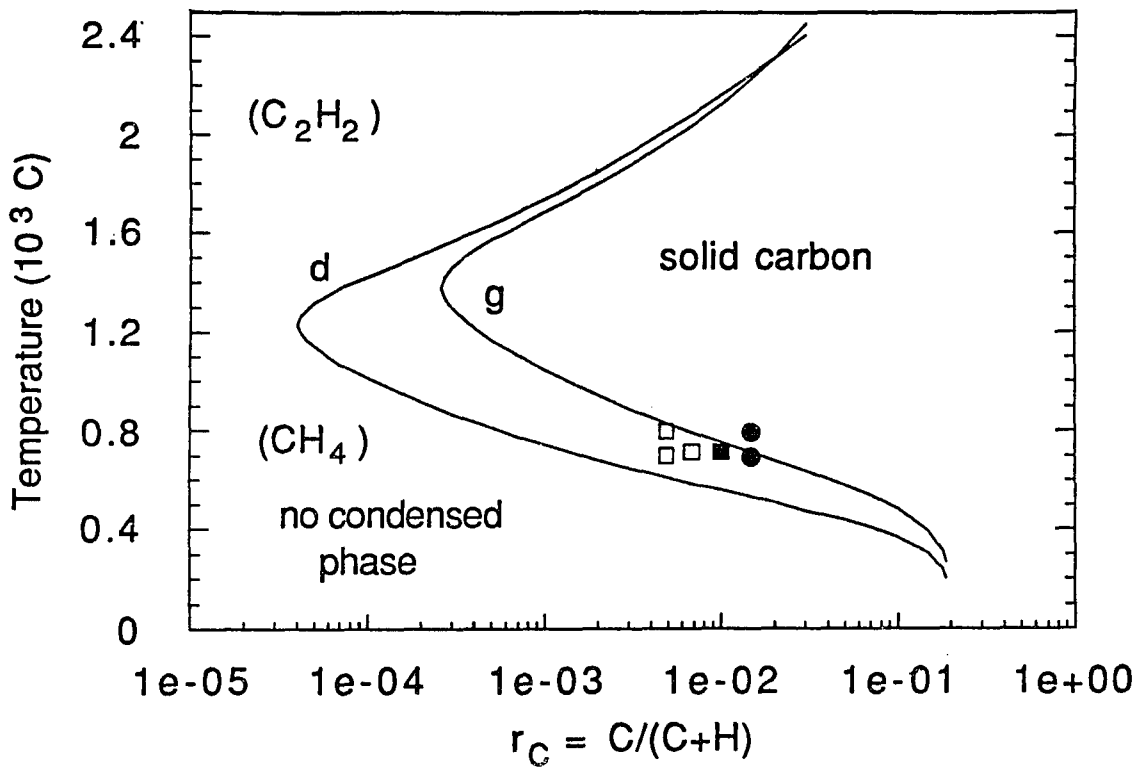

Figure 7.4 Predicted phase diagram for the C-H system (modified to include enhanced etching of graphite by hydrogen) for P = 25 torr. Also included are the experimental results corresponding to samples 1 through 12 from table 7.1. Open squares refer to particles with well-defined diamond crystal habits (samples 1-6), the filled square corresponds to particles where (100) diamond faces coexist with graphitic deposit (samples 9-11), and circles correspond to ball-like particles containing graphitic material (samples 7, 8, and 12).

7.2.2 Effect of Process Parameters on Diamond Deposits

In previous chapters we have established that the optimum conditions for vapor grown diamond are determined by the interdependence of r_C, T_s, and P. Due to the relationship between these process parameters a change in one parameter typically requires the adjustment of at least one of the other two. Expressed differently, if only one parameter deviates from its optimum value, the quality of the deposited diamond can be expected to deteriorate. This behavior has been discussed in section 2.3 and has been explained in terms of the C-H phase diagram in Fig. 3.7. Below, we shall illustrate how the appearance of the deposited particles changes when the reactant ratio r_C is increased and the substrate temperature and system pressure are kept constant.

Samples 5, 6 and 7 (see Table 7.1) were deposited at the same pressure (25 torr) and roughly the same substrate temperature (700-720 °C), but with different reactant ratios, namely 1% CH_4/H_2, 0.7%, and 1.5% C_2H_2/H_2, respectively. When compared in the SEM we notice that all three samples consist of isolated, small particles, approximately 0.5-1 μm in diameter. The low growth rate (< 0.2 μm/hr) is probably related to the low substrate temperature which might pose a kinetic barrier to diamond growth, and the low nucleation rate suggests that the substrates may not have been scratched sufficiently. However, there is a striking difference between these samples concerning the morphologies of the deposited particles. While the particles in samples 5 and 6 can be seen to possess well-defined crystal habitats, the particles in sample 7 are spherically-shaped with cauliflower-type appearances. We would like to remark that the microcrystals in samples 5 and 6 exhibit the same basic structures as have been described in relation to Fig. 7.2, and so can be identified as diamond. On the other hand, spherical particles are typically associated with non-diamond carbon.

Ball-like particles have also been observed in sample 8 which, apart from a higher T_S of 800 °C, was deposited under the same conditions as sample 7 (see Table 7.1). However, due to the higher substrate temperature, growth rates were more than twice as high (~0.5 μm/hr). Fig. 7.5 shows a micrograph of sample 8, which had been mounted in the SEM such that the electron beam was almost parallel to the substrate surface. When viewed in this configuration we notice that the particles are not spheres, but actually have flat bottoms. The resemblance to liquid droplets has lead J. Steiner, a professor of the Earth and Planetary Sciences department at CCNY, to suggest that these particles might actually have been deposited from the liquid phase (private conversation).

Figure 7.5 SEM micrograph of particles deposited onto scratched Si under the following growth conditions: 1.5% C_2H_2/H_2, $T_S \approx 800$ °C, P = 25 torr, T_f = 2300 °C (sample 8).

When the results for the above three samples are plotted in the C-H phase diagram in Fig. 7.4 it is apparent that samples 5 and 6 lie in the zone where diamond is stable, but that samples 7 and 8 fall into the graphite stability region. By comparing samples 1 and 8, we have also confirmed, although not reported here in detail, that a deviation from the optimum substrate temperature at a given pressure and reactant ratio leads to a deterioration of the deposit, in agreement with previous observations

(see section 2.4) and model predictions. Hence the present investigation has confirmed the tendencies that are associated with a variation in the deposition parameters and has also served as a test for the predictions of the QE thermodynamic model (Fig. 3.7).

7.2.3. Effect of Filament Activity on Diamond Deposits

In the preceding two chapters we have provided evidence that W filaments become reactive above a temperature T_1, when patches of the filament surface become free of graphitic carbon, but that the filament surface does not reach a low emissivity until a higher temperature T_2. We now propose 1) that material deposited with C-covered, non-reactive filaments is of lower quality than material deposited with reactive filaments, and 2) that there should be no difference in the quality of the deposit for reactive filaments with a low ε and reactive filaments with a high ε surface. The goal of the following investigation is to prove the validity of these two statements.

In order to establish a relationship between the filament activity and the quality of the deposited diamond we need a series of deposition runs, for which, aside from the condition of the filament surface, the growth parameters do not change. For example, to prove the first claim we wish to compare the results obtained for reactive and non-reactive filaments at the same T_s, r_C, P, and approximately the same T_f. In this way we can isolate changes in the deposited material which are solely caused by the changing filament activity. Hence, in the case of a non-reactive filament, its temperature should be maintained at $T_1-\Delta T$, where T_1 is the temperature at which the jump in power consumption occurs, while a reactive filament should be heated to $T_1+\Delta T$. Obviously, ΔT should not exceed ~25 C^o, in order to minimize the effects of different T_f. The same type of analysis should be performed for filaments at $T_2 \pm \Delta T$.

From chapter 5, Fig. 5.6, we know that the magnitude of the jump in power consumption is correlated with the reactant ratio r_C. In other words, the higher r_C, the

higher the temperature T_1, and the larger the jump in the power consumption. In order to clearly identify T_1, the ratio r_C in our experiment should be greater than ~4.9×10^{-3}, which corresponds to 1% CH_4/H_2 or 0.5% C_2H_2/H_2. We decided to use a mixture of 1% C_2H_2/H_2 (i.e. $r_C \approx 9.9 \times 10^{-3}$) for which, in previous experiments (chapter 5), we have determined the values of T_1 and T_2 to be ~2025 °C and ~2150 °C, respectively. According to the C-H phase diagram the substrate temperatures suitable for diamond growth at $r_C \approx 9.9 \times 10^{-3}$ and P = 25 torr lie approximately between 560 and 750 °C. Note that when the filament temperature is ~2300 °C the substrate temperature can rise to 720 °C (even without heat supplied by the ARI heater), due to irradiation by the filament. To achieve a lower T_s, cooling of the substrate would have been necessary which is not possible with the present setup. Therefore, a substrate temperature of 720 °C was chosen.

It has been pointed out before that, in order to support the statement that reactive and non-reactive filaments yield different results, we have to carry out two deposition runs. In one, the filament is heated to slightly below T_1, i.e. the temperature where the filament surface becomes reactive, while in the second the filament is heated to slightly above T_1. However, when the filament temperature is slightly below or above T_1, the filament surface is in an unstable condition, i.e. very sensitive with respect to small fluctuations in the process parameters (r_C, T_f, ...). For example, if the flow rate of C_2H_2 varies only slightly from 1.0 sccm to 1.0±0.05 sccm the value for T_1, the temperature at which the filament becomes reactive, is predicted to shift by as much as 15 C°, with decreasing r_C corresponding to decreasing T_1. Due to such fluctuations, we found it an impossible task to maintain the filament in either of these states for a long time. During the course of 6-8 hours of deposition the filament surface could change from a reactive to a non-reactive state, or vice versa. The same unstable behavior was observed near T_2. For example, the emissivity of the filament surface could change from

a high (~1.0) to a low (~0.45) value during deposition even though its temperature was held essentially constant.

Samples 9, 10, and 11 in Table 7.1 were all deposited on Si substrates at 720 °C from a mixture of 1% C_2H_2/H_2 at 25 torr, under the following filament conditions. The W filament used to deposit sample 9 was at 2300°C and had a C-free, reactive surface, the W filament for sample 10 was C-covered and initially non-reactive, but it became reactive during deposition, and the W filament for sample 11 was C-covered and reactive from the beginning of the experiment. In Fig. 7.6 we present a micrograph of sample 9, and we would like to remark that samples 10 and 11 exhibit identical growth morphologies. The deposit is seen to consist of nearly perfect (100) faces with defective material between the faces. A strong tendency towards ball-shaped, graphitic particles is clearly visible. Since the filament surface was free of carbon, and therefore undoubtedly reactive, the presence of non-diamond carbon in the deposited material indicates that the substrate temperature might have been too high for our choice of r_C. Indeed, in the C-H phase diagram (Fig. 7.4) the present set of parameters ($T_S \approx 720$ °C, $r_C \approx 0.099$, P=25 torr) lies very close to the graphite phase boundary. It is also conceivable that the actual C/H ratio was higher than anticipated, due to C atoms liberated from the substrate holder assembly, an effect which has been recognized before (see chapter 6). A higher C/H ratio could also explain why the jump in the filament power consumption for the above experiments occurred at a slightly higher temperature than is usual for 1% C_2H_2/H_2 mixtures, 2050 °C instead of 2025 °C.

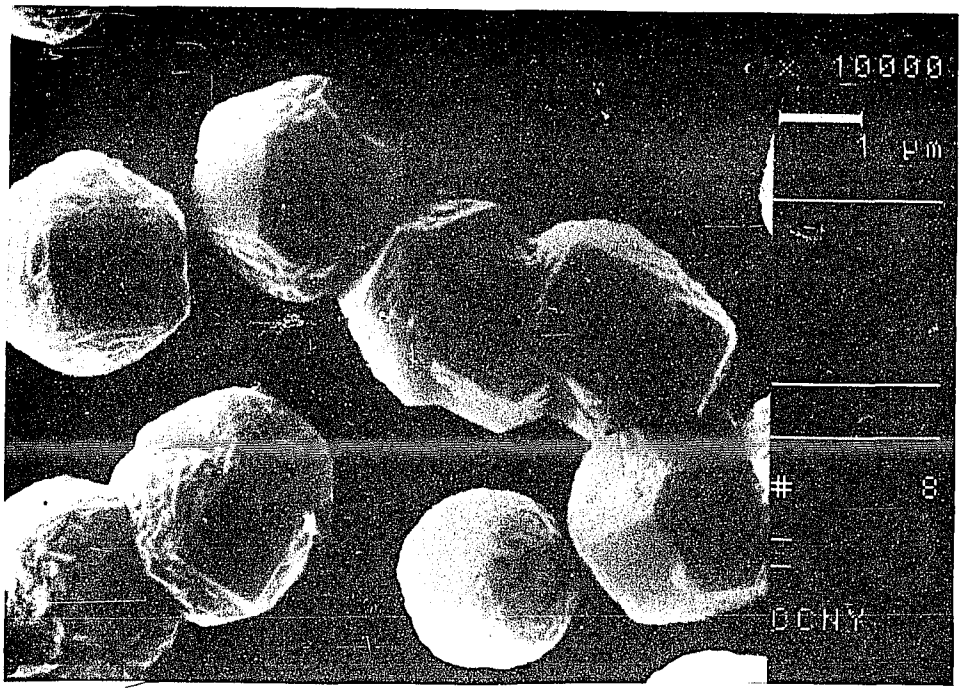

Figure 7.6 SEM micrograph of particles deposited onto scratched Si under the following growth conditions: 1% C_2H_2/H_2, $T_s \approx 720$ °C, P = 25 torr, T_f = 2300 °C (sample 9).

The coexistence of diamond and non-diamond carbon in sample 9 is also confirmed by the Raman spectrum presented in Fig. 7.7. In addition to the relatively narrow peak at 1332 cm^{-1}, which is characteristic of diamond, we observe a broad peak between 1400 and 1600 cm^{-1}, which has been commonly ascribed to sp- and sp^2-hybridized carbon (see chapter 2). It should be noted that the Raman spectra of samples 10 and 11 are essentially indistinguishable from the spectrum shown in Fig. 7.7, and have therefore been omitted.

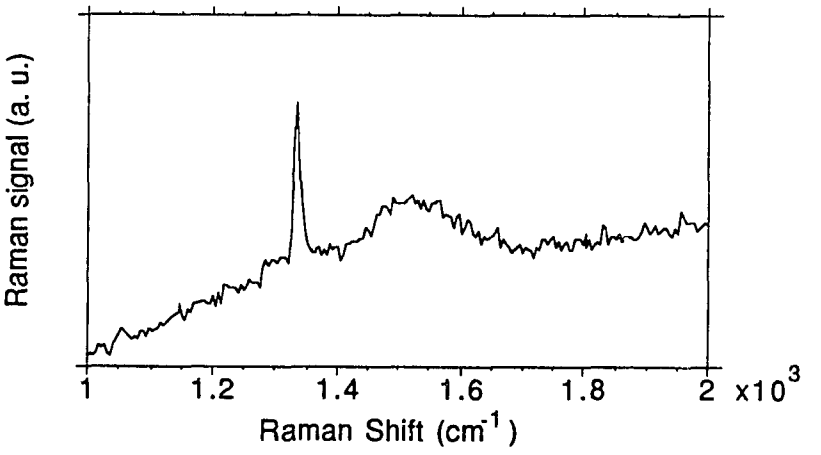

Figure 7.7 Raman spectrum of particles deposited onto scratched Si under the following growth conditions: 1% C_2H_2/H_2, $T_s \approx 720$ °C, P = 25 torr, T_f = 2300 °C (sample 9).

In conclusion, we have not been able to establish a clear relationship between the activity of the filament and the quality of the deposited material, due to the difficulties associated with maintaining the filament in a stable state for a long time. However, it has been demonstrated that *reactive* filaments yield the same type of deposit, regardless of whether their surface emissivities are high (~1.0) or low (~0.45). Even when the filament surface is C-free and reactive, i.e. it is generating atomic hydrogen, good quality diamond is not guaranteed. The nature of the deposit is still determined by the combination of the process parameters r_C, T_s, and P.

7.2.4 Effect of Oxygen on Diamond Deposits

The effect of oxygen on filament activity has been illustrated in the preceding chapter. In this section we shall investigate how the presence of oxygen can influence the appearance of the deposited diamond. The questions that we would like to address are the following: does the addition of O_2 to C/H mixtures 1) improve the quality of the deposit, 2) lead to higher growth rates, and 3) allow diamond deposition at lower substrate temperatures?

To answer the first question, we wish to focus on the deposits obtained for gas mixtures consisting of 3% CH_4/H_2 with 0, 0.5, 1.0, 1.5, and 1.8% O_2 at the same pressure of 25 torr, and substrate temperatures of 700 or 800°C. These conditions correspond to samples 12 through 16 in Table 7.1. Note that reactive filaments were employed for all of these studies.

In the absence of oxygen (sample 12) the deposit consists of small (~1 μm), spherically-shaped particles, very similar to sample 7. (Since 1.5% C_2H_2/H_2 and 3% CH_4/H_2 yield the same value for r_C the deposition conditions are actually identical for these two samples). Upon the addition of increasing amounts of oxygen to the 3% CH_4/H_2 mixture, interesting changes in the morphology of the deposited material can be observed. With 0.5% O_2 (sample 13) spherically-shaped particles together with (100) faces appear. When 1% O_2 is added to the original CH_4/H_2 mixture (sample 14), only faceted particles (~1 μm dia) are observed. Even for a mixture of 1.5% O_2 and 3% CH_4/H_2, which has a C/O ratio equal to unity, a few small particles were grown (sample 15). This result is somewhat surprising since, according to the predictions of our QE thermodynamic model, no solid carbon should be deposited for this mixture. However, it is likely that carbon which might have been introduced into the chamber via the substrate holder assembly contributed to the actual C/H and C/O ratios. This would also explain why the filament resistance increased steadily during deposition, indicating that excess carbon, not tied up in CO, was available for carburization. Due to the presence of this additional source of carbon it is necessary to add as much as 1.8% O_2 to the 3% CH_4/H_2 mixture in order to stop deposition of diamond (or graphite) completely. For this mixture no sign of growth could be detected on the substrate (sample 16). Also, note that after 6 hours of "deposition" the W filament was completely decarburized which indicates that the ratio O/C must have been greater than or equal to one.

This series of experiments confirms that the addition of oxygen to C-H mixtures improves the quality of the deposited material. We will offer an explanation for this

behavior on the basis of a reduced effective C/H ratio in the presence of O_2, an effect which has been described in the previous chapter.

In chapter 6 (Fig. 6.4) we have demonstrated that oxygen reduces the partial pressures of hydrocarbons, such as CH_4 and C_2H_2, by converting them to (mainly) CO and H_2. Since CO, once formed, appears to be chemically inert in the hot-filament environment, we have argued (chapter 6) that in the presence of oxygen the expression for the reactant ratio, which is responsible for the growth of solid carbon, should be changed from r_C = C/(C+H) to r_C(effective) = r_C(1-O/C). In other words, adding oxygen to a CH_4/H_2 mixture is equivalent to reducing the effective C/H ratio, thus leading to a higher quality deposit. The changes in morphology attributed to different C/H ratios have been clearly illustrated above in the case of samples 5, 6 and 7. Now the question arises whether the presence of CO in the reaction chamber, although seemingly irrelevant to the deposition of graphitic carbon on the filament surface, may play a role in the deposition process of diamond. Mucha *et al.* (1989), for example, proposed a reaction mechanism in which CO complexes present on the substrate surface furnish additional paths for the formation of atomic hydrogen.

To answer the above question, we have to compare the material deposited from gas mixtures with the same effective C/H ratio, i.e. we have to compare sample 9 (or 10 and 11) with sample 13, and sample 5 with sample 14. Obviously, a comparison based solely on SEM observations is not sufficient. If one wants to provide a satisfactory answer, more quantitative measurements such as Raman spectroscopy, diffraction studies etc. have to be performed. Unfortunately, at present, we are not in a position to carry out this type of analysis.

Upon careful comparison of sample 9 (1% C_2H_2/H_2), depicted in Fig. 7.6, and sample 13 (3% CH_4/H_2 and 0.5% O_2), not shown, we note that, indeed, their growth morphologies look very similar to one another. In both samples the deposit consists of a mixture of faceted particles and ball-like structures. A close resemblance is also

observed between sample 5 (1% CH_4/H_2) and sample 14 (3% CH_4/H_2 and 1% O_2). Their deposits consist of particles with well-defined crystal habits, which have been described in detail before.

A lot of controversial results have been reported in the literature concerning the effect of oxygen on diamond growth rates. It seems that no consensus has been reached so far on whether oxygen increases or decreases the growth rates. The results of Johnson *et al.* (1990) indicate that, in fact, both statements are correct. It has been demonstrated that diamond growth rates increase initially when up to ~0.4% O_2 is added to a 2% CH_4/H_2 mixture, but that growth rates drop rapidly when more oxygen is added.

On the basis of our experimental results we cannot prove that addition of O_2 to C/H mixtures leads to higher growth rates. However, we have been able to observe a drastic decline in the growth rate when the C/O ratio approaches unity. (Recall that no deposit formed on sample 16). We realize, of course, that it is questionable to define a "diamond growth rate" in terms of individual particles, which vary in size throughout the substrate. To perform a careful analysis, continuous films should be grown and examined.

In addition to the improvements in quality and higher growth rates, there have also been reports about the extension of diamond growth to lower substrate temperatures in the presence of oxygen. Sample 17 was deposited from a mixture of 3% CH_4/H_2 and 0.5% O_2 at a substrate temperature of 650 °C. (This was the lowest temperature attainable when the filament was at 2125 °C). When viewed with bare eyes after deposition, the substrate appears to be clean. Only under the microscope can we recognize some deposit consisting of tiny particles, less than 0.5 μm in diameter, which are sparsely distributed throughout the Si substrate. At a magnification of x20000, the particles are either featureless or can be identified as diamond microcrystallites, with predominantly (111) faces. Based on this result, we cannot confirm that the addition of

oxygen to C-H mixtures extends the range of substrate temperatures suitable for the deposition of diamond to lower values.

7.3 Conclusions

To conclude this chapter let us now summarize the results of this investigation. Firstly, we have verified that substrate pretreatment (scratching) is essential for successful diamond deposition at significant rates. Scratches on the substrate surface provide active sites for diamond nucleation, hence shortening long induction periods. Secondly, with the aid of SEM images we have provided evidence that particles grown via hot-filament assisted CVD under optimum conditions exhibit the diamond structure and that the dominant habit planes are (111) and (100). Multiply-twinned and defective particles are common. When growth parameters deviate from their optimum values, droplet-like structures with cauliflower-type surfaces develop. Thirdly, we have confirmed that the addition of small amounts of oxygen to C-H mixtures can significantly improve the quality of the deposited material. We have offered an explanation for this behavior in terms of a reduced effective C/H ratio, in analogy to the results obtained for hot filaments in C-H-O mixtures (chapter 6). Based on our SEM studies we find that there is no visible difference between the deposit obtained from C-H mixtures with a reactant ratio r_C and the deposit obtained from C-H-O mixtures with an equivalent reactant ratio r_C(effective). It has been shown that no growth resulted from a gas mixture with a C/O ratio equal to unity, in agreement with the predictions of our QE thermodynamic model (Fig. 3.9). When the various samples which were grown from C-H mixtures (samples 1-12) are included in the C-H phase diagram (Fig. 7.4) it is clear that our experimental results are in good agreement with our theoretical predictions concerning the optimum conditions for diamond growth.

Unfortunately, it was impossible to establish a link between the activity of the filament and the quality of the deposited material, due to the unstable condition of the filament surface near T_1 and T_2. In this experimental study the addition of oxygen has not been shown to lead to higher growth rates or to allow diamond growth at lower substrate temperatures.

Chapter 8

Conclusions and Suggestions for Further Research

We have applied the quasiequilibrium (QE) thermodynamic model, first introduced by Batty and Stickney in 1969, to the C-H system in relation to the chemical vapor deposition (CVD) of diamond (chapter 3). When the model is modified to include the observed enhanced etching of graphite by hydrogen (Balooch & Olander 1975) we obtain a C-H phase diagram which can both clarify and even explain qualitatively why diamond grows under the conditions presently being employed. With the aid of our simple model we can identify the important gaseous species in the diamond growth environment and illustrate the tendencies associated with variations in the available growth parameters (substrate temperature T_s, reactant ratio r_C,...).

The QE thermodynamic model has been extended to the CVD of diamond via the oxyacetylene torch and the corresponding C-H-O phase diagram has been determined. However, at this point the stability region of diamond is still found inside the region where graphite is stable. In this case no attempt has been made to incorporate enhanced etching of graphite by oxygen-containing species. In addition, we have examined the possible reactions between a solid carbon surface (graphite or diamond) and fluorine or fluorine/hydrogen mixtures. Although the C-F system has not been included in this discussion, the dominant gaseous species have been specified in both the C-F and C-H-F system and preliminary C-F and C-H-F phase diagrams have been obtained.

Since hot filament-assisted CVD is a widespread technique for the low pressure growth of diamond it is of great importance to understand filament-related processes which take place in the reaction chamber. We have demonstrated that crucial information concerning the activity of W and Re filaments, i.e. their ability to activate the source gases, can be obtained simply by measuring the filament power consumption and partial pressures of CH_4 and C_2H_2 (chapter 5). All of these quantities undergo sharp jumps at the same well-defined temperature, T_1, which depends only on the carbon fraction r_C of the reactant mixture. T_1 was shown to be essentially independent of the type of filament (W or Re), the hydrocarbon source (CH_4 or C_2H_2), or the pressure (9 and 25 torr). These jumps in power consumption and partial pressures are related to transitions from deposition to etching of graphitic carbon on the filament surface. The significance of these results is two-fold: firstly, the observed transitions serve as a probe for the high temperature growth/etching boundary in the predicted C-H phase diagram. It should be noted that theoretical and experimental transition temperatures are in good agreement with each other. Secondly, the observed behavior has practical implications for the thermally activated vapor growth of diamond: filaments should be operated under conditions were they are reactive, i.e. most effective in generating atomic hydrogen.

When W filaments are heated in $CH_4/H_2/O_2$ mixtures (chapter 6), essentially the same behavior is observed as for the oxygen-free analysis. However, in the presence of oxygen, transitions from deposition to etching of carbon on the filament surface are shifted to lower temperatures. We have explained this result in terms of a reduced effective carbon ratio, $r_C(\text{effective}) = r_C(1\text{-}O/C)$, by eliminating from further consideration carbon atoms that are tied up in the form of CO. In fact, no solid carbon (either graphite or diamond) could be deposited from a gas mixture whose C/O ratio equals unity, i.e. $r_C(\text{effective}) = 0$, in agreement with model predictions.

We have accomplished diamond growth from CH_4/H_2 and C_2H_2/H_2 gas mixtures (chapter 7) under deposition conditions that fall into the region where diamond is predicted to be stable in the C-H phase diagram. In addition, it has been shown experimentally that variations in the growth parameters, such as r_C and T_s, lead to changes in the quality of the deposited material which are consistent with the predictions of the QE thermodynamic model. For example, deposition at higher carbon ratios r_C results in graphitic deposit if the substrate temperature is not lowered appropriately. Upon the addition of increasing amounts of oxygen (0-1.8%) to a mixture of 3% CH_4/H_2 the morphology of the deposited particles has been observed to change from ball-like graphitic structures to well-defined diamond microcrystals, and finally to no growth when the O/C ratio reaches unity. The improvement in the quality of the deposit can be explained once again in terms of the reduced effective carbon ratio, $r_C(\text{effective}) = r_C(1\text{-O/C})$, which has been defined above in relation to the behavior of hot filaments in C-H-O mixtures.

We would like to remark that on the basis of our experimental results we cannot confirm that oxygen leads to higher diamond growth rates or allows diamond growth at lower substrate temperatures, as has been reported by Liou *et al.* (1990) and Johnson *et al.* (1990). Also, due to the difficulties associated with keeping the filament surface in a stable condition for a long period of time we have not been able to establish a clear relationship between the quality of the deposit and the activity of the filament.

Clearly, more work needs to be done!

Most of the explanations concerning the quality of the deposited particles (chapter 7) were based solely on the analysis of SEM micrographs. While SEM studies can reveal important details about the structures present in the deposit they cannot provide quantitative information, such as the ratio of diamond to non-diamond material. To obtain this type of information, other techniques such as Raman spectroscopy, have to

be applied. However, in order to perform a careful analysis and arrive at meaningful interpretations continuous films are needed.

Since our deposition experiments have been plagued by extremely low growth rates (< 0.4 μm/hr), we assume that our experimental setup requires some optimization. Firstly, shortening the distance between substrate and filament would prevent the recombination of atomic hydrogen before reaching the substrate. The importance of atomic hydrogen for successful diamond growth is irrefutable (see discussion in chapter 2). Decreasing the filament-substrate distance, however, might make it necessary to provide means to cool the substrate to its desired temperature. Secondly, the use of a series of straight Re wires under tension, instead of one coiled W filament, would guarantee more uniform, and more controllable growth conditions.

As pointed out above, when the QE thermodynamic model is applied to the growth of diamond from C_2H_2/O_2 mixtures (i.e. the oxyacetylene torch) the stability region of diamond in the corresponding C-H-O phase diagram is found within the the region where graphite is stable. Since growth of diamond at atmospheric pressure cannot be explained on purely thermodynamic grounds we have to explore what kinetic factors might be responsible for the selective growth of diamond from C_2H_2/O_2 mixtures. Remember that in the C-H system it was the (observed) enhanced etching of graphite by hydrogen.

Furthermore, theoretical studies of the C-F and C-H-F systems should be expanded and predictions should be investigated experimentally. From our preliminary analysis we have learned that fluorine reacts readily with solid carbon to form (mainly) CF_4 even with hardly any activation, which is in contrast to hydrogen. However, the presence of HF and other "nasty" reaction products requires special precautions in terms of reactor design and exhaust gas disposal.

References

Aisenberg, S. and Chabot, R. 1971. *J. Appl. Phys.* **42**, 2953.

Angus, J. C., Will, H. A., and Stanko, W. S. 1968. *J. Appl. Phys.* **39**, 2915.

Angus, J. C. and Gardner, N. C. 1969. *Us Patent No. 3,611,526.*

Angus, J. C., Gardner, N. C., Poferl, D. J., Chauhan, S. P., Dyble, T. J., and Sung, P. 1971. *Sint. Almazy* **3**, 38.

Angus, J. C., Koidl, P., and Domitz, S. 1986. In *Plasma Deposited Thin Films*, Mort, J. and Jansen, F., eds., CRC Press, Boca Raton, FL, p. 89.

Angus, J. C. and Hayman, C. C. 1988. *Science* **241**, 913.

Anthony, T. R. 1990a. *Phys. Rev. B* **42**, 1104.

Anthony, T. R. 1990b. *Mat. Res. Soc. Symp. Proc.* **162**, 61.

Badzian, A., Simonton, B., Badzian, T., Messier, R., Spear, K. E., and Roy, R. 1986. In *Infrared and Optical Transmitting Material*, Schwartz, R. W., ed. *Proc. SPIE* **683**, SPIE, San Diego, CA, p. 21.

Badzian, A. 1988. *Advances in X-Ray Analysis*, Vol. 31, Barrett, C. S., Gilfrich, J. V., Jenkins, R., Russ, J. C., Richardson, J. W., and Predecki, P. K., eds., Plenum Press, New York, p. 113.

Badzian, A., Badzian, T., and Wang, X. H. 1990. *Carbon* **28**, 804.

Balooch, M., and Olander, D. R. 1975. *J. Chem. Phys.* **63**, 4772.

Barnes, B. T. 1929. *J. Phys. Chem.* **33**, 688.

Batty, J. C., and Stickney, R. E. 1969. *J. Chem. Phys.* **51**, 4475.

Belton, D. N., Harris, S. J., Schmieg, S. J., Weiner, A. M., and Perry, T. A. 1989. *Appl. Phys. Lett.* **54**, 416.

Berman, R. 1965. *Physical Properties of Diamond*, Clarendon Press, Oxford.

Bettler, P. C., Bennum, D. H., and Case, C. M. 1974. *Surf. Sci.* **44**, 360.

Bolton, v., W. 1911. *Z. Elektrochem.* **17**, 971.

Buckley, R. G., Moustakas, T.D., Ye, L., and Varon, J. 1989. *J. Appl. Phys.* **66**, 3595.

Bundy, F. P., Hall, H. T., Strong, H. M., and Wentorf, R. H. 1955. *Nature* **176**, 51.

Burcat, A. 1984. In *Combustion Chemistry*, Gardiner, Jr., W., C., ed., Springer Verlag, New York, p. 455.

Cao, J.-R. and Back, M. H. 1985. *Carbon* **23**, 141.

Carrington, W. A., Hanssen, L. M., Snail, K. A., Oakes, D. B., and Butler, J. E. 1989. *Metall. Trans. A* **20A**, 1282.

Celii, F. G., and Butler, J. E. 1989. *Appl. Phys. Lett.* **54**, 1033.

Celii, F. G., Pehrsson, P. E., Wang, H.-t., and Butler, J. E. 1988. *Appl. Phys. Lett.* **52**, 2043.

Chang, C.-P., Flamm, D. L., Ibbotson, D. E., and Mucha, J. A. 1988. *J. Appl. Phys.* **63**, 1744.

Chauhan, S. P., Angus, J. C., and Gardner, N. C. 1976. *J. Appl. Phys.* **47**, 4746.

Chu, C. J., D'Evelyn, M. P., Hauge, R. H., and Margrave, J. L. 1990. *J. Mater. Res.* **5**, 2405.

Deryagin, B. V., Spitsyn, B. V., Builov, L. L., Klochkov, A. A., Gorodetski, A. E., and Smolyaninov, A. V. 1976. *Dokl. Akad. Nauk SSSR* **231**, 333.

Deryagin, B. V. and Fedoseev, D. V. 1977. Izd. Nauka, Moscow, USSR.

DeVos, J. C. 1954. *Physica* **20**, 690.

DeVries, R. C. 1987. *Ann. Rev. Mater. Sci.* **17**, 161.

Elliot, R. P. 1965. *Constitution of Binary Alloys, First Supplement*, McGraw-Hill, New York, C-Re on p. 226; C-W on p. 236.

Eriksson, G. 1971. *Acta. Chem. Scand.* **25**, 2651.

Evans, T. 1976. *Contemp. Phys.* **17**, 45.

Eversole, W. G. 1962. *US Patent Nos. 3,030,187* and *3,030,188.*

Fedoseev, D. V., Varnin, V. P., and Deryagin, B. V. 1984. *Russ. Chem. Rev.* **53**, 435.

Fedoseev, D. V., Vnukov, S. P., and Deryagin, B. V. 1977. *Zh. Fiz. Khimii* **51**, 26.

Frenklach, M. 1989. *J. Appl. Phys.* **65**, 5142.

Frenklach, M. and Feigelson, E. D. 1989. *Astrophys. J.* **341**, 372.

Frenklach, M. and Spear K. E. 1988. *J. Mater. Res.* **3**, 133.

Frenklach, M. and Wang, H. 1991. *Phys. Rev. B* **43**, 1520.

Hanssen, L. M., Carrington, W. A., Butler, J. E., and Snail, K. A. 1988. *Mater. Letts.* **7**, 289.

Harris, S. J. 1990. *J. Mater. Res.* **5**, 2313.

Harris, S. J. and Weiner, A. M. 1989. *Appl. Phys. Lett.* **55**, 2179.

Harrison, T. R. 1960. *Radiation Pyrometry and Its Underlying Principles of Radiant Heat Transfer*, John Wiley and Sons, New York.

Hayashi, N., Etoh, Y., Kazahaya, T., Katsumata, S., and Aketagawa, M. 1990. Presented at the Second International Conference on New Diamond Science and Technology, Washington, DC, September 23-27.

Henrici, P. 1964. *Elements of Numerical Analysis*, John Wiley and Sons, New York.

Hirose, Y. and Kondo, N. 1988. Program and Abstracts, Japan Applied Physics 1988 Meeting, March, p. 434.

Hirose, Y. and Terasawa, Y. 1986. *Jpn. J. Appl. Phys.* **25**, L519.

Hsu, W. L., Tung, D. M., Fuchs, E. A., McCarty, K. F. 1989. *Appl. Phys. Lett.* **55**, 2739.

Huang, D., Frenklach, M., and Maroncelli, M. 1988. *J. Phys. Chem.* **92**, 6379.

Ito, K., Ito, T., and Hosoya, I. 1988. *Chem. Letts.* **4**, 589.

JANAF Thermochemical Tables 1971. 2nd ed., Stull, D. R. and Prophet, H., eds., US Government Printing Office, Washington, DC, and subsequent supplements.

Jansen, F., Chen, I., and Machonkin, M. A. 1989. *J. Appl. Phys.* **66**, 5749.

Johnson, C. E., Weimer, W. A., Cerio, F. M. 1990. Presented at the Second International Conference on New Diamond Science and Technology, Washington, DC, September 23-27.

Kamo, M., Sato, Y., Matsumoto, S., and Setaka, N. 1983. *J. Cryst. Growth* **62**, 642.

Kawarada, H., Mar, K., and Kiraki, A. 1987. *Jpn. J. Appl. Phys.* **26**, L1032.

Kawato, T. and Kondo, K. 1987. *Jpn. J. Appl. Phys.* **26**, 1429.

Knippenberg, W. F., Lersmacher, B., Lydtin, H., and Moore, A. W. 1967. *Philips Tech. Rev.* **28**, 231.

Kobashi, K., Nishimura, K., Kawate, Y., and Horiuchi, T. 1988. *Phys. Rev. B* **38**, 4067.

Koidl, P., Wild, C., Dischler, B., Wagner, J., and Ramsteiner, M. 1989. *Mater. Sci. Forum* **52**, 41.

Krikorian, O. H., Carpenter, J. H., and Newbury, R. S. 1969. *High Temp. Sci.* **1**, 313.

Kubiak, G. D., Hamza, A. V., Stulem, R. H., Sowa, E. C., Kolasinski, K. W., and Van Hove, M. A. 1990. *Carbon* **28**, 751.

Kurihara, K., Sasaki, K., Kawarada, M., and Koshino, N. 1988. *Appl. Phys. Lett.* **52**, 437.

Lander, J. J., and Morrison, J. 1966. *Surf. Sci.* **4**, 241.

Langmuir, I. J., and Mackay, G. M. J. 1914. *J. Am. Chem. Soc.* **36**, 1708.

Liou, Y., Inspector, A., Weimer, R., and Messier, R. 1989. *Appl. Phys. Lett.* **55**, 631.

Liou, Y., Weimer, R., Knight, D., and Messier, R. 1990. *Appl. Phys. Lett.* **56**, 437.

Matsumoto, S. 1985. *J. Mater. Sci. Lett.* **4**, 600.

Matsumoto, S. and Matsui, Y. 1983. *J. Mater. Sci.* **18**, 1785.

Matsumoto, S., Hino, M., and Kobayashi, T. 1987. *Appl. Phys. Lett.* **51**, 737.

Matsumoto, S., Sato, Y., Kamo, M., and Setaka, N. 1982. *Jpn. J. Appl. Phys.* Part 2, **21**, L183.

Meilunas, R., Wong, M. S., Sheng, K. C., Chang, R. P. H., Van Dyne, R. P. 1989. *Appl. Phys. Lett.* 54, 2204.

Messier, R., Badzian, A., Badzian, T., Spear, K. E., Bachmann, P., and Roy, R. 1987. *Thin Solid Films* **153**, 1.

Meyer, D. E., Dillon, R. O., Woollam, J. A. 1989. Proceedings of the First International Symposium on Diamond and Diamond-Like Films, Electrochemical Society, Pennington, NJ, p. 494.

Meyer, D. E., Ianno, J. N., and Woollam, J. A. 1988. *J. Mater. Res.* **3**, 1397.

Mitomo, T., Ohta, T., Kondoh, E., Ohtsuka, K., and Habu, Y. 1990. Presented at the Second International Conference on New Diamond Science and Technology, Washington, DC, September 23-27.

Moustakas, T. D. 1989. *Solid State Ionics* **32/33**, 861.

Mucha, J. A., Flamm, D. L., and Ibottson, D. E. 1989. *J. Appl. Phys.* **65**, 3448.

Pallmer Jr., P. G., Gordon, R. L., and Dresser, M. J. 1986. *J. Appl. Phys.* **51**, 1798.

Pate, B. B. 1986. *Surf. Sci.* **165**, 83.

Patterson, D. E., Bai, B. J., Chu, J., Hauge, R. H., and Margrave, J. L. 1990. Presented at the Second International Conference on New Diamond Science and Technology, Washington, DC, September 23-27.

Pehrsson, P. E., and Morrish, A. A. 1990. Presented at the Second International Conference on New Diamond Science and Technology, Washington, DC, September 23-27.

Piekarczyk, W., Roy, R., and Messier, R. 1989. *J. Cryst. Growth* **98**, 765.

Poferl, D. J., Gardner, N. C., and Angus, J. C. 1973. *J. Appl. Phys.* **44**, 1418.

Ravi, K. V., and Landstrass, M. I. 1989. Proceedings of the First International Symposium on Diamond and Diamond-Like Films, Electrochemical Society, Pennington, NJ, p. 24.

Robertson, J. 1986. *Advances in Physics* **35**, 317.

Rosenblatt, G. M. 1976. In *Treatise on Solid State Chemistry*, Vol. 6A, Hannay, N. B., ed., Plenum Press, New York, p. 165.

Rosner, D. E. 1980. *Physico-Chemical Hydrodynamics* **1**, 159.

Saito, Y., Sato, K., Tanaka, H., Fujita, K., and Matsuda, S. 1988. *J. Mater. Sci.* **23**, 842.

Sato, Y. 1990. *Carbon* **28**, 778.

Sawabe, A. and Inuzuka, T. 1985. *Appl. Phys. Lett.* **46**, 146.

Schnetzer, S. 1990. *Carbon* **28**, 744.

Setaka, N. 1987. Proceedings of the Tenth International Conference on Chemical Vapor Deposition, Cullen, G. W., and Blocher, Jr., J., eds., Electrochemical Society, Pennington, NJ, p. 1156.

Setaka, N. 1989. *J. Mater. Res.* **4**, 664.

Smith, F. W., and Ghidini, G. 1982. *J. Electrochem. Soc.* **129**, 1300.

Solin, S. A. and Ramdas, A. K. 1970. *Phys. Rev. B* **1**, 1687.

Sommer, M. , Mui, K., and Smith, F. W. 1989. *Solid State Commun.* **69**, 775.

Sommer, M. and Smith, F. W. 1990a. *High Temp. Sci.* **27**, 173.

Sommer, M. and Smith, F. W. 1990b. *Mater. Res. Soc. Symp. Proc.* **162**, 139.

Sommer, M. and Smith, F. W. 1990c. Presented at the Second International Conference on New Diamond Science and Technology, Washington, DC, September 23-27.

Sommer, M. and Smith, F. W. 1991. To be published in *J. Vac. Sci. Technol.*

Spear, K. E. 1976. In *Treatise on Solid State Chemistry*, Vol. 4, Hannay, N. B., ed., Plenum Press, New York, p. 115.

Spear, K. E. 1982. *Pure & Appl. Chem.* **54**, 1297.

Spear, K. E. 1989. *J. Am. Ceram. Soc.* **72**, 171.

Spear, K. E., Phelps, A. W., and White, W. B. 1990. *J. Mater. Res.* **5**, 2277.

Spitsyn, B. V., and Deryagin, D. V. 1956. *USSR Author's Certificate No. 399,134* ; 1980. *USSR Patent No. 399,134.*

Tammann, G. 1922. *Z. Anorg. Allg. Chem.* **115**, 145.

Toulukian, Y. S., and DeWitt, D. P. 1972. *Thermophysical Properties of Matter*, Plenum Press, New York, Vol. 8, p.12.

Tsuda, M., Nakajima, M., and Oikawa, S. 1987. *Jpn. J. Appl. Phys.* **26**, L527.

Varnin, V. P., Teremenskaya, I. G., Fedoseev, D. V., and Deryagin, B. V. 1984. *Sov. Phys. Dokl. (Engl. Transl.)* **29**, 419.

Wagner, J., Ramsteiner, M., Wild, Ch., and Koidl, P. 1989. *Phys. Rev. B* **40**, 1817.

Williams, B. E., and Glass, J. T. 1989. *J. Mater. Res.* **4**, 373.

Winston, H. 1965. In *The Books of Diamonds*, Dickinson, J. Y., Bonanza Books, New York.

Wu, C-H., Tamor, M. A., Potter, T. J., and Kaiser, E. W. 1990. *Mater. Res. Soc. Symp. Proc.* **162**, 133.